

# **Formal Hydrogen Transfer Reactions and the Effects of Non-Redox Active Metal Cations**

by

Jeffrey A. van Santen

B.Sc. Hons. Chemistry, The University of British Columbia, 2015

A THESIS SUBMITTED IN PARTIAL FULFILLMENT OF  
THE REQUIREMENTS FOR THE DEGREE OF

MASTER OF SCIENCE

in

THE COLLEGE OF GRADUATE STUDIES

(Chemistry)

THE UNIVERSITY OF BRITISH COLUMBIA

(Okanagan)

June 2017

© Jeffrey A. van Santen, 2017

---

The undersigned certify that they have read, and recommend to the College of Graduate Studies for acceptance, a thesis entitled: FORMAL HYDROGEN TRANSFER REACTIONS AND THE EFFECTS OF NON-REDOX ACTIVE METAL CATIONS submitted by JEFFREY A. VAN SANTEN in partial fulfilment of the requirements of the degree of Master of Science

---

Supervisor, Professor (please print name and faculty/school above the line)

---

Supervisory Committee Member, Professor (please print name and faculty/school above the line)

---

Supervisory Committee Member, Professor (please print name and faculty/school above the line)

---

University Examiner, Professor (please print name and faculty/school above the line)

---

External Examiner, Professor (please print name and faculty/school above the line)

---

(Date Submitted to Grad Studies)

Additional Committee Members include:

---

(please print name and faculty/school above the line)

---

(please print name and faculty/school above the line)

# Abstract

This is a sample thesis based on the `ubcthesis.cls` template from Michael Forbes. The thesis includes the additional style file `ubcostyle.sty` in accordance to the official standards for the UBCO College of Graduate Studies. This sample thesis together with the style files and templates produces a document that is officially accepted by the UBCO College of Graduate Studies.

If you need a package, look into `ubcostyle.sty` to see if it is not already loaded there. See the file `README.txt` for additional instructions to produce the bibliography, index, and glossary automatically.

# Preface

Preface stuff

If any part of your thesis was co-written, you must include a Co-Authorship statement. Also indicate if part of the thesis was published with the reference.

# Table of Contents

<b>Abstract</b> . . . . .	iii
<b>Preface</b> . . . . .	iv
<b>List of Tables</b> . . . . .	viii
<b>List of Figures</b> . . . . .	ix
<b>List of Schemes</b> . . . . .	xi
<b>List of Symbols and Abbreviations</b> . . . . .	xii
<b>Acknowledgements</b> . . . . .	xiv
<b>Dedication</b> . . . . .	xv
<b>Chapter 1: Introduction</b> . . . . .	1
1.1 Background . . . . .	1
1.2 Details of HAT reactions . . . . .	4
1.3 Research goals . . . . .	8
<b>Chapter 2: Theory</b> . . . . .	11
2.1 The quantum mechanical approach . . . . .	11
2.1.1 Spin and Spatial Orbitals . . . . .	12
2.1.2 The Hartree product . . . . .	12
2.1.3 Slater determinants . . . . .	14
2.1.4 The Hartree-Fock approximation . . . . .	14
2.1.5 Basis sets . . . . .	16
2.1.6 Post-Hartree-Fock methods . . . . .	20
2.1.7 The complete basis set limit . . . . .	23
2.1.8 Composite quantum chemistry methods . . . . .	24

---

**TABLE OF CONTENTS**

---

2.1.9	Density-functional theory . . . . .	24
2.2	Applying theory to chemical problems . . . . .	30
2.2.1	Geometry optimisation . . . . .	30
2.2.2	Molecular vibrations . . . . .	32
2.2.3	Thermochemistry . . . . .	33
2.2.4	Modelling solvent . . . . .	35
2.2.5	Rate constants and transition state theory . . . . .	36
<b>Chapter 3: The Relationship Between Arrhenius Pre-factors with Non-Covalent Binding . . . . .</b>		<b>44</b>
3.1	Introduction . . . . .	44
3.2	Computational methods and details . . . . .	46
3.3	Results and discussion . . . . .	48
3.4	Summary . . . . .	53
<b>Chapter 4: Interrogation of the Bell-Evans-Polanyi Princi- ple: Investigation of the Bond Dissociation En- thalpies correlated with Hydrogen Atom Transfer Rate Constants . . . . .</b>		<b>61</b>
4.1	Introduction . . . . .	61
4.2	Methods . . . . .	65
4.2.1	Quantum chemical composite procedures . . . . .	66
4.2.2	Transition state calculations . . . . .	69
4.3	Comparison of composite method for the prediction of BDEs	69
4.4	Analysis of the Bell-Evans-Polanyi principle . . . . .	76
4.5	Transition state analysis . . . . .	78
4.6	Summary . . . . .	80
<b>Chapter 5: Do non-redox active metal cations have the po- tentials to behave as chemo-protective agents? The Effects on Metal Cations on HAT Reaction Barrier Heights . . . . .</b>		<b>82</b>
5.1	Benchmarking Density Functional Theory for the Binding of Alkali and Alkaline Earth Metals . . . . .	82
5.1.1	Background . . . . .	82
5.1.2	Methods . . . . .	83
5.1.3	Benchmark systems . . . . .	84
5.1.4	Metal cation basis set convergence . . . . .	85
5.1.5	High level results and evaluation of various density- functional theory methods . . . . .	85

*TABLE OF CONTENTS*

---

<b>Chapter 6: Conclusion . . . . .</b>	<b>87</b>
<b>References . . . . .</b>	<b>89</b>
<b>Appendix . . . . .</b>	<b>106</b>
<b>Appendix ABDE data . . . . .</b>	<b>107</b>

# List of Tables

Table 3.1	Table of results for (nearly) thermoneutral reactions studied. . . . .	45
Table 4.1	Bond dissociation enthalpies of the species used to investigate the accuracy of composite methods. . . . .	70
Table A.1	Summary of experimental rate constants and literature bond dissociation enthalpies (BDEs). . . . .	107

# List of Figures

Figure 1.1	A typical reaction coordinate diagram. . . . .	7
Figure 2.1	Schematic representation of a quantum mechanical composite method. . . . .	25
Figure 2.2	A reaction coordinate diagram for a generic reaction. . . . .	37
Figure 2.3	Quantum mechanical tunnelling occurs when a particle penetrates a reaction barrier, rather than surmounting it. Figure adapted from Reference 114. . . . .	41
Figure 3.1	Plot of logarithm of A-factor against binding energy. . . . .	48
Figure 3.2	Three-dimensional structures of pre-reaction complexes 2 (TEMPO-H and 4-oxo-TEMPO) and 3 (di- <i>t</i> -butyl-hydroxylamine and di- <i>t</i> -butyl-nitroxyl). . . . .	50
Figure 3.3	Three-dimensional structure of pre-reaction complex 4 between 2,4,6-tri- <i>t</i> -butylphenol and 4- <i>t</i> -butylphenoxy. . . . .	51
Figure 3.4	Three-dimensional structures of pre-reaction complexes 8 ( <i>t</i> -butylperoxy and phenol) and 9 ( <i>t</i> -butylperoxy and 2-naphthol). . . . .	55
Figure 3.5	Three-dimensional structure of pre-reaction complex 10 between <i>t</i> -butylperoxy and $\alpha$ -tetralin peroxide. . . . .	56
Figure 3.6	Molecular orbitals of hydrogen peroxide-peroxy self-exchange reaction TS complex, demonstrating a PCET mechanism. . . . .	57
Figure 3.7	Reaction coordinate illustrating a conformational change to a second pre-reaction complex prior to transition state. . . . .	58
Figure 3.8	Reaction coordinate illustrating no conformational change before moving to the transition state. . . . .	58
Figure 3.9	Reaction coordinate illustrating a conformational change to a second high energy pre-reaction complex prior to transition state. . . . .	59

## LIST OF FIGURES

---

Figure 3.10	NCIplot <sup>146,147</sup> of complex 5. The blue spheroid between the <i>t</i> -butylperoxyl oxygen centred radical and the 2,4,6-tri- <i>t</i> -butylphenol hydroxyl represents hydrogen bonding. . . . .	60
Figure 4.1	Energy profiles for a series of related exothermic reactions illustrating the Bell-Evans-Polanyi principle. . . . .	62
Figure 4.2	Bell-Evans-Polanyi plot of experimental rate constants against literature BDEs. . . . .	64
Figure 4.3	Summary of deviations of BDEs from literature for composite quantum chemical methods. . . . .	73
Figure 4.4	One-to-one plot of BDEs from literature and as calculated by the W1BD composite method. . . . .	74
Figure 4.5	One-to-one plot comparing calculated BDEs calculated by ROCBS-QB3 to literature and W1BD BDEs. .	75
Figure 4.6	Bell-Evans-Polanyi plot of experimental rate constants (normalised for the number of equivalent hydrogen atoms) for HAT between CumO <sup>•</sup> and substrates. Acetone and acetonitrile are note included in fitting as the experimental rate constants are approximate. Needs revision to move labels around. . . . .	77
Figure 4.7	One-to-one plots of theoretically determined logarithm of rate constant or HAT reactions between CumO <sup>•</sup> and organic substrates against experimental values. . . . .	79
Figure 4.8	Insert better images of CumO <sup>•</sup> -toluene TS complex with A) SOMO and B) HOMO. . . . .	80

# List of Schemes

1.1	Common reactions involved in the protein oxidation. . . . .	3
1.2	Self-exchange reactions of the <b>A.</b> benzyl-toluene couple through direct HAT <b>B.</b> phenoxy-phenol couple through PCET. . . . .	5
1.3	Hyperconjugative overlap in tetrahydrofuran and the effect of non-redox active metal cations on the transition state complex. . . . .	10
4.1	Unimolecular decay of the cumyloxy radical. . . . .	66
4.2	Locally-dense basis set partitioning used in the calculation of BDEs. . . . .	67
5.1	Binding of the calcium cation ( $\text{Ca}^{2+}$ ) to the oxygen lone pairs of N,N-dimethylacetamide. . . . .	83
5.2	Initial proposed benchmark set of molecules and cations. Note this set consists of all combinations of substrates and metal cation, thus there are 60 complexes in the set. . . . .	85
5.3	Revised benchmark set of small substrates and cations. Note this set consists of all combinations of substrates and metal cation, thus there are 35 complexes in the set. . . . .	86

# List of Symbols and Abbreviations

BDE	bond dissociation enthalpy
BEP	Bell-Evans-Polanyi
BnO <sup>•</sup>	benzyloxyl radical
CHD	cyclohexadiene
CumO <sup>•</sup>	cumyloxyl radical
DFT	density-functional theory
DNA	deoxyribonucleic acid
DMA	<i>N,N</i> -dimethylacetamide
DMF	<i>N,N</i> -dimethylformamide
$E_a$	activation energy
FHT	formal hydrogen transfer
$\mathcal{H}$	Hamiltonian operator
HAT	hydrogen atom transfer
HB	hydrogen bond
HF	Hartree-Fock
HOMO	highest occupied molecular orbital
kcal mol <sup>-1</sup>	kilocalories per mole
$K_x$	equilibrium constant
$k_x$	rate constant
KSEs	kinetic solvent effects
LFER	linear free energy relationship
LFP	laser flash photolysis
M	molar concentration
MO	molecular orbital
MDA	malondaldehyde
NCI	non-covalent interaction
PCET	proton coupled electron transfer
PMP	1,2,2,6,6-pentamethylpiperadine
PES	potential energy surface

*List of Symbols and Abbreviations*

---

RNA	ribonucleic acid
ROS	reactive oxygen species
s	seconds
SOMO	singly occupied molecular orbital
SPLET	sequential proton loss electron transfer
STO	Slater-type orbital
TEA	triethylamine
THF	tetrahydrofuran
TS	transition state
Z	atomic number
$\Delta G$	Gibbs free energy of reaction
$\Delta G^\ddagger$	Gibbs free energy barrier of reaction
$\Delta H$	enthalpy of reaction
$\Delta H^\ddagger$	enthalpic reaction barrier of reaction
$\Delta S$	entropic change of reaction
$\nabla^2$	Laplacian operator
$\sigma_X$	Hammett substituent parameter
$\rho$	sensitivity constant, or electron density

# Acknowledgements

This is the place to thank professional colleagues and people who have given you the most help during the course of your graduate work.

# Dedication

The dedication is usually quite short, and is a personal rather than an academic recognition. The *Dedication* does not have to be titled, but it must appear in the table of contents. If you want to skip the chapter title but still enter it into the Table of Contents, use this command `\chapter[Dedication]{}.`

# Chapter 1

## Introduction

### 1.1 Background

Radicals are chemical species that tend to be highly reactive due to the presence of one or more unpaired electrons. Living systems depend on radical processes as part of normal metabolism<sup>1</sup> but biomaterials, such as proteins, are susceptible to radical-induced damage. Radical-induced oxidation of biomaterials has been implicated in a number of degenerative disease states, including cancer, Alzheimer's disease, Parkinson's disease, and multiple sclerosis.<sup>2-5</sup>

In biological systems, radicals are derived from many sources. Exogenous sources include solar radiation and air pollutants, while endogenous sources include *in vivo* transition metal-ion redox processes, such as the electron transport chain involved in cellular respiration.<sup>6</sup> Some redox centres in the electron transport chain may transfer an electron to molecular oxygen, forming the superoxide anion ( $O_2^{\cdot-}$ ). Superoxide is not a strong oxidant on its own, however it may protonated to form the more reactive hydroperoxyl radical,<sup>7</sup> or disproportionate spontaneously, or catalytically through metalloenzymes such as superoxide dismutase, leading to the formation of highly reactive oxygen-centred radicals. In fact, most oxygen-centred radicals derive from reactions of  $O_2$  with redox-active metals.<sup>1</sup>

Oxygen-centred radicals, known as reactive oxygen species (ROSs) in biology, are particularly important and common due to the previously described nature of aerobic respiration. The ROSs which are of primary concern are the highly reactive hydroxyl radicals ( $HO^{\cdot}$ ), alkoxy radicals ( $RO^{\cdot}$ ), superoxide ( $HOO^{\cdot}/O_2^{\cdot-}$ ), and peroxy radicals ( $ROO^{\cdot}$ ).<sup>1</sup> The oxidation of proteins by ROSs occurs through a radical chain mechanism which has been studied experimentally in detail.<sup>8,9</sup> This chain reaction occurs when an ROS initiates a radical chain reaction through hydrogen atom transfer (HAT), single electron transfer, or addition reactions with protein substrates, leading to rapid propagation and formation of new radicals. HAT is an extremely important reaction in the context of oxidative damage. The focus of my work is on developing an understanding of the fundamental chemistry involved in

### 1.1. Background

---

protein oxidation.

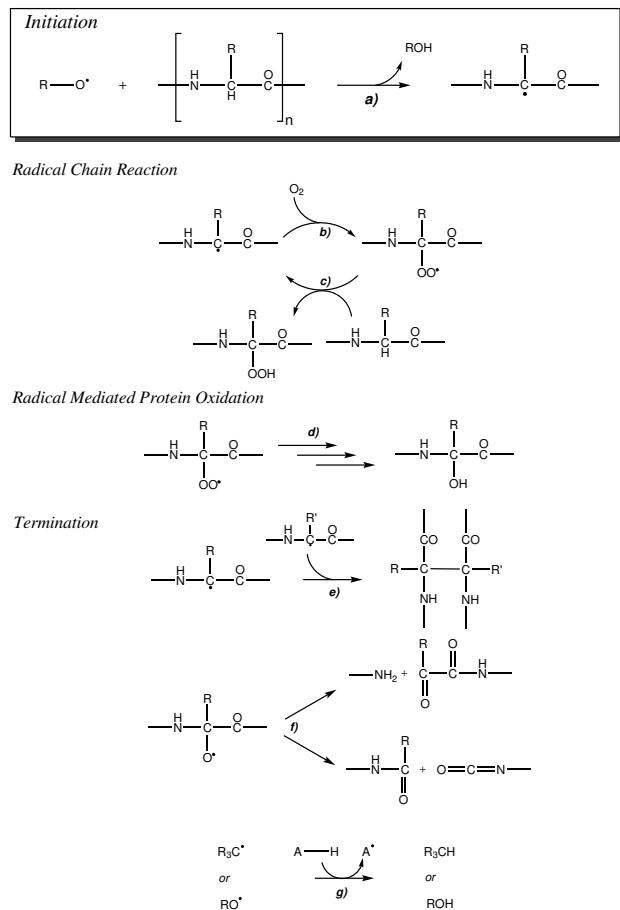
Proteins are the most abundant biomaterial in most biological systems,<sup>10</sup> thus understanding their degradation is essential to understanding degenerative disease. Because proteins are composed of as many as 20 common amino acid side-chains, as well as the common peptide backbone, there are a large number of possible reactions. Some of the reactions involved in protein oxidation are shown in Scheme 1.1.

Initial abstraction (Reaction **a**) often occurs at the  $\alpha$ -carbon position ( $\alpha\text{-CH}$ ), forming a carbon-centred radical ( $\alpha\text{-C}^\bullet$ ) which is partially delocalised in the  $\pi$ -system of the neighbouring amide and carbonyl groups. Many studies have indicated that the stability of  $\alpha\text{-C}^\bullet$  is determined by stereo-electronic considerations related to the planarity of the amide group. As such, steric bulk in the side-chains, as well as local protein structure (helix, sheet, etc.) can constrain radical geometries. For example, the most stable  $\alpha$ -carbon radicals occur at glycine residues in antiparallel  $\beta$ -sheets, whereas other bulkier residues and secondary structures lead to loss of captodative stabilisation.<sup>11</sup> Amino acid side-chains are also susceptible to oxidation. Those side-chains containing sulphur,<sup>12</sup> as well as tyrosine (which has a fairly weak phenolic O-H bond of about 89 kcal mol<sup>-1</sup>),<sup>13</sup> are particularly susceptible to oxidation.

Propagation of the radical chain reaction occurs through various processes. In the presence of molecular oxygen, rapid addition occurs at the newly formed  $\alpha\text{-C}^\bullet$  (Reaction **b**), generating a peroxy radical, which can carry forward through further HAT reactions (Reaction **c**).<sup>14</sup> The mechanism involved in the radical mediated oxidation of proteins has been studied experimentally using techniques involving ionising radiation.<sup>15,16</sup> The course of this process is complexly dependent on the availability of either singlet oxygen ( ${}^1\text{O}_2$ ), or superoxide ( $\text{O}_2^\bullet^-$ ) or the protonated form, peroxy radical ( ${}^\bullet\text{OOH}$ ). A detailed analysis of this process is outside the scope of this thesis, but ultimately, these reactions lead to the generation of a hydroxyl-amide (Reaction **d**).

The radical chain reaction can be terminated through several mechanisms, including protein-protein cross-linking (Reaction **e**), or protein fragmentation (Reaction **f**). Reactions with antioxidants (A–H, Reaction **g**) also terminate the chain reaction by removing the radical from the protein system. The sum total of all these processes contribute to the accumulation of oxidised proteins which are associated with many degenerative diseases.<sup>17</sup> HAT reactions which are important steps in the initiation, propagation, and termination reactions of protein oxidation are investigated in this thesis.

### 1.1. Background



Scheme 1.1: Common reaction involved in the protein oxidation. The reactions are as follows: **a)** initiation of radical chain through abstraction by an oxygen centred radical to generate an  $\alpha$ -carbon radical, **b)** radical addition of molecular oxygen, **c)** propagation of the radical chain reaction generating another  $\alpha$ -carbon radical and an peroxide. **d)** Radical mediated protein oxidation proceeds through multiple steps involving oxygen centred radicals and molecular oxygen result in the generation of a hydrogen-amide. Termination of the radical chain reaction can occur in several ways, including: **e)** possible cross-linking mechanism of two carbon-centred radicals, **f)** possible fragmentation pathways of an oxygen-centred radical intermediate, or **g)** HAT with an antioxidant.

## 1.2 Details of HAT reactions

Developing an understanding of protein and other biomolecular oxidation requires an understanding of the deceptively simple HAT reactions involved. Formal HAT reactions are a fundamental radical chemical transformation that have been studied for more than a century.<sup>18,19</sup> From an experimental perspective, HAT reactions which involve oxygen-centred radicals and non-radical organic substrates, are reasonably well characterised: the effects of different solvents are well understood.<sup>20</sup> However, the main challenge faced by many experiments is elucidating the mechanistic details of a reaction. This is a problem that can be examined by quantum chemistry, which is the approach that I shall take. Background on the theory used in this thesis is given in Chapter 2.

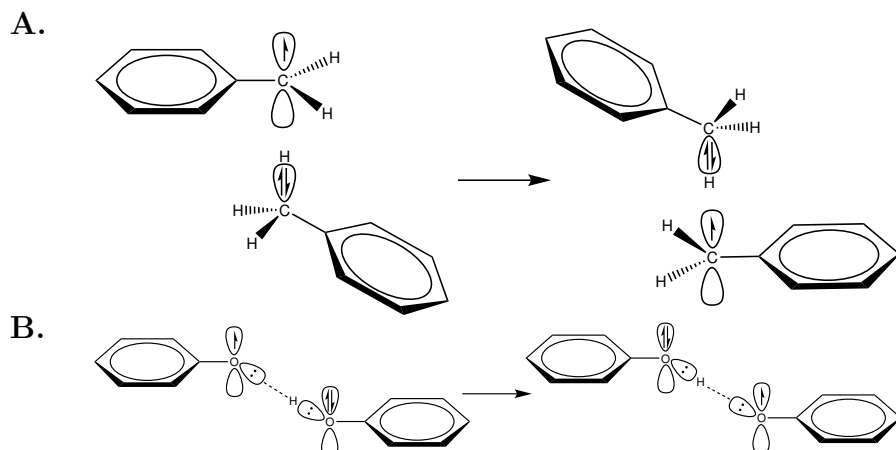
In order to investigate HAT reactions, we need to consider the mechanism in detail. For a simple HAT reaction, there exists several possible mechanisms by which this transformation can occur. The two most common concerted mechanisms are direct HAT and proton-coupled electron transfer (PCET). At the basic level, direct HAT involves the transfer of an electron and proton through the same set of acceptor/donor orbitals, while PCET involves the transfer of an electron and proton through different sets of orbitals. In practise, this distinction is poorly described, and this topic is still in active discussion in the literature.<sup>21–31</sup>

The prototypical example demonstrating the difference between direct HAT to PCET comes from the work of Mayer et al.,<sup>22</sup> that describes the self-exchange reactions of benzyl-toluene and phenoxy-phenol, shown in Scheme 1.2. In their work, the transition state (TS) structures were obtained through theoretical studies. These complexes are oriented so that the aromatic rings are trans relative to one another. In this geometry, the benzyl-toluene pair undergoes direct HAT, with the  $2p - \pi$  orbital of the benzylic carbon radical oriented at the benzylic hydrogen on toluene. This is described as direct HAT, as the orbital containing the radical overlaps with the C-H  $\sigma^*$  anti-bonding orbital, and thus the transfer of the H atom occurs through the same set of orbitals (see Scheme 1.2 A).

For the phenoxy-phenol pair (see Scheme 1.2 B), a fairly strongly hydrogen bonded pre-reaction complex is first formed with a binding enthalpy  $\Delta H$  of  $-8.1\text{ kcal mol}^{-1}$ . As a result of this strong interaction, the TS structure is such that the phenoxy radical nominally occupies an oxygen  $2p$  orbital. Therefore, in order to undergo direct HAT, the hydrogen bond between the OH and O lone-pair must break, and a new, weaker hydrogen bond with the nominally O-centred radical must form. Alternatively, the hydrogen bonded

## 1.2. Details of HAT reactions

---



Scheme 1.2: Self-exchange reactions of the **A.** benzyl-toluene couple through direct HAT **B.** phenoxy-phenol couple through PCET.

pre-reaction complex geometry does allow the orbital containing the radical to overlap with the  $2p$  lone pair of and the phenol moiety, and the conjugated aromatic  $\pi$  systems. As a result, the TS complex singly occupied molecular orbital (SOMO) is of  $\pi$ -symmetry and highly delocalised. Accordingly, the proton and electron are transferred through different sets of orbitals. The reaction has an enthalpic barrier height ( $\Delta H^\ddagger$ ) of  $5.0\text{ kcal mol}^{-1}$  relative to the hydrogen bonded complex, so that the barrier is  $3.1\text{ kcal mol}^{-1}$  below the separated reactants.

The work by Mayer et al.<sup>22</sup> suggests that hydrogen bonding is a necessary, but not sufficient, condition for PCET to occur. This then implies that PCET is not possible between molecules which do not possess hydrogen bonding moieties, such as carbon atoms. Work by other authors has shown this to be untrue.<sup>25,32</sup> In particular, DiLabio and Johnson<sup>25</sup> demonstrated that Mayer et al.<sup>22</sup> neglected the important contributions of  $\pi - \pi$  interactions and lone pair- $\pi$  interactions. Additional calculations revealed the existence of a TS structure for the benzyl-toluene couple which is  $3.7\text{ kcal mol}^{-1}$  lower in energy than previously reported. This structure orients the aromatic rings  $34^\circ$  relative to one another, allowing for optimal  $\pi - \pi$  overlap. Analysis of the TS structure highest-occupied molecular orbital (HOMO) reveals bonding character between the two  $\pi$ -systems, while the SOMO shows anti-bonding character between the  $\pi$ -systems, as well

## 1.2. Details of HAT reactions

---

as both C-H bonds. Thus, there exists a net partial bonding interaction between the two  $\pi$ -systems, opening up an additional electronic channel for PCET to occur. DiLabio and Johnson also suggest that the phenol-phenoxy couple likely prefers a  $\pi$ -stacked TS structure, and compare this to a structural analogue, a naturally occurring tyrosyl-tyrosine couple, which they demonstrated proceeds through a PCET mechanism. Other authors have confirmed the existence of a  $\pi$ -stacked TS structure for the phenol-phenoxy couple.<sup>30,31,33</sup> In the work of Muñoz-Rugeles et al.<sup>31</sup>, an approach utilising natural population analysis along the intrinsic reaction coordinate, it was demonstrated that both the benzyl-toluene couple and phenoxy-phenol couple favour a  $\pi$ -stacked TS structure and undergo formal HAT through a PCET mechanism. Interestingly, they also showed that reaction barrier heights for the PCET mechanism are systematically lower than those for related direct HAT mechanism.

Bearing in mind there is not an obvious way to explore the related differences in mechanism experimentally, computational examination of formal HAT reactions enables analysis of the mechanism of these reactions. Through careful investigation, a general distinction between a direct HAT mechanism and PCET mechanism can be achieved. In doing so, important insight is gained from understanding the electronic behaviour of these reactions. In this vein, the investigation of the physico-chemical nature of HAT reactions shall be the central theme of this thesis.

Consider for a moment the potential energy surface (PES) for an arbitrary chemical reaction, which is a complex hypersurface that depends on many variables. Theoretical methods can be used to generate a full PES, however, this quickly becomes computationally infeasible as the number of atoms in a system increases. Typically this problem can be simplified by examining only the relevant degrees of freedom. Often, the two most important coordinates can be isolated, giving a three-dimensional PES. Furthermore, in chemistry we often simplify this problem to two-dimensions using the so-called intrinsic reaction coordinate, which is the lowest energy cross section of a higher dimension PES. This yields a reaction coordinate diagram, as is illustrated below in Figure 1.1.

In a typical reaction coordinate diagram, the reactants begin to interact and form a pre-reaction complex (A). Given sufficient energy, the reaction will proceed over the top of the energy barrier through a transition state (TS) complex (B). After the chemical transformation is completed, a post-reaction complex (C) is formed until the products are able to separate. This is a somewhat simplified description, as it only broadly describes a chemical transformation. In particular, the roles of substrate-radical and

## 1.2. Details of HAT reactions

---

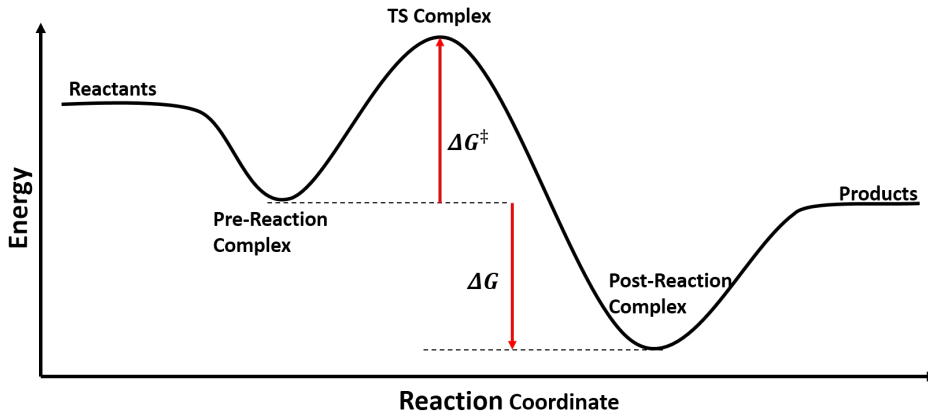


Figure 1.1: A typical reaction coordinate diagram.

substrate-radical-medium interactions along the reaction coordinate are not fully described. This is in fact a key point, as a thorough understanding of these interactions continues to be a hole in the literature.

Consequently, recent work from our group, in collaboration with our experimental colleagues at the University of Rome Tor Vergata, has focused on the importance of substrate-radical interactions in determining the kinetics of HAT reactions. Specifically, it has been shown that the three-dimensional structures of oxygen-centred radicals, as well as the organic substrates, impact the nature of the interactions involved in HAT reaction pathways.<sup>34</sup> In our work, we utilise primarily the benzyloxy (BnO<sup>•</sup>) and cumyloxy (CumO<sup>•</sup>) radicals, which serve as a proxy to biological oxygen-centred radicals. This is primarily due to the fact that reactions involving BnO<sup>•</sup> and CumO<sup>•</sup> are relatively long lived in solution, and can be monitored using time resolved laser flash photolysis (LFP) techniques. These radicals are somewhat different than biologically relevant radicals such as HO<sup>•</sup>, and as a result, the reactivity trends pertaining to the substrates can be somewhat masked by the properties of the radical, such as steric bulk,<sup>35</sup> or non-covalent binding.<sup>36</sup> Nonetheless, through a careful combination of theoretical and experimental techniques, reactions involving BnO<sup>•</sup> and CumO<sup>•</sup> with a variety of organic substrates have been used to develop a great deal of insight with respect to the role of structure in both the radicals and substrates, and resulting intermolecular interactions.

### 1.3. Research goals

---

## 1.3 Research goals

With respect to the work in this thesis, in Chapter 3 the importance of the left-hand side of Figure 1.1 shall be examined by studying how the pre-reaction complex impacts HAT reactions. There has been limited investigation of the importance of pre-reaction complex formation for HAT reaction.<sup>37</sup> This is problematic, as oxygen-centred radicals can hydrogen bond with substrates as both acceptors and donors.<sup>38</sup> These hydrogen bonding interactions, in addition to the other non-covalent interactions between the radical and substrate, lead to the formation of a pre-reaction complex. Accordingly, the formation of a pre-reaction complex is a fundamental step in protein oxidation.

The specific aim of Chapter 3 is to investigate the effects of non-covalent binding in the pre-reaction complex, with respect to the well-known, but phenomenological Arrhenius equation. As of yet, there is no framework which relates the non-covalently bound pre-reaction complex to kinetic results. I ask the simple question: does there exist a direct correlation between the Arrhenius pre-factor for a HAT reaction and the non-covalent binding that occurs in the pre-reaction complex formed in near identity reactions? To address this question, I examine the non-covalent binding in the pre-reaction complex in a series of related HAT reactions. Arrhenius parameters for the systems of interest in this work were previously tabulated,<sup>39</sup> and consist of thermoneutral or nearly thermoneutral reactions involving the formation and destruction of oxygen-centred radicals. These reactions are related to the phenol-phenoxy self-exchange reaction, where a relatively strong pre-reaction complex is expected.

Then in Chapter 4, the right-hand side of Figure 1.1 is considered, where the effects of bond dissociation enthalpies (BDEs) on HAT rate constants are examined. BDEs are central to the understanding of reactions with respect to thermodynamics. In addition to this, there exists a tremendous amount of literature in which BDEs are linked to chemical reactivity, especially for HAT reactions.<sup>18,24,40–42</sup> There exists a linear free energy relationship (LFER) called the Bell-Evans-Polanyi (BEP) principle,<sup>43,44</sup> which states that the difference in activation energy ( $E_a$ ) for two related reactions is proportional to the differences in reaction enthalpy ( $\Delta H$ ):

$$E_a = E_0 + \alpha\Delta H \quad (1.1)$$

where  $E_0$  is the activation energy of a reference reaction, and  $\alpha$ , a constant which characterises the position of the TS along the reaction coordinate.

### 1.3. Research goals

---

This relationship has been more generally used to compare larger families of reactions. Despite the widespread use of the BEP principle, the validity of this relationship is not well described.

I probe the validity of the BEP principle, with the aim to determine how generally it may be applied. This is achieved by relating accurate, theoretically determined C-H BDEs for species that undergo abstraction at the appropriate C-H position, to the experimentally determined HAT rate constants. HAT reaction rate constants depends on many factors. However, by using rate constants determined under specific conditions (LFP with CumO<sup>•</sup> in acetonitrile at 298K), the difference in reactivity depend mainly on the differences in chemical properties of the substrates of interest. Therefore, we hypothesise that there should exist two BEP relationships for C-H bonds: one in which the incipient radical is delocalised into a  $\pi$ -system (benzylic-allylic), and the other in which the remaining alkyl radicals are largely localised.

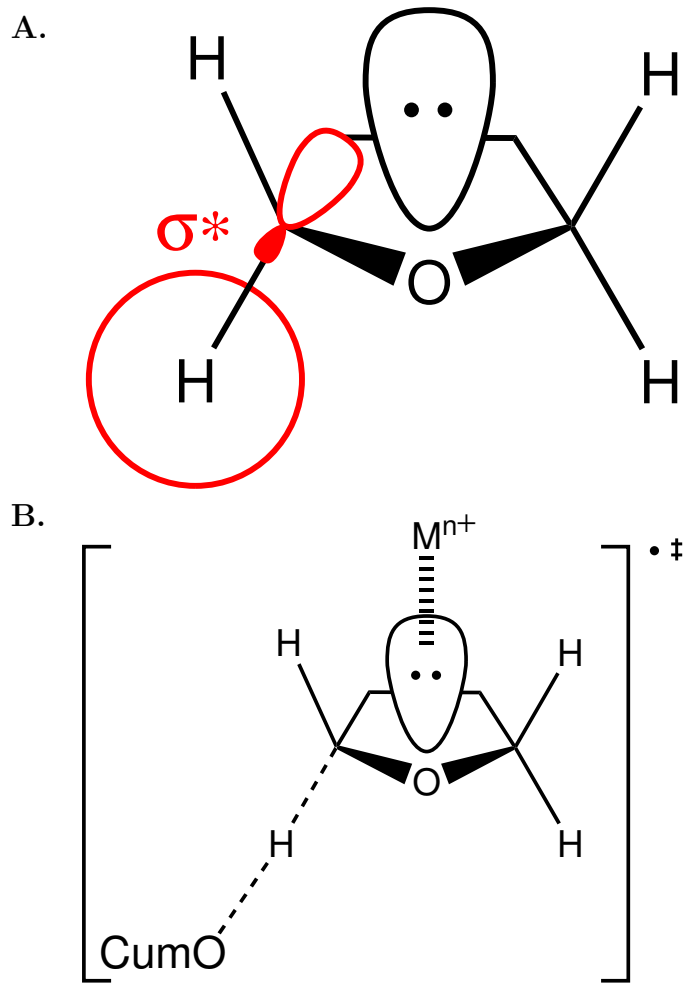
Finally, recent experimental results show that non-redox active metal cations, which are found ubiquitously in biological systems, have an inhibitory effect on HAT reactions involving oxygen-centred radicals. This has been demonstrated experimentally for substrates which undergo abstraction from sites adjacent to heteroatoms (e.g. amines, amides, and ethers). Under various stoichiometric ratios, these metal cations have effects ranging from full inhibition to partial deactivation of HAT reactivity.<sup>45–47</sup> This effect has been attributed partially to the effects of hyperconjugative overlap. Take for example tetrahydrofuran (THF), shown in Scheme 1.3. Normally, there exists C-H bond weakening hyperconjugative overlap of electron density from one of the oxygen lone-pairs and the adjacent C-H  $\sigma^*$  anti-bonding orbitals. The interaction of a metal cation with the oxygen lone-pairs removes electron density from this interaction, thus increasing the C-H bond strength. As a result, the reactivity of this bond is decreased, as observed from the experimentally measured 3.2-fold decrease in the rate constant for HAT with CumO<sup>•</sup> in acetonitrile from  $6.65 \times 10^7 \text{ M}^{-1}\text{s}^{-1}$  to  $7.0 \times 10^7 \text{ M}^{-1}\text{s}^{-1}$  in the presence of 1.0 M Mg(ClO<sub>4</sub>)<sub>2</sub>.<sup>45</sup>

The nature of the interactions between non-redox active metal cations and organic substrates is poorly understood. This problem is explored in Chapter 5, with the aim to understand the fundamental physico-chemical properties that lead to the experimentally observed trends in reactivity. The experimentally observed effects have led us to hypothesise that the presence of non-redox active metal cations has a chemo-protective effect against the radical-induced oxidation of biomaterials such as proteins.

In using theory to study HAT reactions, I hope to contribute to a better

### 1.3. Research goals

---



Scheme 1.3: **A.** Hyperconjugative overlap in tetrahydrofuran. **B.** The non-redox active metal cation accepts electron density from the heteroatom lone pair, reducing overlap with the C-H  $\sigma^*$  anti-bonding orbital, and increasing the C-H bond strength, thus destabilising the TS complex.

understanding of the fundamental properties which govern these reactions, and thus develop insights into the many important biological processes in which HAT takes place.

# Chapter 2

## Theory

### 2.1 The quantum mechanical approach

The fundamental properties governing all of chemistry are dictated by the quantum mechanical wave functions,  $\Psi$ . Therefore, in quantum chemistry we seek solutions to the non-relativistic time-independent Schrödinger equation

$$\mathcal{H} |\Psi\rangle = E |\Psi\rangle \quad (2.1)$$

where  $\mathcal{H}$  is the Hamiltonian operator for a system of nuclei and electrons, and  $\Psi$  is the wave function, defined as the set of eigenvectors with energy eigenvalues  $E$ .<sup>48</sup> For a system with  $N$  electrons and  $M$  nuclei, the full Hamiltonian in atomic units is

$$\begin{aligned} \mathcal{H} = & -\sum_{i=1}^N \frac{1}{2} \nabla_i^2 - \sum_{A=1}^M \frac{1}{2M_A} \nabla_A^2 - \sum_{i=1}^M \sum_{A=1}^M \frac{Z_A}{r_{iA}} \\ & + \sum_{i=1}^N \sum_{j>i}^N \frac{1}{r_{ij}} + \sum_{A=1}^M \sum_{B>A}^M \frac{Z_A Z_B}{R_{AB}} \end{aligned} \quad (2.2)$$

In this equation,  $Z_A$  is the atomic number of nucleus  $A$  with a mass  $M_A$  divided by the mass of an electron. The Laplacian operators  $\nabla_i^2$  and  $\nabla_A^2$  represent differentiation with respect to the coordinates of the  $i$ th electron and  $A$ th nucleus. The first and second terms are the kinetic energies of the electrons and nuclei, respectively. The third term represents the Coulomb attraction between electrons and nuclei with distance  $r_{iA}$ . The fourth and fifth terms represent repulsion between two electrons with distance  $r_{ij}$ , and between two nuclei with distance  $R_{AB}$ , respectively.

Nuclei move slowly relative to electrons, due to their much greater mass. This is the central pillar of the Born-Oppenheimer approximation that is nearly always applied in molecular electronic structure calculations. The application of this approximation allows for the simplification of Equation 2.2: using a separation of electronic and nuclear variables, the second term for

## 2.1. The quantum mechanical approach

---

nuclear kinetic energy is solved separately. Also, the last term of nuclear repulsion is constant, and thus is generally ignored. This leaves us with the electronic Hamiltonian

$$\mathcal{H}_{elec} = - \sum_{i=1}^N \frac{1}{2} \nabla_i^2 - \sum_{i=1}^M \sum_{A=1}^M \frac{Z_A}{r_{iA}} + \sum_{i=1}^N \sum_{j>i}^N \frac{1}{r_{ij}} \quad (2.3)$$

Unfortunately, it is only possible to exactly solve the Schrödinger equation for the full electronic Hamiltonian  $\mathcal{H}_{elec}$  in the simplest of cases: when there is only one electron ( $H$ ,  $H_2^+$ ,  $He^+$ ,  $Li^{2+}$ , etc). Note that since we will always work within the Born-Oppenheimer approximation, the subscript *elec* is usually dropped. In order to proceed to systems with multiple electrons, we must make further approximations.

### 2.1.1 Spin and Spatial Orbitals

We will refer to the wave function of a single particle as an orbital. Naturally then, as we will deal with electrons in molecules, we shall refer to their wave functions as molecular orbitals (MOs). To fully describe electrons we must consider a spatial and spin component to the overall wave function. A spatial orbital  $\psi_i(\mathbf{r})$ , is a function of the position vector  $\mathbf{r}$ , and describes the distribution of an electron in all space. It is usually assumed that spatial MOs form an orthonormal set such that

$$\langle \psi_i(\mathbf{r}) | \psi_j(\mathbf{r}) \rangle = \int d\mathbf{r} \psi_i^*(\mathbf{r}) \psi_j(\mathbf{r}) = \delta_{ij} \quad (2.4)$$

where the left-hand side is standard Dirac *bra-ket* notation representing the same integral in the middle. The right-hand side of Equation 2.4 is the standard Kronecker delta.

The spin of an electron is represented by two orthonormal functions  $\alpha(\omega)$  and  $\beta(\omega)$ , or spin up and spin down. If a wave function describes both the spatial distribution and spin of an electron it is a spin orbital,  $\chi_i(\mathbf{x})$ , where  $\mathbf{x}$  represents both the spatial distribution and spin coordination of an electron ( $\mathbf{x} = \{\mathbf{r}, \omega\}$ ). Since  $\psi_i(\mathbf{r})$  and  $\alpha(\omega)/\beta(\omega)$  are orthonormal, so too is  $\chi_i(\mathbf{x})$

$$\langle \chi_i(\mathbf{x}) | \chi_j(\mathbf{x}) \rangle = \delta_{ij} \quad (2.5)$$

### 2.1.2 The Hartree product

The first steps towards describing an  $N$  electron wave function come from the work in the late 1920s by Hartree. The early *Hartree method* took an

## 2.1. The quantum mechanical approach

---

approach in which the wave function of  $N$  non-interacting electrons ( $\Psi^{HP}$ ) is described by the product of  $N$  spin orbitals, known as a *Hartree product*:

$$\Psi^{HP}(\mathbf{x}_1, \mathbf{x}_2, \dots, \mathbf{x}_N) = \chi_i(\mathbf{x}_1)\chi_j(\mathbf{x}_2)\dots\chi_k(\mathbf{x}_N) \quad (2.6)$$

In such a system the Hamiltonian has the form of a sum of  $N$  independent operators

$$\mathcal{H} = \sum_{i=1}^N \hat{h}(i) \quad (2.7)$$

where  $\hat{h}(i)$  is

$$\hat{h}(i) = -\frac{1}{2}\nabla_i^2 + V(\mathbf{r}_i) \quad (2.8)$$

such that the first term describes an electron's kinetic, and the second term describes potential felt by a single electron. If we consider the case which ignores electron-electron repulsion, then case  $V$  describes only the nuclear-electron attraction. Alternatively, the electron-electron repulsion may be included as an average potential.

Solutions to the Schrödinger equation for this system of non-interacting electrons are facile to obtain as each  $h(i)$  depends only on the variables of  $\chi_i(\mathbf{x}_i)$ , so that

$$\mathcal{H} |\Psi^{HP}\rangle = E |\Psi^{HP}\rangle \quad (2.9)$$

gives an eigenvalue energy solution  $E$  that is the sum of  $N$  spin orbital energies  $\varepsilon_i$

$$E = \varepsilon_1 + \varepsilon_2 + \dots + \varepsilon_N \quad (2.10)$$

While this theory does allow one to calculate energies for an  $N$  electron system, it has a basic deficiency: the antisymmetry principle of wave functions is not obeyed. The antisymmetry principle states that the electronic wave function must change sign (be antisymmetric) with respect to the exchange of spacial and spin coordinate of any two electrons. Hartree accounted for this by nominally applying the Pauli exclusion principle, however, this description is still incomplete in the sense that it does not describe the statistical nature of quantum particles.

### 2.1.3 Slater determinants

In order to satisfy the antisymmetry principle, a linear combination of Hartree products can be taken. Although the method was first utilised independently by Heisenberg<sup>49</sup> and Dirac,<sup>50</sup> this method is called a *Slater determinant* after Slater.<sup>51</sup> For an  $N$  electron system, a Slater determinant is written as

$$\Psi(\mathbf{x}_1, \dots, \mathbf{x}_N) = \frac{1}{\sqrt{N!}} \begin{vmatrix} \chi_i(\mathbf{x}_1) & \chi_j(\mathbf{x}_1) & \cdots & \chi_k(\mathbf{x}_1) \\ \chi_i(\mathbf{x}_2) & \chi_j(\mathbf{x}_2) & \cdots & \chi_k(\mathbf{x}_2) \\ \vdots & \vdots & \ddots & \vdots \\ \chi_i(\mathbf{x}_N) & \chi_j(\mathbf{x}_N) & \cdots & \chi_k(\mathbf{x}_N) \end{vmatrix} \quad (2.11)$$

where  $1/\sqrt{(N!)}$  is a normalisation factor. This simple mathematical trick ensures antisymmetry since the interchange of two electrons requires the exchange of two rows in the determinant, which changes the sign. Normally the short-hand form, which implicitly includes the normalisation factor and assumes the ordering of electrons is  $\mathbf{x}_1, \mathbf{x}_2, \dots, \mathbf{x}_N$ , is written as only the diagonal elements of the determinant:

$$\Psi(\mathbf{x}_1, \mathbf{x}_2, \dots, \mathbf{x}_N) = |\chi_i \chi_j \cdots \chi_k\rangle \quad (2.12)$$

Slater determinants are completely dependent on the spin orbitals from which it is formed, to within a sign. Therefore, Slater determinants also form an orthonormal set. Additionally, the introduction of antisymmetry into the Hartree product incorporates so-called *exchange correlation*. This means that the motion of two electrons with parallel spin are correlated. However, since the motion of electrons with opposite spin are not correlated, a single determinant wave function is said to be uncorrelated.

### 2.1.4 The Hartree-Fock approximation

Now that we have a method for describing many-electron wave functions, we can consider the computation of molecular properties. The cornerstone of quantum chemistry is the *Hartree-Fock method* (HF), otherwise known as the self-consistent field method. The main principle of the HF method is to approximate electron-electron interactions with an average potential. We begin with a single Slater determinant for an  $N$  electron system in the ground state:

$$|\Psi_0\rangle = |\chi_1 \chi_2 \cdots \chi_N\rangle \quad (2.13)$$

## 2.1. The quantum mechanical approach

---

By applying the variational method to the Schrödinger equation, we hope to find the lowest possible ground state energy,  $E_0$ . One applies the variational principle by choosing a trial wave function ( $\phi$ ) dependent on some number of parameters. These parameters are optimised so that the expectation value of the energy is minimised:

$$E_0 \leq \langle \phi | \mathcal{H} | \phi \rangle \quad (2.14)$$

The trial wave function minimises  $E_0$  only when  $\phi = \Psi_0$ , the ground state wave function.

Within the Hartree-Fock approximation, we approximate the full electronic Hamiltonian  $\mathcal{H}$  with a related operator  $\hat{H}_0$ :

$$\hat{H}_0 = \sum_{i=1}^N \hat{f}(i) \quad (2.15)$$

where  $\hat{f}(i)$  is the Fock operator of the  $i$ -th electron, defined as

$$\hat{f}(i) = -\frac{1}{2} \nabla_i^2 + \sum_{A=1}^M \frac{Z_A}{r_{iA}} + v^{HF}(i) \quad (2.16)$$

The first two terms are familiarly the non-interacting one electron Hamiltonian,  $\hat{h}(i)$ . The third term,  $v^{HF}(i)$ , is the average potential experienced by each electron in the presence of other electrons.

With these approximations, the quantum problem is now reduced to solving the eigenvalue Hartree-Fock equation of the form

$$\hat{f}(i)\chi(\mathbf{x}_i) = \epsilon_i\chi(\mathbf{x}_i) \quad (2.17)$$

Solving Equation 2.17 directly is computationally very challenging, as there are infinite possible solutions. However in 1951, Roothaan<sup>52</sup> demonstrated that the problem can be simplified by expanding each spin orbital into a linear combination of a known finite number  $K$  basis functions:

$$\chi_i = \sum_{\mu=1}^K C_{\mu,i} \phi_{\mu} \quad (2.18)$$

where  $C_{\mu,i}$  is a weighting coefficient and  $\phi_{\mu}$  is a basis function. As  $K$  approaches  $\infty$ , the set  $\{\phi_{\mu}\}$  becomes more complete and the energy approaches the so-called *Hartree-Fock limit*, or the exact energy in the Hartree-Fock approximation. One is, however, always limited to a finite number of basis functions, leaving deficiencies in the desired wave function  $\Psi_0$ .

## 2.1. The quantum mechanical approach

---

The expansion of spin orbitals into a basis allows Equation 2.17 to be written in terms of the *Roothaan matrix equation*

$$\mathbf{FC} = \mathbf{SC}\varepsilon \quad (2.19)$$

where  $\mathbf{F} = \sum_{l,m} \langle \chi_l | \hat{f}(i) | \chi_m \rangle$  is the Fock matrix,  $\mathbf{S} = \sum_{l,m} = \langle \chi_l | \chi_m \rangle$  is the orbital overlap matrix.  $\mathbf{C}$  is the orbital coefficient matrix, and  $\varepsilon$  is the diagonal matrix of orbital energies  $\varepsilon_i$ , which are generally the desire solutions. By performing a transformation of basis to an orthonormal basis, the overlap matrix  $\mathbf{S}$  becomes the identity matrix  $\mathbb{1}$ , and simplifies the problem. Thus, utilising 2.19 reduces the problem to the of diagonalisation  $\mathbf{F}$ . Unfortunately, this must be done iteratively, as  $\mathbf{F}$  depends on its own solution, hence the name self-consistent field method.

### 2.1.5 Basis sets

Choosing optimal basis functions can help significantly in terms of determining the ground state wave function  $\Psi_0$ . Quantum chemists rely on the choice of *basis sets*, defined as the vector space in which an *ab initio* problem is defined. Basis sets usually refer to the set of one particle functions, which are used to form MOs in a linear combination of atomic orbitals (LCAO-MO) like approach. For a system with  $N$  electrons, the LCAO-MO approach gives  $N/2$  occupied orbitals in the ground state. The remaining basis functions in a set are combined to give *virtual* (unoccupied) orbitals.

Early basis sets were composed of *Slater-type orbitals* (STOs), due to their resemblance to the atom orbitals (AOs) of the hydrogen atom. These are functions of the form

$$\phi_i^{STO}(\zeta, n, a, b, c, x, y, z) = N r^{n-1} e^{-\zeta r} x^a y^b z^c \quad (2.20)$$

where  $N$  is a normalisation constant,  $\zeta$  is a constant related to the effective nuclear charge of the nucleus,  $r$  is the distance of the electron from the atomic nucleus,  $n$  is a natural number that plays the role of the principle quantum number, and  $x$ ,  $y$ , and  $z$  are cartesian coordinates. The angular component  $x^a y^b z^c$  describes the shape of the function, such that if  $a+b+c=0$   $\phi_i^{STO}$  is of *s*-type; if  $a+b+c = 1$ ,  $\phi_i^{GTO}$  is of *p*-type, and so forth. Although STOs approximate the long and short range behaviour of atomic orbitals correctly, performing integration with these functions is computationally very demanding, due primarily to the complexity of the integrals involved describing in electron-electron interactions.

$$\phi_i^{GTO}(\alpha, a, b, c, x, y, z) = Ne^{-\alpha r^2} x^a y^b z^c \quad (2.21)$$

where  $N$  is a normalisation constant,  $\alpha$  is the orbital exponent coefficient,  $x$ ,  $y$ , and  $z$  are cartesian coordinates,  $r$  is the radius ( $r^2 = x^2 + y^2 + z^2$ ), and the angular portion is described the same as in an STO. It takes a linear combination of several GTOs to represent the same function as an STO. These linear combinations of GTOS are known as *contracted GTOs* (CGTO) with  $n$  GTOs combined as

$$\phi_i^{CTGO}(\alpha, a, b, c, x, y, z) = N \sum_{i=1}^n c_i e^{-\alpha r^2} x^a y^b z^c \quad (2.22)$$

where  $c_i$  is referred to as the contraction coefficient which describes the weighting of each GTO. Although it requires more GTOs than STOs to accurately describe the atomic orbitals, the integrals can be computed 4–5 times faster, and thus calculations involving GTOs are much more efficient.<sup>53</sup>

### Basis set nomenclature

Standard basis sets are composed of basis functions which represent atomic orbitals and that each basis function is a CGTO composed of several GTOs. A *minimal basis set* is one in which each AO is represented by a single basis function. To more accurately represent AOs, more basis functions should be used, although basis set size needs to be balanced with computational cost. Larger basis sets are referred to by their cardinal number, the number of basis functions which represent each AO. When two basis functions are used to represent each AO, this is called a *double-zeta* basis set. If three basis functions represent each AO, this is called a *triple-zeta* basis set. Generalised, a basis set is  $N$ -zeta in size when  $N$  basis functions are used per AO.

A *split-valence* basis set is one in which a single basis function is used to represent each core AO, while more basis functions are used to represent the valence AOs. Constructing basis sets in this way can help reduce the computational cost while still accurately representing the electrons which are most important to chemistry.

Additional basis functions are often added to basis sets in order to correctly describe molecular properties. *Polarisation functions* are basis functions which are one or more angular momentum channels greater than the natural electronic configuration of an atom. For example, a single *p*-type

## 2.1. The quantum mechanical approach

---

basis function can be added to the minimal basis of a hydrogen atom. Polarisation functions are essential to accurately describe chemical bonding, as the presence of other atoms distorts the spherical symmetry of a single atom's AOs.<sup>54</sup> *Diffuse functions* are basis functions which extend further into space, typically by the inclusion of a very shallow Gaussian function (small  $\zeta$  exponent). Diffuse functions are necessary to accurately describe anions, very electronegative atoms, and large systems in which NCIs are important.

### Commonly used basis sets

A large number of basis sets currently exist in the literature.<sup>55</sup> While not all basis sets are created equally, we shall briefly describe four of the most commonly used basis sets used in quantum chemistry. (I have only included the first citation for the basis sets. Maybe include more.)

#### Pople-style basis sets

Perhaps the most utilised basis sets in chemistry are those arising from the group of Pople.<sup>56</sup> These basis sets were defined by fitting to HF wave functions. The earliest of these basis sets are the minimal STO-NG basis sets, where  $N$  describes the number of GTOs that go into each contraction.

The practise of using minimal basis sets has diminished significantly as technology has advanced, thus these basis sets are largely considered out of date. It is more common to utilise the split-valence basis sets, denoted as  $n - ijG$  or  $n - ijkG$  for double and triple zeta split-valence basis sets, respectively. In this system of notation,  $n$  represents the number of GTOs that comprise the core AOs, and  $i, j, k$  describe the number of GTOs for contractions in the valence AOs. Polarisation functions are denoted either with asterisks or with the specific shell and number of functions which are being added. Diffuse functions are denoted with either a single or double “+”, indicating diffuse  $s$  and  $p$ -type functions for non-hydrogen atoms, and the addition of diffuse  $s$ -type functions for hydrogen, respectively. For example, the  $6-31+G(d,p) \equiv 6-31+G^{**}$  double-zeta basis set is one which has: 6 GTOs per core AO, 3 GTOs for the first valence set of AOs, and 1 GTO for the second, along with  $s$  and  $p$  diffuse functions of the heavy atoms, a single  $d$  polarisation function of heavy atoms, and a single  $p$  polarisation function of hydrogen atoms.

#### Correlation consistent basis sets

Post-Hartree-Fock methods (*vide infra*) are commonly used in quantum

## 2.1. The quantum mechanical approach

---

chemistry. In 1989, Dunning<sup>57</sup> identified that the use of basis sets optimised for HF were inappropriate for post-HF methods. The basis sets that came from Dunning and co-workers, which are referred to as “correlation consistent” basis sets are commonly used in, but not limited to, state of the art wave function calculations. These basis sets are said to be correlation consistent as they treat electron correlation (*vide infra*) in a manner which systematically approached the complete basis set limit. Correlation consistent basis sets are denoted as “cc-pVNZ”, where  $N=D,T,Q,5,6,\dots$  is the cardinal number of the basis set. These are large sets containing polarisation functions by default and can be additionally augmented with diffuse functions, denoted by “aug.” A commonly used basis set is aug-cc-pVTZ, which is a triple-zeta basis set with implicit polarisation functions and specified diffuse functions on all atoms.

### Polarisation consistent basis sets

The polarisation consistent basis sets have been developed by Jensen and coworkers.<sup>58</sup> The polarisation consistent basis sets have been developed to systematically complete basis set limit in density-functional theory calculations through the use of higher order polarisation functions. The notation adopted is “pc- $X$ ”, where  $X$  is the cardinal number of the basis set minus one (i.e.  $X = N-1$ ). Polarisation functions are included by default in these basis sets, and additional diffuse functions can be specified with the same “aug” notation as the correlation consistent basis sets.

### Ahlrich basis sets

The last basis sets we will mention are those developed by Ahlrich and coworkers.<sup>59,60</sup> These are the “Def2” basis sets, named as such because they are the second generation of default basis set in the Turbomole quantum chemistry package.<sup>61</sup> Additionally, these basis sets have been developed so that consistent errors are obtained for nearly every element on the periodic table: a unique trait among modern basis sets. The nomenclature for these basis sets is fairly straightforward where either SV is used for split valence, or NZ is used for cardinal number. Addition of polarisation and diffuse functions is specified with a P and D, respectively. For example, Def2-SVP is the basis set of split-valence double-zeta quality with polarisation functions; Def2-TZVP is the triple-zeta basis set with polarisation functions; Def2-QZVPD is the quadruple-zeta basis set with polarisation and diffuse functions.

### 2.1.6 Post-Hartree-Fock methods

The HF method gives an approximation to the ground state wave function of a molecule for a reasonable computational cost (scaling with  $N^4$  number of basis function). There is however, a lack of the complete description of *dynamical electron correlation*,<sup>62</sup> and thus significant deviations from experimental results can be observed. Dynamical electron correlation is a measure of how much one electron's movement is affected by the presence of other electrons. As described previously, the HF method includes correlation through the average electron field potential term, however this field is in general, not static, thus correlation must be treated directly in order to obtain accurate results. The majority of methods take the HF wave function  $\Psi_0$  as the starting point. Normally, the total energy is obtained by inclusion of an energy term for correlation  $E_{corr}$ , which can be defined as

$$E_{corr} = \Xi_{exact} - E_0 \quad (2.23)$$

$E_{corr}$  is the difference between the full non-relativistic energy from the Schrödinger equation,  $\Xi_{exact}$ , and a reference ground state energy  $E_0$ , usually the HF energy.

We shall briefly describe two important methods for accounting for electron correlation and obtaining  $E_{corr}$ : Møller-Plesset perturbation theory, and the related configuration interaction and coupled cluster theories.

#### Møller-Plesset perturbation theory

Møller-Plesset (MP) perturbation theory is a special case of Rayleigh-Schödinger perturbation theory in which the Hamiltonian for a system can be approximated by

$$\hat{H} = \hat{H}_0 + \lambda \hat{V} \quad (2.24)$$

where  $\hat{H}_0$  is an unperturbed Hamiltonian,  $\hat{V}$  is a small perturbation, and  $\lambda$  is an arbitrary parameter which controls the size of the perturbation. The perturbed wave function and energy are expressed as a power series in  $\lambda$ :

$$\Psi = \lim_{m \rightarrow \infty} \sum_{i=0}^m \lambda^i \Psi^{(i)} \quad (2.25)$$

$$E = \lim_{m \rightarrow \infty} \sum_{i=0}^m \lambda^i E^{(i)} \quad (2.26)$$

## 2.1. The quantum mechanical approach

---

The MP method applies perturbations to HF by defining a *shifted* Fock operator  $\hat{H}_0$  and *correlation potential*  $\hat{V}$  as

$$\hat{H}_0 = \hat{F} + \langle \phi_0 | (\hat{H} - \hat{F}) | \phi_0 \rangle \quad (2.27)$$

$$\hat{V} = \hat{H} - \hat{H}_0 \quad (2.28)$$

where  $\phi_0$  is the ground state Slater determinant of the Fock operator.

Within this formulation, the zeroth-order energy is the expectation of  $\hat{H}$ , which gives the HF energy. The first-order energy is

$$E_{MP1} = \langle \phi_0 | \hat{V} | \phi_0 \rangle = 0 \quad (2.29)$$

by Brillouin's Theorem of singly excited determinants. Thus, the first useful correction occurs at the second order of perturbation, which is known as MP2. Additional orders of perturbation are referred to as MP3, MP4, etc. The MP2 method has been popular in quantum chemistry because it scales with  $N^5$  number of basis functions and is a significant improvement on the treatment of electron correlation compared to HF. One may expect higher order of perturbation theory to more accurately describe a system. Practically however, the expansions used in MPN theory do not converge smoothly to a limit with higher order of perturbation.<sup>63</sup> As a result, for molecular properties calculated with MP3 or higher are not guaranteed to give more accurate results than MP2.

## Configuration interaction and coupled cluster theory

The solutions to the HF method give a single determinant wave function which only describes the ground state electronic configuration. Configuration interaction (CI) is a post-HF method which describes a linear combination of Slater determinants to more accurately represent a system's wave function. The additional Slater determinants represent excited electronic configurations and can be singly excited (S), doubly excited (D), and so forth. This is represented as follows:

$$|\Psi\rangle = (1 + \sum_{j=1}^N C_j) |\phi_0\rangle \quad (2.30)$$

where  $C_j$  are operators which describes the  $j$ -th excitations of electrons. If all possible excitations are included in the CI equation, this is referred to as

## 2.1. The quantum mechanical approach

---

*full CI* (FCI). Extending FCI to an infinite basis set gives the exact solution to the Schrödinger equation.

Coupled cluster (CC) theory<sup>64</sup> is a similar approach to CI, but uses the so-called *exponential ansatz*

$$|\Psi\rangle = e^{\hat{T}} |\phi_0\rangle \quad (2.31)$$

where  $\hat{T}$  is the cluster operator, defined by  $n$ -electron excitation operators  $\hat{T}_n$ :

$$\hat{T} = \hat{T}_1 + \hat{T}_2 + \hat{T}_3 + \dots \quad (2.32)$$

Within the exponential ansatz,  $e^{\hat{T}}$  is usually truncated and expanded in a Taylor series. For example, truncation at the  $\hat{T}_2$  excitation operator gives

$$\begin{aligned} |\Psi\rangle &= e^{\hat{T}_1 + \hat{T}_2} |\phi_0\rangle \\ &= (1 + \hat{T}_1 + \hat{T}_2 + \frac{1}{2!} \hat{T}_1^2 + \hat{T}_1 \hat{T}_2 + \frac{1}{2!} \hat{T}_2^2 + \dots) |\phi_0\rangle \end{aligned} \quad (2.33)$$

Considering both CI and CC with single and double excitation (CISD and CCSD), the wave functions will include similar excitations, however inclusion of cross terms ( $\hat{T}_1 \hat{T}_2$ ) in CCSD implicitly includes higher excitation levels. Additionally, the use of the exponential operator makes the CC formulation *size consistent*, which is the largest short coming of the CI method. Size consistency refers to the additivity of energies for an ensemble of molecules. That is, for a pair of molecules A and B, their energies must follow the relation

$$E_{AB}(r \rightarrow \infty) = E_A + E_B \quad (2.34)$$

Size consistency is a necessary requirement of a theoretical treatment to treat systems of molecules accurately. It is for this reason that CC has superseded CI as the dominant highly correlated method in quantum chemistry.

The inclusion of higher order excitations becomes decreasingly important with degree of excitation; however, the inclusion of triples is often found to be necessary for the accurate description of electron correlation (i.e. CCSDT). The computation of triples is prohibitively expensive in all but the simplest of systems, thus approximations based on perturbation theory are often used in substitution. The most commonly used perturbative triples method is CCSD(T), where the parenthesis indicate the use of perturbative arguments.

## 2.1. The quantum mechanical approach

---

Note also that traditionally, the use of CCSD(T) implies excitation of only the valence electrons, unless otherwise stated.

CCSD(T) is commonly referred to as the *gold standard* in quantum chemistry and is often used to obtain benchmark quality results for thermochemistry and NCIs.<sup>65</sup> However, CCSD(T) scales with  $N^7$  number of basis functions, and is thus significantly more computationally expensive than HF or MP2, restricting its application to small systems of molecules. Quadratic configuration interaction (QCI) is closely related to CC, except that it uses quadratic operators in place of exponential ones. QCISD(T) and CCSD(T) gives very similar results.<sup>66</sup>

### 2.1.7 The complete basis set limit

#### Complete basis set extrapolation

In accordance with the variational principle, the energy obtained by a particular method will always be greater than or equal to the exact energy. The exact energy can only be achieved with an infinite basis set, a value known as the *complete basis set* (CBS) limit.<sup>67</sup> Since this is computationally infeasible, specific tricks have been developed to approximate the CBS limit. Specifically, molecular properties calculated using the HF and post-HF methods have been shown to asymptotically approach the CBS limit in a smooth manner when appropriate basis sets are used. Therefore, to obtain results estimating a molecular property at the CBS limit ( $Y(\infty)$ ), properties can be fit to three-parameter<sup>68,69</sup> or two-parameter functions:<sup>70,71</sup>

$$Y(x) = Y(\infty) + Ae^{-x/B} \quad (2.35)$$

$$Y(x) = Y(\infty) + A/x^3 \quad (2.36)$$

where the molecular property as a function of basis set cardinal number  $Y(x)$  is fit using parameters  $A$  and  $B$ . Typically calculations of this nature are performed using the correlation consistent basis sets (cc-pVNZ), however there is evidence that the polarisation consistent basis sets (pc-X) more rapidly approach the CBS limit for some molecular properties.<sup>72</sup> The true *gold standard* in quantum chemistry is referred to as CCSD(T)/CBS, which typically means CCSD(T) with complete basis set extrapolation with aug-cc-pVNZ basis sets, where  $N=D, T, Q$ , or 5. Although extrapolation is useful for approximating highly accurate results, there is an inherent amount of uncertainty associated with the final fitted results, which may be unclear from the nomenclature.

### Explicit correlation methods

A new technique which is gaining popularity among post-HF methods is the inclusion of so called *explicit correlation*.<sup>73,74</sup> The introduction of additional functions dependent on inter-electronic distance coordinates allows for explicit correlation of electrons.<sup>75</sup> As a result, the dynamical correlation of electrons is treated more accurately with reduced basis sets, therefore accurate results can be achieved at a reduced computational cost. Basis set extrapolation can also be performed on explicitly correlated results: this is quickly become the standard approach.<sup>76</sup>

#### 2.1.8 Composite quantum chemistry methods

In order to calculate thermochemical and kinetic properties that are within a sub-kcal mol<sup>-1</sup> range of experiment, multistep *ab initio* procedures which are referred to as *composite methods* have been developed.<sup>77</sup> These procedures work by including important energy terms which contribute to molecular properties. Generally, composite methods make use of a combination of low correlation methods with large basis sets and high correlation methods with small basis sets, as is illustrated in Figure 2.1. Some of the relevant energy terms include: core-valence, relativistic, spin-orbital, Born-Oppenheimer, and zero-point vibrational energy corrections. There exist many composite methods, each of which makes use of a variety of quantum mechanical (QM) methods and different basis set extrapolation techniques in order to best approximate energy terms which are relevant, with the ultimate goal of achieving the exact energy of a system. In our work, we have made use of several composite methods including: the G4 and G4(MP2) methods,<sup>78,79</sup> CBS-QB3 and CBS-APNO methods,<sup>80–82</sup> and the W1BD method.<sup>83</sup> A description of these methods will be provided in Chapter 4.

#### 2.1.9 Density-functional theory

Density-functional theory (DFT) is the most popular quantum chemical method applied to date. It relies on the two Hohenberg-Kohn theorems, the first of which states that there exists a unique electron density  $\rho$  that defines the properties of a many-electron system. The second theorem defines an energy functional of the electron density and demonstrates that the correct ground state electron density minimises the energy functional through the variational theorem.<sup>84,85</sup> These theorems alone do not provide the solutions to the Schrödinger equation.

## 2.1. The quantum mechanical approach

---

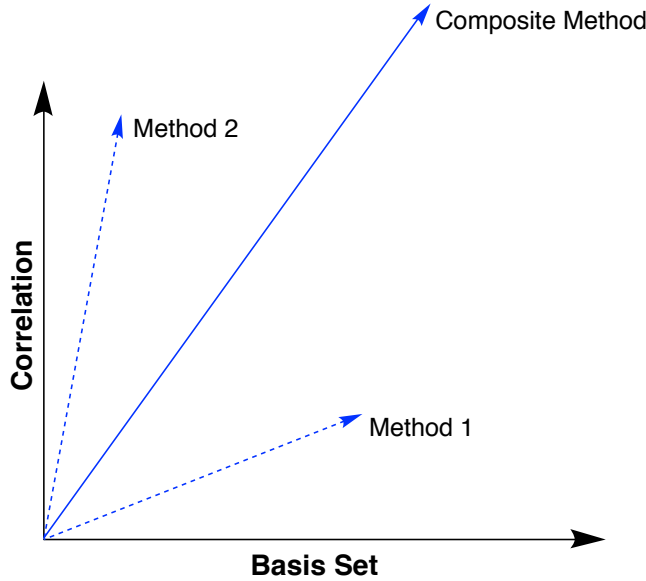


Figure 2.1: Schematic representation of a quantum mechanical composite method. The exact energy can only be achieved at the limits of an infinite basis set and complete correlation. Using a combination of Method 1 (low correlation/large basis set) and Method 2 (high correlation/small basis set), the Composite method approaches the exact energy.

It wasn't until the formulation of Kohn-Sham DFT<sup>86</sup> that the theory began gaining ground as a useful quantum theory. Kohn-Sham DFT scales formally with  $N^3$  number of electrons<sup>62</sup> which is better than HF by a factor of  $N$ . In addition, DFT is a complete theory like FCI; however, there is no straightforward way to determine the correct functionals of the electron density as the exact form of the functionals is unknown. Nonetheless, the drive for the development of the correct density-functional has been one of the main endeavours in quantum chemistry in the last two decades.

The framework behind conventional DFT is built into the description of the full energy functional  $E$ :

$$E[\rho] = T_{ni}[\rho] + V_{ne}[\rho] + V_{ee}[\rho] + \Delta T[\rho] + \Delta V_{ee}[\rho] \quad (2.37)$$

where  $T_{ni}$  is the kinetic energy of non-interacting electrons,  $V_{ne}$  is the potential of nuclear-electron interactions, and  $V_{ee}$  is the classical electron-electron repulsion. The last two terms are collectively referred to as the exchange-correlation (XC) functionals, where  $\Delta T$  is the dynamical correlation term,

## 2.1. The quantum mechanical approach

---

and  $\Delta V_{ee}$  is the non-classical correction to electron-electron repulsion. All the functionals, except the XC functionals have an exact form. It is therefore the XC functionals in which there is currently empiricism.

The ultimate goal in describing XC functionals is to find the “correct” XF functional which gives the exact energy of a system from the electron density. At this point, this must be done using approximations, for which there are several degrees of complexity. These approaches follow a hierarchical scheme, commonly referred to as the “Jacob’s ladder” of DFT.<sup>87</sup> The first rung represents the simplest approximation which is known as local-density approximations (LDAs), which approximate the exchange-correlation density at a given point by the electron density at that same point. The form of these functionals is:

$$E_{XC}^{LDA} = \int \rho(\mathbf{r}) \varepsilon_{XC}(\rho(\mathbf{r})) d\mathbf{r} \quad (2.38)$$

where  $\varepsilon_{XC}(\rho(\mathbf{r}))$  is the exchange-correlation energy per particle (energy density) of a uniform electron gas of density  $\rho(\mathbf{r})$ . This approximation is overly simple and applies only when the electron density is constant at all points, and are thus not generally applied in chemical problems. Nonetheless, LDA based approaches are commonly employed in solid state physics.

The second rung on the ladder corresponds to generalised-gradient approximation (GGA) based functionals, which are still amongst some of the most popular density-functionals. GGAs depend on both the electron density and the gradient of the electron density at a point:

$$E_{XC}^{GGA} = \int \rho(\mathbf{r}) \varepsilon_{XC}^{GGA}(\rho(\mathbf{r}), \nabla \rho(\mathbf{r})) d\mathbf{r} \quad (2.39)$$

where,  $\varepsilon(\rho(\mathbf{r}), \nabla \rho(\mathbf{r})) d\mathbf{r}$  is the energy density associated with a given GGA. GGA functionals provide a substantial improvement over LDAs, and most are constructed so that they correct the LDA energy:

$$\varepsilon_{XC}^{GGA}(\rho(\mathbf{r}), \nabla \rho(\mathbf{r})) = \varepsilon_{XC}^{LDA}(\rho(\mathbf{r})) d\mathbf{r} + \Delta \varepsilon_{XC} \left( \frac{\nabla \rho(\mathbf{r})}{\rho^{4/3}(\mathbf{r})} \right) \quad (2.40)$$

A step above GGAs on the third rung of the ladder are meta-GGAs, which depend on the electron density, as well as the first derivative of electron density at a point, and the kinetic-energy density,  $\tau(\mathbf{r})$ , defined as:

$$\tau(\mathbf{r}) = \sum_i^{\text{occupied}} \frac{1}{2} |\nabla \chi_i(\mathbf{r})|^2 \quad (2.41)$$

## 2.1. The quantum mechanical approach

---

where  $\chi_i(\mathbf{r})$  are the self-consistently determined Kohn-Sham orbitals. Meta-GGAs improve upon the accuracy of GGAs at a comparable cost.<sup>62</sup>

The XC functionals described up to this point (LDAs, GGAs, meta-GGAs) depend only on the electron density and derivatives of the electron density. The fourth and fifth rungs of the ladder improve upon the prior functionals by inclusion of terms dependent on additional properties. While this approach improves upon the accuracy of these functionals, it comes with an increase in computational cost. On the fourth rung sit functionals which depend to some percentage on the HF exact exchange. When the ratio of HF exchange is fixed, these functionals are termed hybrid functionals. Alternatively, functionals are said to be range-separated corrected if a different amount of exact-exchange to describe long and short-range behaviours. In the cases of hybrid and range-separated functionals, the added computational cost comes from the calculation of the HF exact exchange.

Alternatively, one can describe the fourth rung functionals as the depending upon the properties of the occupied molecular orbitals. The fifth rung then, is said to depend on the properties of unoccupied molecular orbitals. These functionals are typically referred to as double-hybrids, and incorporated correlation energy from a post-HF method, typically MP2.<sup>88</sup> Double-hybrid DFT methods are once again more accurate than the lower rung methods, however, calculating the MP2 correlation energy is considerably more computationally demanding than traditional DFT approaches. Therefore, double-hybrid DFT methods have not gained popularity in the literature.

There are many published XC functionals. Fortunately, there is a fairly standard system of nomenclature, such that density functionals are described as *exchange functional-correlation functional*. The most commonly used density functional is the B3-LYP, which uses the 3-parameter hybrid exchange functional of Becke,<sup>89</sup> and the correlation functional of Lee, Yang, and Parr.<sup>90</sup> There are also standalone functionals which have built in exchange and correlation functionals. A common example of these are the Minnesota family of functionals from the Truhlar group.<sup>91,92</sup>

Aside from the problem of choosing density-functionals, solving DFT is computationally very similar to the HF method. Within Kohn-Sham (KS) DFT, we define a fictitious system of non-interacting electrons with the same electron density as the real system. This is achieved by the use of a Hamiltonian in which there is an effective local potential,  $V_s(\mathbf{r})$ :

## 2.1. The quantum mechanical approach

---

$$\hat{H}_s = -\frac{1}{2} \sum_i^N \nabla_i^2 | \sum_i^N V_S(\mathbf{r}_i) \quad (2.42)$$

The ground state wave function of this non-interacting Hamiltonian is represented by a single Slater determinant with spin orbitals ( $\chi$ ), completely analogous to the HF problem. These spin orbitals, referred to as *Kohn-Sham orbitals* are determined by

$$\hat{h}_i^{KS} \chi_i = \varepsilon_i \chi_i \quad (2.43)$$

where the one-electron Kohn-Sham operator  $\hat{h}^{KS}$  is defined as

$$\hat{h}_i^{KS} = -\frac{1}{2} \nabla^2 + V_s(\mathbf{r}) \quad (2.44)$$

It is crucial to realise that this procedure does not give us the exact energy of a system, but rather is used to determine an electron density which represents our real system. The connection between this fictitious system comes from the choice of the effective potential such that the density of our real system is a result of summing over the squared moduli of the KS orbitals:

$$\rho(\mathbf{r}) = \sum_i |\chi_i|^2 \quad (2.45)$$

Once again in analogy to HF theory, one applies the variational principle to minimise the total energy functional in Equation 2.37 with respect to  $\chi$ . The effective potential which variationally minimises the energy is given by<sup>93</sup>

$$\begin{aligned} V_s(\mathbf{r}) &= \frac{\delta J[\rho]}{\rho(\mathbf{r})} + \frac{\delta E_{XC}[\rho]}{\delta \rho(\mathbf{r})} + \sum_A^M \frac{Z_A}{r_{iA}} \\ &= \int \frac{\rho(\mathbf{r}_2)}{r_{12}} + V_{XC} + \sum_A^M \frac{Z_A}{r_{iA}} \end{aligned} \quad (2.46)$$

where the first term describes the Coulombic potential between two electrons, the last term is the potential between the electron and each nucleus. The middle term is once again the unknown XC potential. The electron density obtained from the fictitious system of non-interacting particles is finally used in Equation 2.37 to find the total energy of the system. Since

## 2.1. The quantum mechanical approach

---

$V_s(\mathbf{r})$  depends on the electron density, these equation must be solved iteratively, as with HF theory. Note however, that if the exact form of  $E_{XC}[\rho]$  was known, this method would give the exact ground state electron density of the system, and thus the exact energy.

### Challenges for density-functional theory methods

Pure DFT has low computational cost and potentially good accuracy, hence its popularity as a quantum chemical treatment. However, there are several problems which common DFT methods experience that lead to erroneous results in many cases.<sup>94</sup> It is well established that traditional DFT methods completely fail at describing non-covalent interactions.<sup>95</sup> This shortcoming leads to poor descriptions of chemistry beyond equilibrium geometries, including transition states. Fortunately, there are several methods which can correct for this problem, commonly through the addition of an energy correction term  $E_{disp}$  to the DFT energy  $E_{DFT}$ , as

$$E_{tot} = E_{DFT} + E_{disp} \quad (2.47)$$

It is common to employ the empirical D3 pair-wise correction of Grimme,<sup>96</sup> paired with the Becke-Johnson damping functions,<sup>97</sup> denoted as D3(BJ). This correction works by calculating the dispersion interactions between all pairs of atoms  $A$  and  $B$  separated by distance  $R_{AB}$ , with the following equation:

$$E_{disp} = \sum_{A>B} \frac{C_6^{AB}}{R_{AB}^6} f_6(R_{AB}) + s_8 \frac{C_8^{AB}}{R_{AB}^8} f_8(R_{AB}) \quad (2.48)$$

where  $C_6$  and  $C_8$  are dispersion coefficients,  $s_8$  is an empirically determined scaling parameter, and  $f_n$  are the damping functions which limit the range of dispersion correction, avoiding near singularities at small  $R_{AB}$ . Another approach to correcting for dispersion is to add parameters directly to the functional, as is the case in the Minnesota functionals.<sup>91,91</sup> Both of these empirical corrections have the benefit of adding negligible computational time, but must be parametrised for each DFT method with which they are employed.

Another striking issue with DFT is the unphysical ability of an electron to interact with itself, termed *self-interaction error*. This is most obvious in what is known as *delocalisation error*, which is a result of many-electrons interacting with themselves, or many-electron self-interaction error. In HF theory, self-interaction error is exactly cancelled, thus DFT methods which

have a high portion of HF exchange in their formulation are able to account for this issue. Consider for a moment a one electron system: there should be exactly zero electron correlation. In terms of the energy functionals shown in Equation 2.37, the electronic repulsion term  $V_{ee}[\rho]$  should cancel exactly with the XC term ( $V_{ee}[\rho] = -E_{XC}[\rho]$ ).<sup>62</sup> Unfortunately, all pure DFT methods fail to reproduce this expected behaviour. An obvious manifestation of delocalisation error is the incorrect treatment of charge-transfer in intramolecular interactions,<sup>98,99</sup> as well as in transition state complexes. Even for the simplest HAT reaction  $\text{H}_2 + \text{H}^\bullet \longrightarrow \text{H}^\bullet + \text{H}_2$ , the calculated barrier height is underestimated by 8–9 kcal mol<sup>-1</sup> using a GGA functional.<sup>100</sup> Charge-transfer occurs when a fraction of an electron is transferred between molecular entities. Specifically, charge-transfer is mistreated at longer ranges, thus either high percentage exact exchange hybrid functionals, or range-separated functionals are suggested for systems in which charge-transfer may occur.

As is the case for most experimental methods, identifying the correct theoretical methods requires the careful consideration of the problem at hand. Choosing a DFT based method requires calibration, however, once a method has been tested and is known to provide reasonably accurate results, DFT methods have the ability to help understand chemical problem with relatively low computational costs.

## 2.2 Applying theory to chemical problems

### 2.2.1 Geometry optimisation

All QM methods depend parametrically on the geometry of a molecular system. That is the electronic energy of a system depends on the positions of the nuclei. While the wave functions can describe any arbitrary geometry, we are typically only interested in certain geometries of a molecule. These geometries of interest are normally stationary states along a the potential energy surface (PES) of a system, that is, points where the gradient of energy with respect to nuclear coordinates is zero. Therefore, we perform *geometry optimisation* calculations to determine these points.

Molecular systems have complex PESs. For a non-linear molecule, the nuclear PES has  $3N-6$  dimensions, where  $N$  is the number of nuclei present.<sup>101</sup> In geometry optimisation, we seek the local minima (reactants, products, or intermediates) and local maxima (TS complexes). Consider only local minima for a moment. Often complex molecules have more than one possible conformation, and each conformation represents a different local minimum

## 2.2. Applying theory to chemical problems

---

along the PES. It is therefore important to ensure the correct conformation, typically the lowest energy structure (global minimum), is used when approaching chemical problems.

In order to efficiently perform geometry optimisation, numerical analysis techniques are employed. All geometry optimisation methods follow the same general framework.<sup>102</sup> First, energy and necessary derivatives are computed from an initial geometry. Second, the geometry is modified to step towards the nearest stationary state. And last, some test is performed to determine if the new geometry is near enough to the stationary state along the PES. The most efficient method to do this is the *Newton method*, in which the energy is expanded in a Taylor series (truncated at the second order point) about the current point,  $\mathbf{x}_0$ :

$$E(\mathbf{x}) = E_0 + \mathbf{g}_0 \Delta \mathbf{x} + \frac{1}{2} \Delta \mathbf{x} \mathbf{H}_0 \Delta \mathbf{x} \quad (2.49)$$

where  $E_0$ ,  $\mathbf{g}_0$ , and  $\mathbf{H}_0$  are the energy, gradient (Jacobian), and second derivative (Hessian) at point  $\mathbf{x}_0$ , and  $\Delta \mathbf{x} = \mathbf{x}_i - \mathbf{x}_0$ . The aim of the Newton method is to minimise the gradient of the Taylor expansion,  $\mathbf{g}(\mathbf{x})$ , such that

$$\mathbf{g}(\mathbf{x}) = \mathbf{g}_0 + \mathbf{H}_0 \Delta \mathbf{x} \quad (2.50)$$

Solving for  $\Delta \mathbf{x}$  gives the so-called Newton step that leads to minimisation:

$$\Delta \mathbf{x} = -\mathbf{H}_0^{-1} \mathbf{g}_0 \quad (2.51)$$

The analytic computation of the Hessian is very expensive, especially for large systems. Therefore, to simplify the problem at the beginning of geometry optimisation, the Hessian matrix is approximated and updated at each step in the optimisation, using clever algorithms.<sup>102</sup> This is called the *quasi-Newton method*, and is the default optimisation routine in the Gaussian<sup>103</sup> quantum chemistry package, as well as many other quantum chemistry packages.

Some additional caution must be taken in optimising molecular structures. Normal algorithms which optimise structures stop when the gradient of energy is sufficiently close to zero; however, often PES can be flat or very shallow in regions and structures that are not fully optimised can be obtained. To avoid this, geometries are always subject to molecular vibration analysis.

### 2.2.2 Molecular vibrations

The computation of molecular vibrations can be performed simply given a set of molecular coordinates.<sup>104</sup> Assuming a non-linear molecule, we start with  $3N-6$  internal coordinates which are non-coupled (orthogonal). We then apply the *harmonic approximation*, in which we assume each normal mode follows Hooke's Law

$$F = kx \quad (2.52)$$

where  $F$  is the force,  $k$  is the force constant, and  $x$  is the displacement along one normal mode's coordinates. This approximation assumes the PES along the normal mode is parabolic, which in general is not true, but is a good approximation near the minima. Deviations from this approximation are known as *anharmonicity*. In practise, however, at normal temperatures ( $\sim 298\text{K}$ ) the harmonic approximation is sufficient to describe molecular vibrations as displacements are assumed to be small.

Typically to obtain molecular frequencies, one computes the mass-weighted Hessian matrix elements  $F_{ij}$

$$F_{ij} = \frac{1}{\sqrt{m_i m_j}} \mathbf{H}_{ij} \quad (2.53)$$

where the partial derivatives of internal coordinates  $x_i$  of the potential energy  $U$  are taken for  $3N$  atoms with mass  $m$ . One then seeks to diagonalise this  $3N \times 3N$  matrix to obtain eigenvalues  $\lambda_i$ , which describe the force constant of each normal mode. The harmonic frequencies  $\nu_i$  are then obtained by

$$\nu_i = \frac{\sqrt{\lambda_i}}{2\pi} \quad (2.54)$$

and the lowest 6 modes are then discarded to account for  $3N-6$  normal modes. These lowest energy modes generally correspond the internal rotations, and thus must be discarded to correctly obtain thermochemical corrections.

From these frequencies, the *zero-point vibrational energy* (ZPE,  $E_{ZPE}$ ) is calculated:

$$E_{ZPE} = \sum_{i=1}^{3N-6} \frac{h\nu_i}{2} \quad (2.55)$$

## 2.2. Applying theory to chemical problems

---

The ZPE is an important quantum correction to the classical potential, giving the electronic potential energy

$$U = E_{elec} + E_{ZPE} \quad (2.56)$$

where  $E_{elec}$  is the QM electronic energy.

If a normal mode describes a non-minimum along the PES, the energy gradient will be negative (imaginary) instead of positive. Only energy maxima or saddle-points (TS structures) should have a single imaginary mode. Therefore, if a non-TS molecular structure calculation yields one or more imaginary modes, the geometry optimisation has yielded a structure which is not at minimum on the PES. In this situation additional steps must be taken to find a corrected structure.

### 2.2.3 Thermochemistry

Up until this point we have been viewing molecules from a microscopic perspective; however, this is not useful for describing properties of bulk systems. Fortunately, fundamental statistical thermodynamics can be used to approximately describe a system in bulk.<sup>105,106</sup> We approximate our system as an ensemble of non-interacting particles: the ideal gas. Within statistical thermodynamics, the fundamental starting point is the partition function  $Q$ ,<sup>107</sup> from which all thermodynamic properties can be calculated. For our ensemble, the molecular partition function is

$$Q = \sum_j e^{\varepsilon_j / k_B T} \quad (2.57)$$

where a Boltzmann distribution of  $j$  energy states  $\varepsilon$  is taken at temperature  $T$ , and  $k_B$  is the Boltzmann constant. All calculations herein are defined under conditions of temperature  $T = 298.15$  K and pressure  $P = 1$  atm.

Normally, the molecular partition function is decomposed into contributions from translational, vibrational, rotational, and electronic motion:

$$Q = q_{trans} q_{vib} q_{rot} q_{elec} \quad (2.58)$$

The equation describing the translational partition function  $q_{trans}$  is

$$q_{trans} = \left( \frac{2\pi m k_B T}{h^2} \right)^{3/2} \frac{k_B T}{P} \quad (2.59)$$

where  $m$  is the mass of the molecule,  $h$  is Planck's constants.

## 2.2. Applying theory to chemical problems

---

The vibrational partition function  $q_{vib}$  depends on the contributions of each of  $K$  vibrational modes. Only the  $3N-6$  (or  $3N-5$  for linear molecules) real vibrational modes of a molecule are considered, and imaginary frequencies are ignored. Therefore, for molecules which posses an imaginary frequency this thermodynamic analysis is invalid. TS complexes do posses a single imaginary frequency which is ignored, as it is assumed to not contribute to the overall vibrational partition function as no formal bond is said to be formed in the acceptor-donor system. Each vibrational mode has a characteristic vibrational electronic temperature,  $\Theta_{\nu,K} = h\nu/k_B$ , and the partition function is

$$q_{vib} = \prod_K \frac{e^{-\Theta_{\nu,K}/2T}}{1 - e^{-\Theta_{\nu,K}/T}} \quad (2.60)$$

The rotational partition function depends on the geometry of a system. For a single molecule  $q_{rot}=1$ . For a linear molecule, the rotational partition function is

$$q_{rot} = \frac{1}{\sigma_r} \left( \frac{T}{\Theta_r} \right) \quad (2.61)$$

where  $\sigma_r$  is the symmetry number for rotation which depends on the molecular symmetry, and  $\Theta_r = h^2/8\pi^2Ik_B$ .  $I$  is the moment of inertia. Finally, for a non-linear polyatomic molecule, the rotational partition function is

$$q_{rot} = \frac{\sqrt{\pi}}{\sigma_r} \left( \frac{T^{3/2}}{\sqrt{\Theta_{r,x}\Theta_{r,y}\Theta_{r,z}}} \right) \quad (2.62)$$

where  $\Theta_{r,x}$ ,  $\Theta_{r,y}$ , and  $\Theta_{r,z}$  describe contributions of the moment of inertia in each of the x, y, and z-planes.

Finally, we make an important assumption that electronic contributions are assumed to exist in only the ground state, as excited states are generally safely assumed to be much larger than  $k_BT$  in energy. The full electronic partition function is

$$q_{elec} = \sum_{i=0} \omega_i e^{-\epsilon_i/k_BT} \quad (2.63)$$

where  $\omega$  is the degeneracy of an energy level with energy  $\epsilon$ . Applying our assumption, and by setting the ground state energy  $\epsilon_0 = 0$ , our problem simplifies dramatically, such that  $q_{elec} = \omega_0$ , which is simply the spin multiplicity of the molecule.

## 2.2. Applying theory to chemical problems

---

We now have all the information needed to calculate the thermodynamic quantities we are interested in. In chemistry we are concerned with the Gibbs free energy  $G$ , which is defined by the entropy  $S$  and enthalpy  $H$  as

$$G = H - TS \quad (2.64)$$

From each of the partition functions, the entropy of a system with  $N$  moles,  $S_{tot} = S_{trans} + S_{vib} + S_{rot} + S_{elec}$ , is calculated using the relation

$$S = Nk_B + Nk_B \ln \left( \frac{Q}{N} \right) + Nk_B T \left( \frac{\partial \ln Q}{\partial T} \right)_V \quad (2.65)$$

Similarly, the internal energy of a system,  $E_{int,tot} = E_{int,trans} + E_{int,vib} + E_{int,rot} + E_{int,elec}$ , is given by the relation

$$E_{int} = Nk_B T^2 \left( \frac{\partial \ln Q}{\partial T} \right)_V \quad (2.66)$$

Finally, the enthalpy is obtained from

$$H_{tot} = E_{int,tot} + k_B T \quad (2.67)$$

Using very simple statistical thermodynamic arguments, the properties of a bulk system are easily computed. It is important to emphasise that these results are for particles in the gas phase, thus additional steps must be taken if one desires to compare results to experiments performed in solvent.

### 2.2.4 Modelling solvent

It is in principle possible to include solvent molecules explicitly in QM calculations: this is in practise, extremely cost prohibitive. In order to approximate the important contributions of solvation, so-called *implicit continuum solvent models* are generally employed.<sup>62,108</sup> Mathematically, one describes this as

$$\hat{H}^{tot}(\mathbf{r}_m) = \hat{H}^{mol}(\mathbf{r}_m) + \hat{V}^{mol+sol}(\mathbf{r}_m) \quad (2.68)$$

where a perturbation  $\hat{V}^{mol+sol}$  dependent only on the coordinates of the solute ( $\mathbf{r}_m$ ; thus implicit) is applied to the Hamiltonian of the solute. The perturbation term is composed of interaction operators which contribute to the net free energy:

$$G_{solv} = G_{cavity} + G_{electrostatic} + G_{dispersion} + G_{repulsion} + G_{solv\ kinetic} \quad (2.69)$$

## 2.2. Applying theory to chemical problems

---

where the total solvation free energy  $G_{solv}$  contains terms from: the formation of a solvation cavity  $G_{cavity}$ , the electrostatic interactions between solvent and solute  $G_{electrostatic}$ , the dispersion interactions between solvent and solute  $G_{dispersion}$ , the QM exchange repulsion between solvent and solute  $G_{repulsion}$ , and the movement of solvent molecules  $G_{solv\ kinetic}$ .

A widely used model for solvation comes from the Truhlar group, and is known as SMD.<sup>109</sup> The main parameter in implicit solvent models is the solvent dielectric constant ( $\epsilon$ ) with contributions from surface tension and the solvent-solute interface. SMD also includes terms which depend on the electron density of the solute. While many other implicit solvent models require the use of the same QM method as they were parametrised,<sup>110</sup> SMD is a *universal* model which was parametrised using several QM methods. Therefore, it does not require the use of a specific QM method and can be applied broadly in both single point energy and geometry optimisation calculations.

### 2.2.5 Rate constants and transition state theory

In the discussion of chemical kinetics, the rate ( $r$ ) of a bimolecular reaction



is determined by the *rate law*, which can generally be described as

$$r = \frac{dC}{dt} = \frac{dD}{dt} = k[A]^a[B]^b \quad (2.71)$$

where  $k$  is the rate constant,  $t$  is time,  $A, B, C$ , and  $D$  are chemical species with stoichiometric coefficients  $a, b, c$ , and  $d$ , and  $k$  is the rate constant. Computational chemistry is in general, not useful for determining rate laws: this must be done experimentally. Where computational studies can be useful, is in determining reaction mechanisms, and how the reaction barrier height can be altered. In doing so, we focus entirely on  $k$ .

Most chemists are intimately familiar with the phenomenological *Arrhenius equation*

$$k_{Arr} = Ae^{-E_a/RT} \quad (2.72)$$

where  $A$  is a constant,  $R$  is the gas constant, and  $E_a$  is the *activation energy*, which is an experimental measure of the reaction barrier height. This equation dates back to the 1880s, when Arrhenius noticed that the

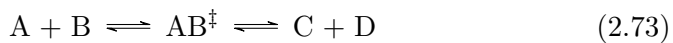
## 2.2. Applying theory to chemical problems

---

reactions depended more heavily on temperature than was intuitive, and thus introduced the  $A$  constant, known often as the Arrhenius pre-factor.<sup>111</sup> The Arrhenius pre-factor is an empirical measure of how factors other than kinetic energy affect the rate constant. From the perspective of theory, Equation 2.72 has little meaning as the parameters are empirical. Thus, to study rate constants theoretically we must turn to *transition state theory*.

### Transition state theory

The study of transition state theory (TST) originates in the 1930s, and was developed primarily by Eyring.<sup>111,112</sup> In TST we focus on the TS complex, which is defined as a transient species which exists at the top of the energy barrier of a reaction. If we consider the same reaction in Equation 2.70, and set all the coefficients to 1, then TST states the reaction proceeds in two steps, the first of which includes a quasi-equilibrium between the reactants and TS complex



with an equilibrium constant ( $K_c^\ddagger$ ) expression

$$K_c^\ddagger = \frac{[AB^\ddagger]/c^0}{[A]/c^0[B]/c^0} \quad (2.74)$$

where  $c^0$  is the standard-state concentration (normally taken to be 1 M).

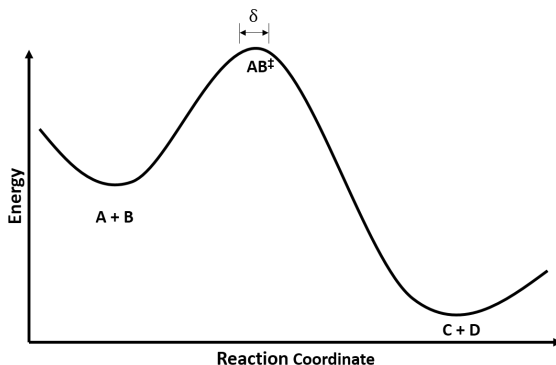


Figure 2.2: A reaction coordinate diagram for the reaction of Equation 2.73. The TS complex is defined to exist in the small region  $\delta$  above the reaction barrier.

## 2.2. Applying theory to chemical problems

---

In TST, we define the TS complex to exist throughout a small region of width  $\delta$  above the reaction barrier (Figure 2.2). From the second step of the reaction in Equation 2.73, we can define a reaction rate dependent on the concentration  $[AB^\ddagger]$  and  $v_c$ , a factor which defines the frequency with which the complexes proceed over the barrier:

$$r = v_c[AB^\ddagger] \quad (2.75)$$

From Equations 2.70 and 2.73, we now have two equivalent expressions for the reaction rate, which allows us to derive the following

$$r = k[A][B] = v_c[AB^\ddagger] \quad (2.76)$$

and solving Equation 2.74 for  $[AB^\ddagger]$  results in

$$r = v_c \frac{[A][B]K_c^\ddagger}{c^0} \quad (2.77)$$

or

$$k = \frac{v_c K_c^\ddagger}{c^0} \quad (2.78)$$

We must now invoke the statistical thermodynamics to make sense of Equation 2.78. We can rewrite the equilibrium expression  $K_c^\ddagger$  in terms of partition functions of each molecular species:

$$K_c^\ddagger = \frac{[AB^\ddagger]/c^0}{[A]/c^0[B]/c^0} = \frac{(q^\ddagger/V)c^0}{(q_A/V)(q_b/V)} \quad (2.79)$$

where  $V$  is the volume, and  $q_A$ ,  $q_B$ , and  $q^\ddagger$  are the partition functions of A, B, and  $AB^\ddagger$ , respectively.

Since we have defined the reaction to be occurring with one degree of freedom, the translational partition function  $q_{trans}$  can be defined as

$$q_{trans} = \frac{\sqrt{2\pi m^\ddagger k_B T}}{h} \delta \quad (2.80)$$

where  $m^\ddagger$  is the mass of the TS complex. The partition function of the TS complex can be written as the product  $q^\ddagger = q_{trans}q_{int}^\ddagger$ , where the second term accounts for all remaining degrees of freedom of the TS complex. We can use this and rewrite Equations 2.79 and 2.78 as

$$K_c^\ddagger = \frac{\sqrt{2\pi m^\ddagger k_B T}}{h} \delta \frac{(q_{int}^\ddagger/V)c^0}{(q_A/V)(q_b/V)} \quad (2.81)$$

## 2.2. Applying theory to chemical problems

---

and

$$k = v_c \frac{\sqrt{2\pi m^\ddagger k_B T}}{hc^0} \delta \frac{(q_{int}^\ddagger/V)c^0}{(q_A/V)(q_b/V)} \quad (2.82)$$

We are now left with the two terms  $v_c$  and  $\delta$  which are ill-defined. However, the product of these two terms is the average speed at which the TS complex crosses the barrier,  $\langle u_{TS} \rangle = v_c \delta$ . A Maxwell-Boltzmann distribution is used to calculate the value of  $\langle u_{TS} \rangle$ :

$$\langle u_{TS} \rangle = \left( \frac{m^\ddagger}{2\pi k_B T} \right)^{1/2} \int_0^\infty ue^{-m^\ddagger u^2/2k_B T} du = \left( \frac{m^\ddagger}{2\pi k_B T m^\ddagger} \right)^{1/2} \quad (2.83)$$

Substituting Equation 2.83 into Equation 2.82 for  $v_c \delta$  yields

$$k = \frac{\sqrt{k_B T}}{hc^0} \frac{(q_{int}^\ddagger/V)c^0}{(q_A/V)(q_b/V)} = \frac{k_B T}{hc^0} K_c^\ddagger \quad (2.84)$$

Now, define the standard Gibbs free energy of activation ( $\Delta^\ddagger G^0$ ) to be the change in Gibbs free energy in going from reactants to TS. The thermodynamical expression is

$$\Delta^\ddagger G^0 = -RT \ln K_c^\ddagger \quad (2.85)$$

which can be substituted into Equation 2.84

$$k = \frac{k_B T}{hc^0} e^{-\Delta^\ddagger G^0 / RT} \quad (2.86)$$

The standard Gibbs free energy of activation can be expressed in terms of enthalpy and entropy as

$$\Delta^\ddagger G^0 = \Delta^\ddagger H^0 - T\Delta^\ddagger S^0 \quad (2.87)$$

which, upon substitution gives the equation

$$k = \frac{k_B T}{hc^0} e^{-\Delta^\ddagger S^0 / R} e^{-\Delta^\ddagger H^0 / RT} \quad (2.88)$$

At this point, we can draw a direct comparison to the Arrhenius equation (Equation 2.72) by expressing  $E_a$  in terms of  $\Delta^\ddagger H^0$  and  $A$  in terms of  $\Delta^\ddagger S^0$ . We must differentiate the natural logarithm of Equation 2.84, as well as Equation 2.72 (assuming that  $A$  is independent of temperature):

$$\frac{d \ln k}{dT} = \frac{1}{T} + \frac{d \ln K_c^\ddagger}{dT} \quad (2.89)$$

$$\frac{d \ln k_{Arr}}{dT} = \frac{E_a}{RT^2} \quad (2.90)$$

Next, we use the fact that  $d \ln K_c / dT = \Delta U^0 / RT^2$  for an ideal gas, then Equation 2.89 becomes

$$\frac{d \ln k}{dT} = \frac{1}{T} + \frac{\Delta^\ddagger U^0}{RT^2} \quad (2.91)$$

Additionally,  $\Delta^\ddagger H^0 = \Delta^\ddagger U^0 + RT\Delta^\ddagger n$  ( $\Delta^\ddagger n = 1$ ), as so Equation 2.91 can be rewritten as

$$\frac{d \ln k}{dT} = \frac{\Delta^\ddagger H^0 + 2RT}{RT^2} \quad (2.92)$$

Therefore, by comparison of Equation 2.92 and 2.90, we get

$$E_a = \Delta^\ddagger H^0 + 2RT \quad (2.93)$$

which then converts Equation 2.88 into the form

$$k = \frac{e^2 k_B T}{hc^0} e^{\Delta^\ddagger S^0 / R} e^{-E_a / RT} \quad (2.94)$$

Therefore, a statistical thermodynamical picture of the Arrhenius equation arises from TST, and the Arrhenius pre-factor  $A$  can be expressed as

$$A = \frac{e^2 k_B T}{hc^0} e^{\Delta^\ddagger S^0 / R} \quad (2.95)$$

In practise, we use the form of Equation 2.86 to compute the rate constant of a reaction, which we shall denote as  $k_{TST}$ . The conventional TST makes an assumption that the reaction coordinate is static along the lowest energy pathway. This can be corrected by the use of *variational transition state theory*.<sup>113</sup> We shall not consider variational TST in this work, as with careful application, conventional TST does a remarkably good job at accounting for the magnitude and temperature dependence of a wide range of reactions.<sup>112</sup> Additionally, if one makes corrections for *QM tunnelling*, conventional TST can easily give a more complete description of the rate constant.

### Quantum mechanical tunnelling

Atoms are quantum mechanical particles, and are thus subject to the strange probabilistic behaviours observed at the microscopic level. QM tunnelling refers to the ability of particles to penetrate the reaction barrier, rather than surmounting it classically (Figure 2.3). While all reactions are subject to QM tunnelling, we will show that due to the low mass of the hydrogen atom, QM tunnelling can play a significant role in HAT reactions.

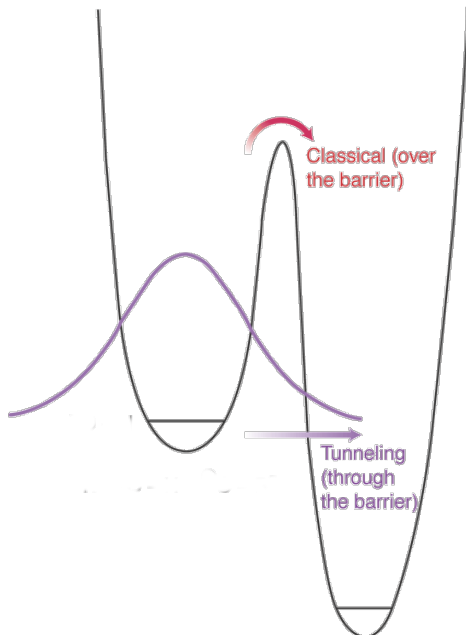


Figure 2.3: Quantum mechanical tunnelling occurs when a particle penetrates a reaction barrier, rather than surmounting it. Figure adapted from Reference 114.

In order to determine the effects of scattering, one must find transmission coefficients ( $\kappa$ ) by solving the Schrödinger equation.<sup>48</sup> This is done by approximating the reaction barrier with an analytical potential, thus simplifying the problem mathematically. The earliest model potentials were introduced by Bell, who used a parabolic function to approximate the reaction barrier.<sup>115</sup> To obtain  $\kappa$ , and thus the observed rate constant ( $k_{obs}$ ), the following equations were used:

$$k_{obs} = \kappa A e^{-E_a/RT} \quad (2.96)$$

## 2.2. Applying theory to chemical problems

---

$$\kappa = \frac{e^\alpha}{\beta - \alpha} (\beta e^{-\alpha} - \alpha e^{-\beta}) \quad (2.97)$$

$$\alpha = E_a/RT \quad (2.98)$$

$$\beta = \frac{2a\pi^2(2mE_a)^{1/2}}{h} \quad (2.99)$$

where the Arrhenius equation was used to estimate the rate constant,  $m$  is the mass of the tunnelling particle, and  $2a$  is the width of the barrier. Since the equation is dependent on the mass of the particle, tunnelling occurs more often when lighter particles are involved. As a consequence, tunnelling is more common in HAT reactions than other atom transfer reactions. Also, the height and width of the barrier are important factors in determining the contributions to tunnelling: reactions with small barriers have low tunnelling contributions; narrow barriers result in higher tunnelling contributions.

The Bell model is a poor representation of an actual reaction barrier. One which is a much better approximation is the *Eckart potential*.<sup>116</sup> The form of this potential is

$$V = -\frac{Ay}{1-y} - \frac{By}{1-y^2} \quad (2.100)$$

$$y = -e^{2\pi x/L} \quad (2.101)$$

where  $x$  is the variable along the reaction coordinate and  $L$  is called the characteristic length. If  $A = 0$  the potential becomes a symmetric function, further simplifying the problem; however, most reactions do not have a symmetric potential.  $A$ ,  $B$  and  $L$  are related to the change in barrier height in the forward and reverse direction,  $\Delta V_1$  and  $\Delta V_2$ , respectively:

$$A = \Delta V_1 - \Delta V_2 \quad (2.102)$$

$$B = ((\Delta V_1)^{1/2} + (\Delta V_2)^{1/2})^2 \quad (2.103)$$

$$\frac{L}{2\pi} = (-\frac{2}{F^*})^{1/2} [\frac{1}{(\Delta V_1)^{1/2}} + \frac{1}{(\Delta V_2)^{1/2}}]^{-1} \quad (2.104)$$

where  $F^* = d^2V/dx^2$  evaluated at the maximum of the potential. In this formulation,  $V$  is a placeholder energy. Note that if a reaction is endoergic, tunnelling does not occur. Alternatively, one says tunnelling only occurs in exoergic or energy-neutral reactions.

The solutions to the Schrödinger equation for the Eckart potential are analytical, thus that transmission coefficient  $\kappa$  can easily be computed using

## 2.2. Applying theory to chemical problems

---

standard numerical techniques. These tunnelling corrections will be applied, where applicable as

$$k_{calc} = \kappa k_{TST} = \kappa \frac{k_B T}{hc^0} e^{-\Delta^\ddagger G^0} \quad (2.105)$$

# Chapter 3

## The Relationship Between Arrhenius Pre-factors with Non-Covalent Binding

### 3.1 Introduction

DiLabio and Ingold<sup>39</sup> previously investigated the formal HAT reaction of the iminoxyl/oxime self-exchange reaction. In this paper, they compiled a table of parameters from the phenomenological Arrhenius equation for a series of interesting reactions, which appear here in Table 3.1.<sup>37,117–123</sup> These are thermoneutral self-exchange reactions of oxygen-centred  $\pi$ -radicals,<sup>i</sup> and other nearly thermoneutral reactions involving the destruction and formation of oxygen-centred  $\pi$ -radicals, reactions 3.1 and 3.2, respectively:

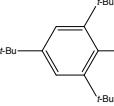
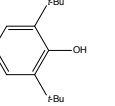
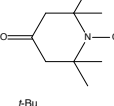
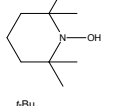
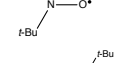
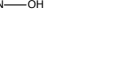
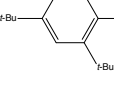
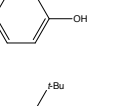
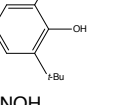
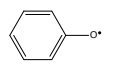
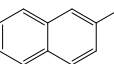
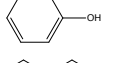
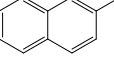
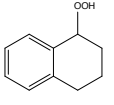


Although it is well known that reactions of this nature involve remarkably low activation energies ( $E_a$ ),<sup>124–127</sup> they also have unusually low Arrhenius pre-exponential factors ( $A$ ), or as we shall refer to them, *A-factors*. As a result, these reactions are generally slower than expected, evidence for which is summarised in Table 3.1: The measured A-factors are small, and range from  $\times 10^{3.5}$ – $\times 10^{8.3}$  M<sup>-1</sup>s<sup>-1</sup>. In this past, this has been attributed to steric shielding around the oxygen atoms, resulting in a large entropic barrier.<sup>39</sup> Importantly, it was noted that the degree of steric shielding on

<sup>i</sup>A  $\pi$ -radical is one in which the SOMO is orthogonal to the plane of the molecular framework, i.e. of  $\pi$ -symmetry. Note that free alkoxyl radicals cannot be distinguished as either  $\sigma$  or  $\pi$ -radicals, as the SOMO is degenerate, or free to rotate with respect to the rest of the molecular framework. Therefore, only the geometry of the radical-molecule complex can resolve the symmetry of the SOMO.

### 3.1. Introduction

Table 3.1: Table of results for (nearly) thermoneutral reactions studied. Unit for  $\Delta H$ ,  $E_a$ , and calculated binding energy (BE) are kcal mol<sup>-1</sup>, and  $\log A$  and  $k$  are M<sup>-1</sup>s<sup>-1</sup>. Adapted with permission from Reference 39. Copyright (2005) American Chemical Society.

ID	$\text{RO}^\bullet/\text{R}'\text{O}^\bullet$	$\text{ROH}$	$\Delta H$	$\log A$	$E_a$	$k$	BE
1 <sup>37</sup>			0.0	3.7	1.2	$3.3 \times 10^2$	-10.8
2 <sup>117</sup>			-2.0	3.8	3.8	10	-14.8
3 <sup>37</sup>			0.0	5.1	3.5	$3.3 \times 10^2$	-10.1
4 <sup>118,119</sup>			4.2	5.5	4.8	93	-10.0
5 <sup>120</sup>	$t\text{-BuOO}^\bullet$		-7.0	4.2	0.5	$7 \times 10^3$	-6.8
6 <sup>37</sup>	$\text{Ph}_2\text{NO}^\bullet$	$\text{Ph}_2\text{NOH}$	0.0	>7	-	$>10^7$	-14.8
7 <sup>121</sup>			-2.2	8.3	2.3	$4 \times 10^6$	-8.6
8 <sup>122</sup>	$t\text{-BuOO}^\bullet$		0.3	7.2	5.2	$3 \times 10^3$	-5.5
9 <sup>122</sup>	$t\text{-BuOO}^\bullet$		-1.9	6.4	2.6	$3 \times 10^4$	-5.6
10 <sup>123</sup>	$t\text{-BuOO}^\bullet$		1.4	6.0	4.5	$7 \times 10^2$	-8.0

the oxygen atom appears to play an important role in the order of the A-factor; systems with greater bulk have lower A-factors, while non-shielded systems have larger A-factors.

Steric-electronic effects are known to play an important role in HAT, and have been studied extensively.<sup>35,128–134</sup> Although the abstraction of a specific bond may be more thermodynamically favourable than others on a given substrate, if it is not accessible due to steric constraints, abstraction will not occur at this site. Otherwise, additional steric bulk can

### 3.2. Computational methods and details

---

lead to significant reductions in reactivity, through destabilisation of the TS complex. For example, in reactions of tertiary acetamides with CumO<sup>•</sup>,<sup>134</sup> where abstraction occurs mainly from C-H bonds  $\alpha$  to the nitrogen atom, a two-fold decrease in the normalised rate constant is observed in going from *N,N*-dimethylacetamide to *N,N*-diisobutylacetamide ( $k_H = 2.0 \times 10^5$  and  $7.8 \times 10^4 \text{ M}^{-1}\text{s}^{-1}$ , respectively).

Upon first inspection, all of the reactions in Table 3.1 appear to be of a similar nature. Each reaction involves the formation and destruction of O-H bonds as the thermodynamic driving force. All of these bonds expected to be of comparable strength, therefore, differences should not contribute significantly to reaction barriers in a Bell-Evans-Polanyi principle fashion. Hence, the large degree of variance in their rate constants ( $k$ ) is somewhat surprising. For the closely related self-exchange reaction between phenol and phenoxyl,<sup>22</sup> a strong molecule-radical pre-reaction complex is formed, ca. 10 kcal mol<sup>-1</sup> below the separated reactants. It is therefore expected that most, if not all, of the systems in Table 3.1 should exhibit a similar molecule-radical complex, granted, the strength of the interaction will vary because of steric repulsion.

Currently, there is no literature which describes the relationship between the pre-reaction complex and the kinetics of a reaction. Using the reactions and data in Table 3.1, we ask the question: *Do A-factors have a correlation with non-covalent binding energies of the pre-reaction complex?* This is a reasonable question as non-covalent binding and steric hinderance represent a loss of degrees of freedom and therefore entropy,<sup>ii</sup> which ultimately determines the A-factor magnitude. If the answer to the question is yes, then non-covalent binding may be useful as a diagnostic for the “looseness” or “tightness” of a TS complex, in addition to providing an important link between theory and experiment.

## 3.2 Computational methods and details

Density-functional theory (DFT) calculations were carried out using the Gaussian-09 software package.<sup>103</sup> Care was taken to obtain minimum energy structures through detailed conformational analysis. For this, I utilised the BLYP density-functional<sup>90,135</sup> paired with the empirical D3 dispersion correction<sup>96</sup> with the recommended Becke-Johnson damping functions,<sup>97</sup> as well as our groups’ own *basis set incompleteness potentials* (BSIPs),\* (update

---

<sup>ii</sup>Recall from Equation 2.95 that the A-factor can be related to TST such that the primary variable is entropy ( $\Delta^\ddagger S^0$ ).

### 3.2. Computational methods and details

---

citation) and minimal MINIs basis sets.<sup>136</sup> The use of minimal basis sets corrected for basis set incompleteness allows DFT-based methods (as opposed to semi-empirical or force-field based approaches) to be used efficiently in performing a large number of calculations. Minimum energy conformers of the monomers (substrates and radicals) were first obtained by manual manipulation of the necessary dihedral bond angles, followed by geometry optimisation and vibrational analysis.

The lowest energy radicals and substrates were combined to generate the appropriate pre-reaction complexes. These pre-reaction complexes were subject to conformational analysis using the same BLYP-D3(BJ)-BSIP/MINIs method. Geometries were initially manipulated by hand. It became apparent that manual manipulation resulted in an unsatisfactory exploration of the conformational space. To solve this, all the necessary dihedral angles were scanned systematically using a combination of scripts.<sup>137</sup> All manipulated geometries were subject to optimisation. For each complex, the top 5–10 complex geometries were subject to further optimisation using a higher level of theory (BLYP-D3(BJ)/pc-1) to obtain the final minimum energy pre-reaction complex structures. Due to the free rotation of *t*-butyl and methyl groups, some of the optimised pre-reaction complex structures contain small imaginary frequencies, and thus do not represent proper stationary states. Several measures were taken to resolve this, however, no resolution was obtained. Regardless, the complexes adequately represent the pre-reaction complex and differences in “true” binding energies should be negligible.

To obtain accurate pre-reaction complex binding energies, the substrates and complexes were subject to single-point energy calculations using the LC- $\omega$ PBE long-range corrected density functional<sup>138,139</sup> with D3(BJ) dispersion corrections and pc-2 basis sets with truncated *f*-type functions (pc-2-spd).<sup>140</sup> This method was selected on the recommendation of work by Johnson et al.<sup>140</sup>, which demonstrated the accuracy of this method for the calculation of NCIs. On the basis of the reported mean absolute error in Reference 140 for the S66 benchmark set of sixty-six different non-covalently interacting dimers,<sup>141</sup> the calculated binding energies reported herein from the LC- $\omega$ PBE-D3(BJ)/pc-2-spd level of theory carry an estimated 0.2 kcal mol<sup>-1</sup> margin of error.

### 3.3. Results and discussion

The theoretically determined electronic binding energies calculated for the lowest energy pre-reaction complex of each system are listed in Table 3.1. The logarithm of A-factor against binding energy was plotted, as shown in Figure 3.1. The overall correlation is quite poor ( $R^2=0.33$ ), however, the majority of the data is grouped about a single, well correlated line ( $R^2=0.95$ ). Interestingly, the intercept of the fitted line which corresponds to zero binding energy is 8.63, a result which is in line with the observed A-factor in “normal” HAT reactions, *viz.*  $10^{8.5\pm0.5} \text{ M}^{-1}\text{s}^{-1}$ .<sup>142</sup> This suggests that the observed correlation is valid, that is, NCIs may have an impact on A-factors. I shall demonstrate that the data which do not correlate are reasonable outliers. In fact, using simple rational I shall demonstrate that different regimes of sterics result in different processes leading to the TS complex. As a result, deviations from the relationship between A-factor and binding energy are observed.

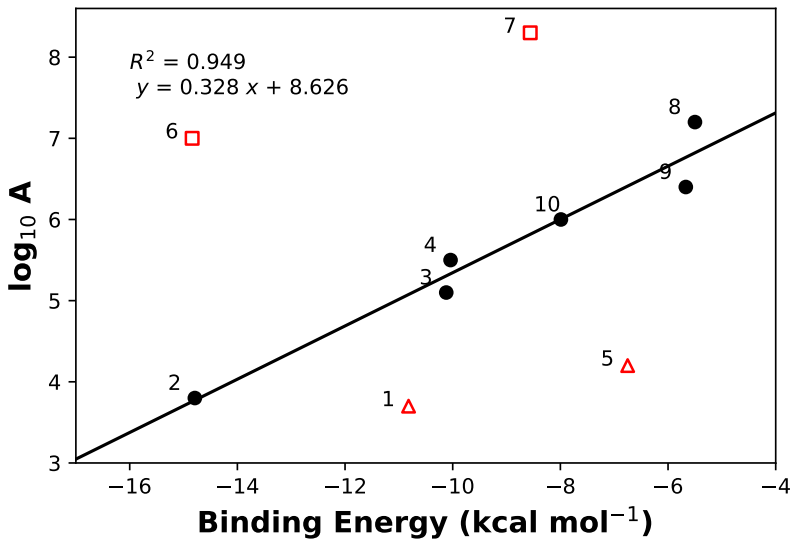


Figure 3.1: Plot of logarithm of A-factor against binding energy. Black points only were included in the line fitting (slope = 0.328 kcal mol<sup>-1</sup>, intercept = 8.626 kcal mol<sup>-1</sup>, and  $R^2 = 0.949$ ). Red points with open faced markers indicate outliers, *vide infra*. The inclusion of complexes 1, 5, and 7 result in an  $R^2=0.334$ . Complex 6 is always omitted as the experimental A-factor is approximate.

### 3.3. Results and discussion

---

In order to illustrate this, consider the fundamental properties of the HAT reaction involved here; the two important concerted reaction mechanisms which can occur, direct HAT and PCET. Specifically, we must consider the geometric constraints in which these reactions occur. For direct HAT to occur, the SOMO of the radical must overlap with the O-H  $\sigma^*$  anti-bonding orbital. Often this requires the rotation of the hydroxyl group out of the plane, the barrier to which can be as much as 3.1 kcal mol<sup>-1</sup> on the basis of the rotational barrier in phenol.<sup>143</sup> In PCET, there are two possibilities: the SOMO of the radical must be able to overlap with the corresponding oxygen *p*-orbital, as seen in the work of Mayer et al.<sup>22</sup>; or a lone pair- $\pi$  or  $\pi$ - $\pi$  overlap must occur, as seen in the work of DiLabio and Johnson<sup>25</sup>. Due to time constraints, I did not seek to obtain TS complex structures. Nonetheless, from the pre-reaction complex one can surmise as to the TS complex. Thus, by applying these basic principles, it is possible to rationalise the trend observed in Figure 3.1.

We shall begin by examining the points which fall on the expected line, complexes 2–4 and 8–10, all of which require small conformational changes to proceed through HAT reactions. Complexes 2 and 3 are shown in Figure 3.2, and are very similar in structure, both are hydroxylamine-nitroxyl couples with similar degrees of steric bulk adjacent to the reacting centres. Both the *t*-butyl and methyl groups prevent the alignment of the NO-H-ON frameworks in a PCET manner. Additionally both pre-reaction complexes must undergo the rotation of the hydroxyl group for direct HAT. In the most stable stacked conformation, complex 4 cannot undergo PCET as the steric clash of the para-position *t*-butyl groups prevent  $\pi$ - $\pi$  overlap. In order to react *via* HAT, the hydroxyl group must rotate out of the plane. Alternatively, an open conformation for complex 4 is possible, which lies ca. 2 kcal mol<sup>-1</sup> higher in energy than the stacked complex, a result which is also consistent with the observed trendline. From the open conformation, PCET is still not possible due to the steric bulk of the ortho-position *t*-butyl groups of the radical, thus this reaction likely proceeds through direct HAT.

Complexes 8 and 9 are similar systems, in which *t*-BuOO<sup>•</sup> reacts with unhindered phenolic substrates. As seen by the structures in Figure 3.4, the bound complexes are somewhat dissimilar. The hydroxyl group of complex 8 is rotated out of the plane 24°, while this is not true for complex 9. It is likely that the larger aromatic system of 2-naphthol results in a larger OH rotational barrier, and thus the most favourable conformation is entirely in the plane. Complex 8 was previously studied by DiLabio and Johnson<sup>25</sup>, where it was demonstrated that a partial bonding interaction exists between the peroxy lone-pair and phenolic  $\pi$ -system, giving a PCET

### 3.3. Results and discussion

---

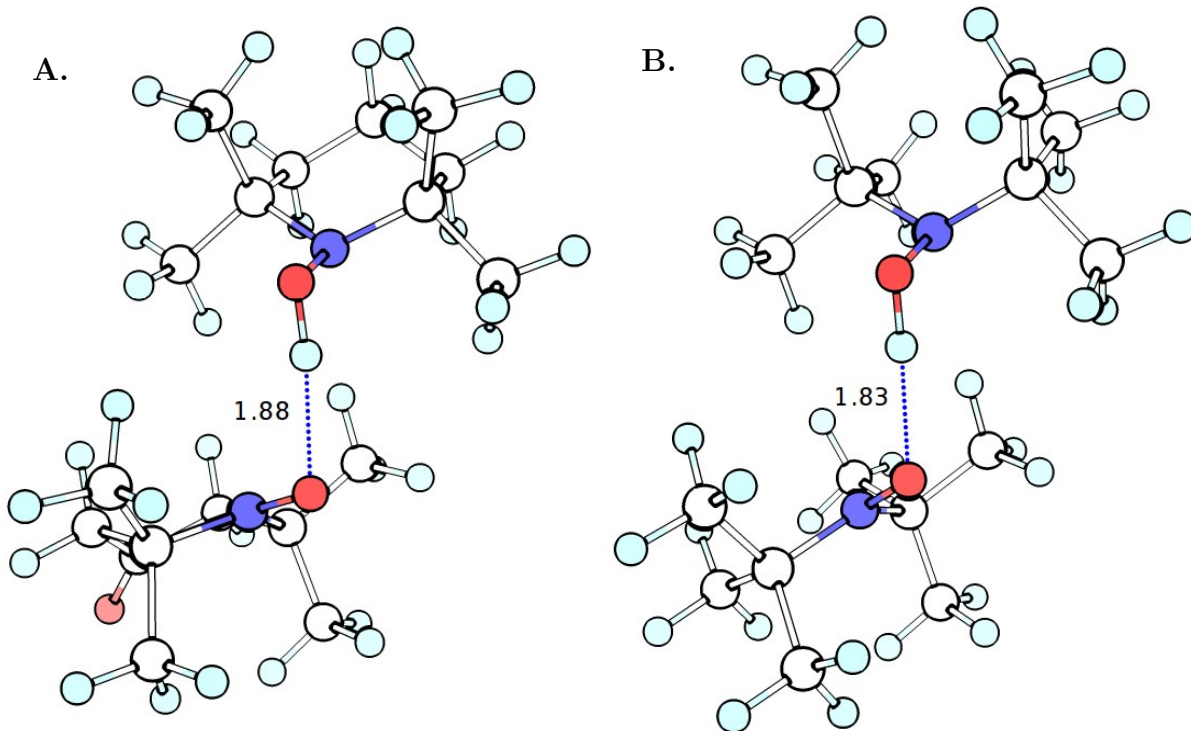


Figure 3.2: Three-dimensional structures of **A** complex 2, and **B** complex 3. Hydrogen bond distances are shown in units of Å. The elements are coloured as white for carbon, light blue for hydrogen, red for oxygen, and blue for nitrogen.

mechanism. Although the pre-reaction complexes are somewhat dissimilar, the conformational changes necessary to reach the PCET TS complex, similar to that reported in reference 25, are likely not dramatically different in terms of energetic barriers. Any small differences that are observed result in noise in the observed trend.

Complex 10 is unique in that it is the only reaction between a peroxide and a peroxy radical. The self-exchange reaction between  $\text{HOO}^\bullet$  and  $\text{HOOH}$  can be considered the simplest reference for the reaction of  $\alpha$ -tetralin peroxide with *t*-butylperoxy. To the best of my knowledge, the mechanism of the hydroperoxyhydrogen peroxide couple has not been characterised previously in the literature, although the TS structure has been previously reported.<sup>144</sup> Using this structure, calculations reveal a lone pair-lone pair interaction leading to partial bonding in the TS, i.e. a PCET mechanism.

### 3.3. Results and discussion

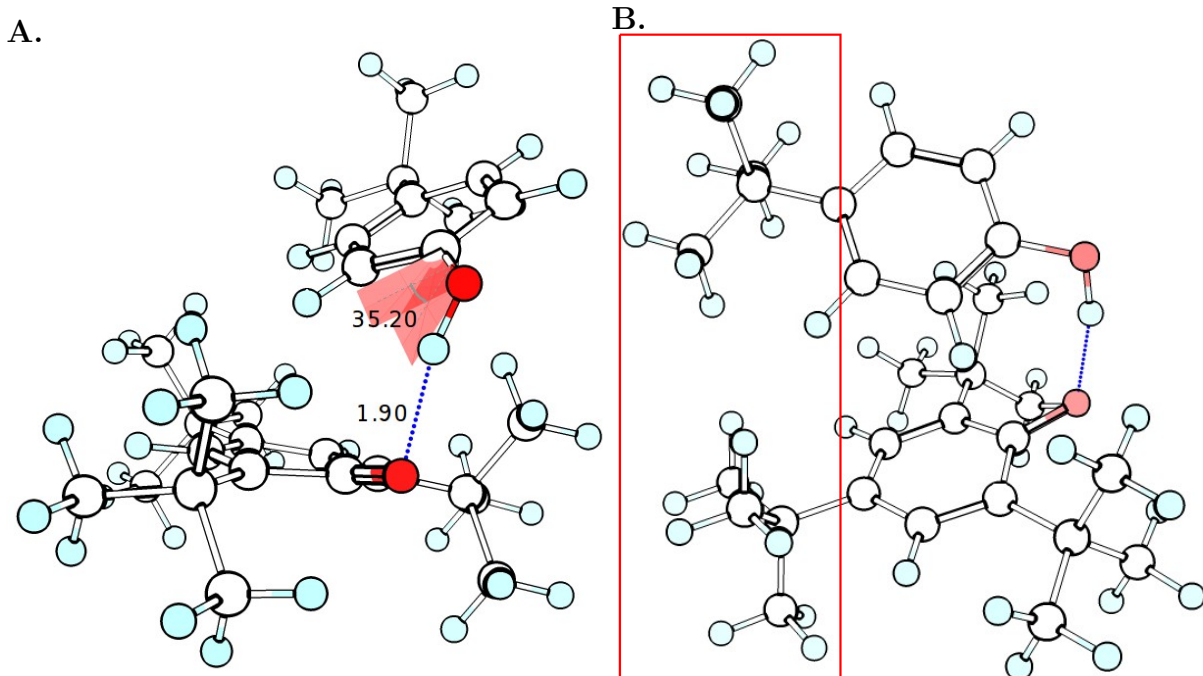


Figure 3.3: Three-dimensional structure of pre-reaction complex 4 between 2,4,6-tri-*t*-butylphenol and 4-*t*-butylphenoxy. **A** demonstrates the hydrogen bond distances in units of Å, and the out-of-plane rotation by 35.2° of the phenolic hydroxyl group. **B** demonstrates the steric clash (highlighted by red box) between the para-position *t*-butyl groups. The elements are coloured as white for carbon, light blue for hydrogen, and red for oxygen.

Details of this can be found in Appendix X. For complex 10 to achieve the same lone pair-lone pair interaction, the two species must rotate by approximately 30° relative to one another. This is somewhat unfavourable due to steric clash.

#### (Add HOOH-OOH TS details to appendix)

All the the complexes which follow the observed trend must undergo an additional process with a barrier that is likely about 3 kcal mol<sup>-1</sup>(on the basis of the phenolic rotational barrier) to reach the TS complex. This is illustrated in in Figure 3.7.

Consider next the points which sit above the trendline, complexes 6 and 7. The A-factor for complex 6 is approximate and thus does not get factored into the line fitting. In both cases, the non-covalently bound complexes are in a slipped-parallel π-stacked conformation. Complex 7 in particular is

### 3.3. Results and discussion

---

very similar to the phenol-phenoxy couple, except with 2-naphthol instead of phenol. Therefore, it is possible to infer that both of these reactions take place through a PCET mechanism. Specifically, these pre-reaction complexes do not require an additional conformational change to approach the TS complexes, as illustrated in Figure 3.8.

Finally, consider the points which fall below the trendline, complexes 1 and 5. In both cases, a high degree of steric repulsion likely does not allow for a PCET mechanism. Complex 1 is the reaction with the most steric shielding surrounding the reaction centres, with four ortho-position *t*-butyl groups in total. As a result, the most stable pre-reaction complex does not have a hydrogen bond, which is unique among the ten reaction couples studied here. A higher energy ( $0.6 \text{ kcal mol}^{-1}$ ) pre-reaction complex 1 does exist, and possesses an open conformation hydrogen bond. This higher energy conformer is likely that which leads to HAT through a direct mechanism. The geometry is such that the hydrogen group must rotate and the *t*-butyl groups must approach one another to approach the TS complex. This higher energy complex is still inconsistent with the trendline.

Complex 5 possesses an unusual hydrogen bond. Normally hydrogen bonds are nearly linear so that there is both a dipole-dipole interaction and an orbital interaction such that the lone pair of the acceptor donates electron density into the OH  $\sigma^*$  anti-bonding orbital.<sup>145</sup> In the case of complex 5, the hydrogen bond is nearly perpendicular, resulting in only an orbital interaction.<sup>iii</sup> This is due to the steric repulsion between the *t*-butyl groups of *t*-butylperoxy and 2,4,6-tri-*t*-butylphenol. This structure is comparable to of complex 8, the TS of which as published in reference 25. Complex 8 which takes place through PCET, however, due to steric shielding it is apparent that complex 5 cannot conform to the correct geometry for PCET to occur. In order for this reaction to proceed, an open conformation complex must form so that a direct HAT mechanism can take place.

For complexes 1 and 5 which fall below the trendline, the lowest energy pre-reaction complex does not correspond to one which will lead to HAT. Therefore, one can describe an additional higher energy pre-reaction complex which leads to HAT, similar to the trend observed, but likely much higher in energy, as illustrated in Figure 3.9.

---

<sup>iii</sup>The hydrogen bonding nature of this interaction has been verified using the NCIplot software.<sup>146,147</sup> These results can be found in Appendix X.

### *3.4. Summary*

---

## **3.4 Summary**

In this investigation, I report the lowest energy pre-reaction complexes for a series of thermoneutral or nearly thermoneutral HAT reactions. I have plotted the theoretically determined electronic binding energies against the logarithm of experimentally determined A-factors. These results demonstrate that the A-factor is correlated to some extent with the binding energy, given that the reactions proceed through energetically similar pathways. The results herein can be sorted into three bins: 1. Complexes which require small conformational changes to approach the TS structure. This appears to be the most likely case for formal HAT reactions. 2. Complexes which are optimally aligned to approach the TS structure. 3. Complexes which require a large conformational change to approach the TS structure.

These results suggest that different regimes of steric interactions lead to different chemical processes in seemingly similar reactions. As a result, non-covalent binding can be used as a metric for kinetics parameters, however, they cannot tell the whole story. One must first determine the relationship between the pre-reaction and TS complexes.

Additional work is necessary to extend these results. In particular, a larger sample of data points should be used. Regardless, the results herein represent a novel attempt to link theory and experiment. Given that obtaining the full PES for large molecules is computationally impractical, these results serve as a seed for developing a fundamental understanding of complex formal HAT reactions.

### *3.4. Summary*

---

#### **Appendix NCI Plot**

### 3.4. Summary

---

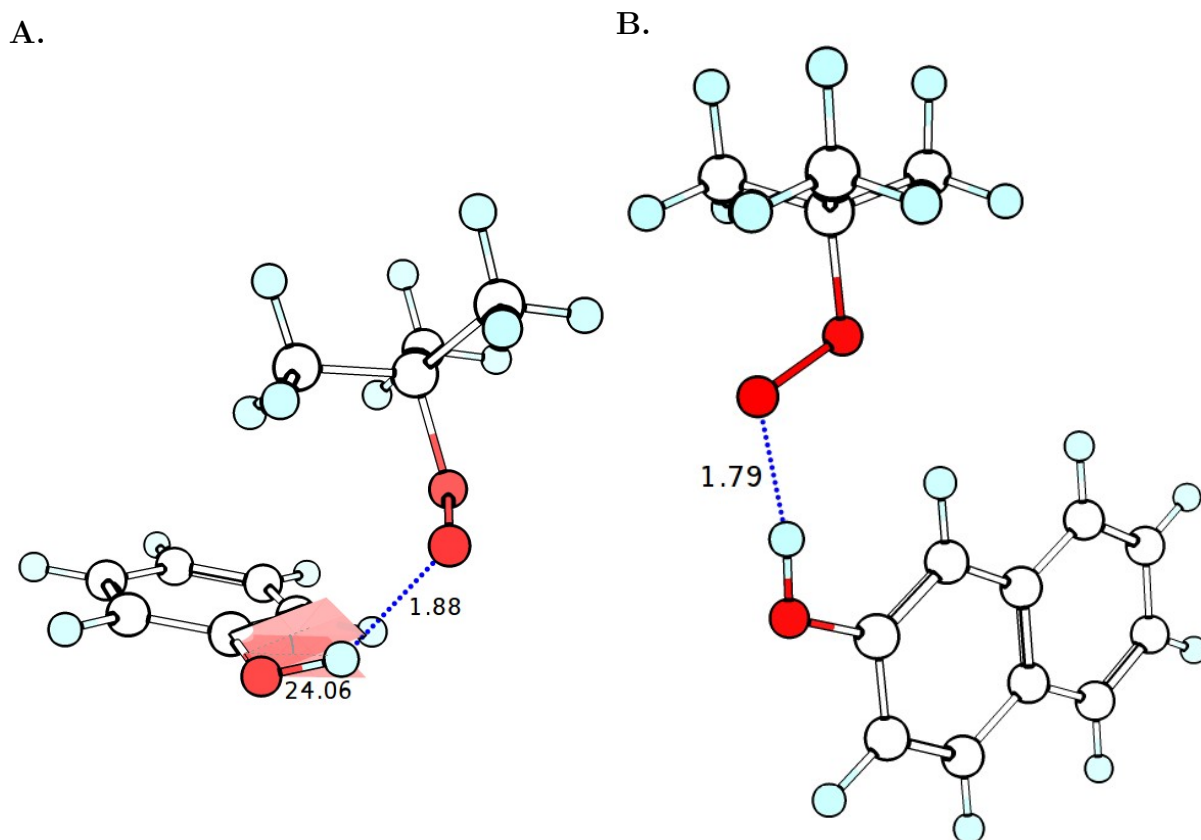


Figure 3.4: Three-dimensional structures of pre-reaction complexes **A.** 8 (*t*-butylperoxy and phenol) and **B.** 9 (*t*-butylperoxy and 2-naphthol). Hydrogen bond distances are shown in units of Å. Complex 8 has an out of plane rotation of the phenolic hydroxyl group of  $24.1^\circ$ . The elements are coloured as white for carbon, light blue for hydrogen, and red for oxygen.

### 3.4. Summary

---

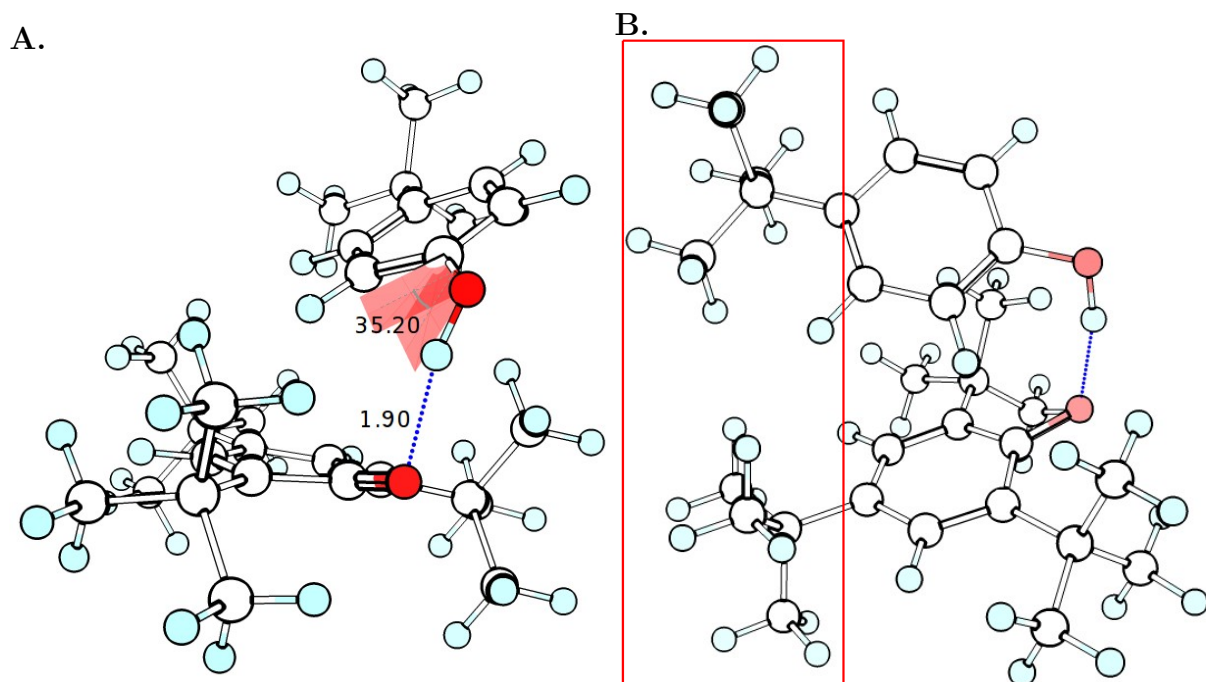


Figure 3.5: Three-dimensional structure of pre-reaction complex 10 between *t*-butylperoxyl and  $\alpha$ -tetralin peroxide. **A** demonstrates the hydrogen bond distances in units of Å, and the out-of-plane rotation by  $35.2^\circ$  of the phenolic hydroxyl group. **B** demonstrates the steric clash (highlighted by red box) between the para-position *t*-butyl groups. The elements are coloured as white for carbon, light blue for hydrogen, and red for oxygen.

### 3.4. Summary

---

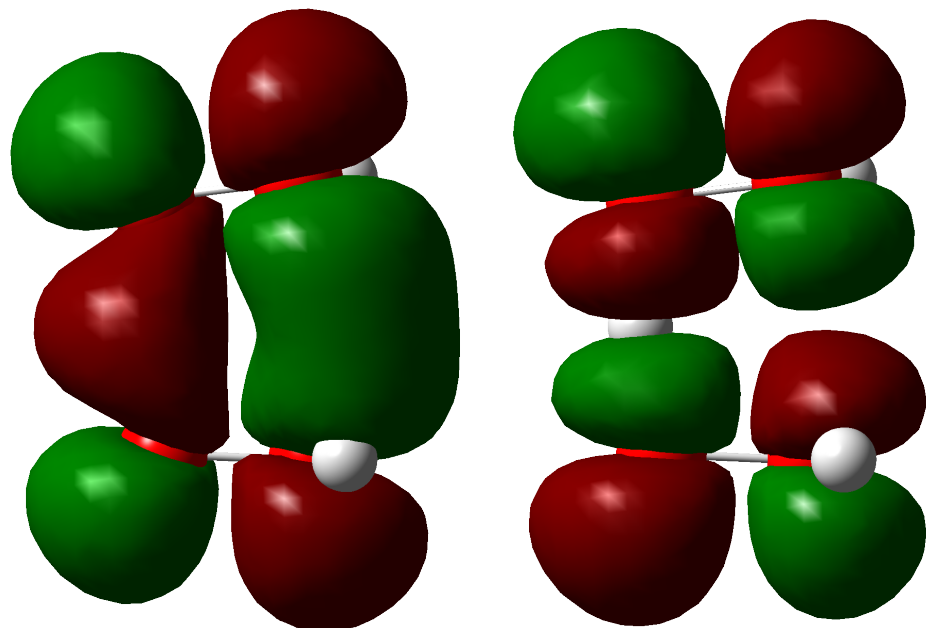


Figure 3.6: Molecular orbitals of hydrogen peroxide-peroxyl self-exchange reaction TS complex, demonstrating a PCET mechanism. Left is the HOMO-1 and right is the SOMO. Together they demonstrate a lone pair-lone pair net half bonding interactions, consistent with PCET.

### 3.4. Summary

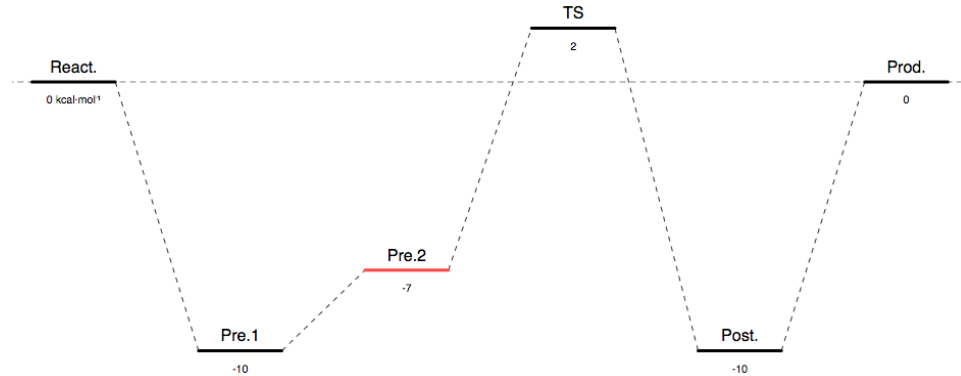


Figure 3.7: Reaction coordinate illustrating a conformational change to a second pre-reaction complex prior to transition state. All energies are arbitrarily estimated based on the phenol-phenoxy self-exchange reaction. React. = reactants, Pre.1 = lowest energy pre-reaction complex, Pre.2 = postulated higher energy pre-reaction complex, TS = transition state, Post. = post-reaction complex, Prod. = products.

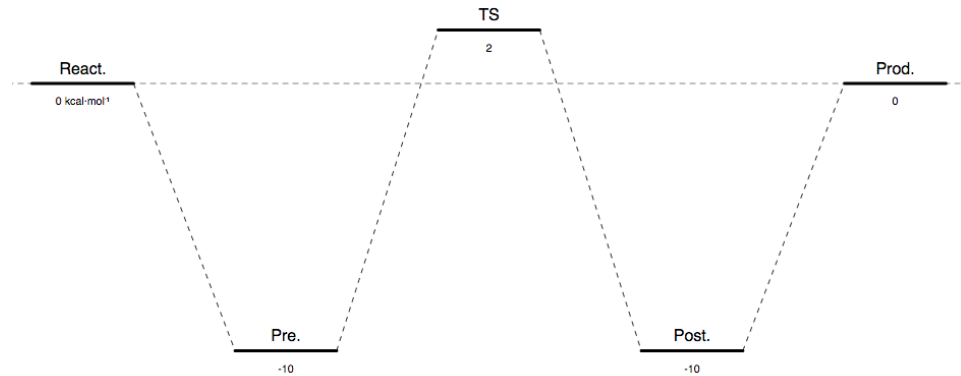


Figure 3.8: Reaction coordinate illustrating no conformational change before moving to the transition state. All energies are arbitrarily estimated based on the phenol-phenoxy self-exchange reaction. React. = reactants, Pre. = lowest energy pre-reaction complex, TS = transition state, Post. = post-reaction complex, Prod. = products.

### 3.4. Summary

---

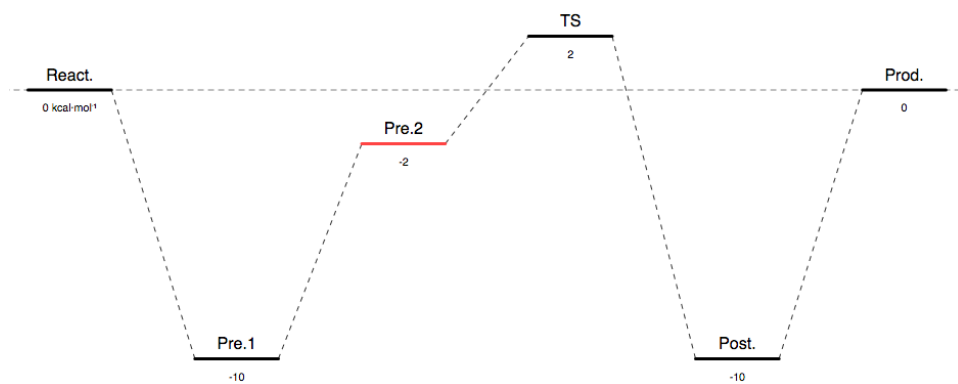


Figure 3.9: Reaction coordinate illustrating a conformational change to a second high energy pre-reaction complex prior to transition state. All energies are arbitrarily estimated based on the phenol-phenoxy self-exchange reaction. React. = reactants, Pre.1 = lowest energy pre-reaction complex, Pre.2 = postulated higher energy pre-reaction complex, TS = transition state, Post. = post-reaction complex, Prod. = products.

### 3.4. Summary

---

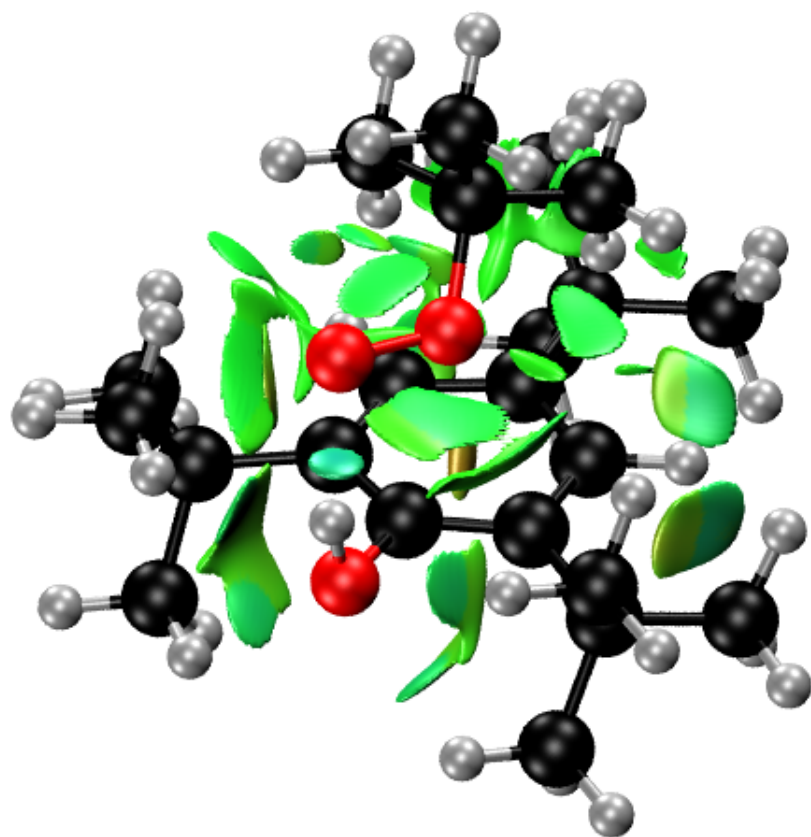


Figure 3.10: NCIplot<sup>146,147</sup> of complex 5. The blue spheroid between the *t*-butylperoxyl oxygen centred radical and the 2,4,6-tri-*t*-butylphenol hydroxyl represents hydrogen bonding.

## Chapter 4

# Interrogation of the Bell-Evans-Polanyi Principle: Investigation of the Bond Dissociation Enthalpies correlated with Hydrogen Atom Transfer Rate Constants

### 4.1 Introduction

The Bell-Evans-Polanyi (BEP) principle is a conceptual framework that states, for two closely related reactions, the difference in activation energy is proportional to the difference in their enthalpy of reaction.<sup>43,44,148</sup> This is commonly expressed as the linear free energy relationship:  $E_a = E_0 + \alpha\Delta H$  (Equation 1.1). Initially, the BEP principle was used as a simple model to explain the Brønsted catalysis law, which states that the stronger and acid is, the faster the catalysed reaction will proceed.<sup>149</sup> A key assumption is made for the BEP principle: the position of the TS along the reaction coordinate is the same for all reactions. The relationship can be described schematically: the more stable the product, the lower the reaction barrier, as seen in Figure 4.1.

A modern use of the BEP principle is to estimate rate constants of related reactions. In application, plots of the logarithm of the rate constant against BDEs are used:  $\log(k_H) = \alpha\Delta H + \text{constant}$ . For HAT reactions involving abstraction by CumO<sup>•</sup>,  $\Delta H$  is directly related to the strength of the breaking bond:  $\Delta H = \text{BDE}(\text{C}-\text{H}) - \text{BDE}(\text{CumO}-\text{H})$ . If the relationship holds for

#### 4.1. Introduction

---

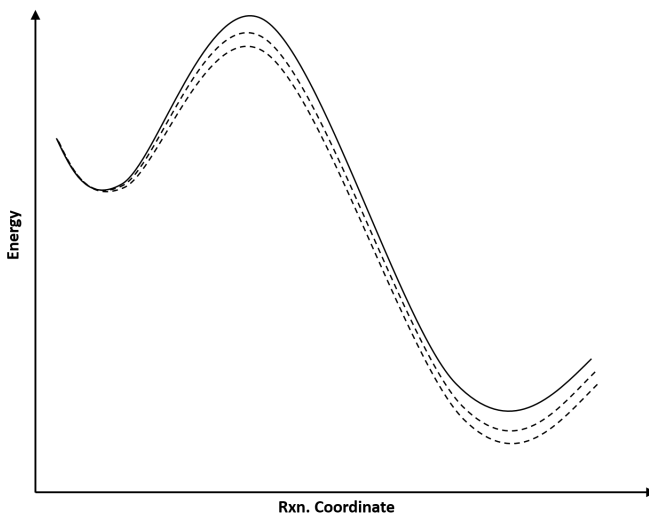


Figure 4.1: Energy profiles for a series of related exothermic reactions illustrating the Bell-Evans-Polanyi principle.

a series of related HAT reactions, then bond dissociation enthalpies (BDEs) should correlate with the activation energy. It would then stand that an increase in bond strength represents a destabilisation in the TS complex, and thus a decrease in reaction rate. This concept is also important for the work in Chapter 5, where the interaction of non-redox active metals cations results in an increase in effective bond strength, and decrease in rate constant. It is also important to note, that if the BEP principle breaks down for reactions which appear related, then additional physico-chemical factors, such as non-covalent binding *viz.* Chapter 3, may be influencing the reaction barrier.

An interesting application of the BEP principle is the work of Pratt et al.<sup>150</sup>, in which the free radical oxidation of unsaturated lipids was examined. They studied the correlation of theoretically determined allylic or benzylic C–H and C–OO<sup>•</sup> bond strengths with experimentally measured HAT rate constants and O<sub>2</sub> addition rate constants, respectively. BEP plots (log  $k$  vs. BDE) for a large range of polyunsaturated fatty acid models show good correlation for C–OO<sup>•</sup> bonds examined, and reasonable correlation for C–H bonds. This demonstrates that BDEs can have a direct impact on the reaction barrier height, thus providing validation of the BEP principle. Additionally, these results provide the important ability of predicting rate constants for HAT and oxygen addition reactions related to unsaturated

#### 4.1. Introduction

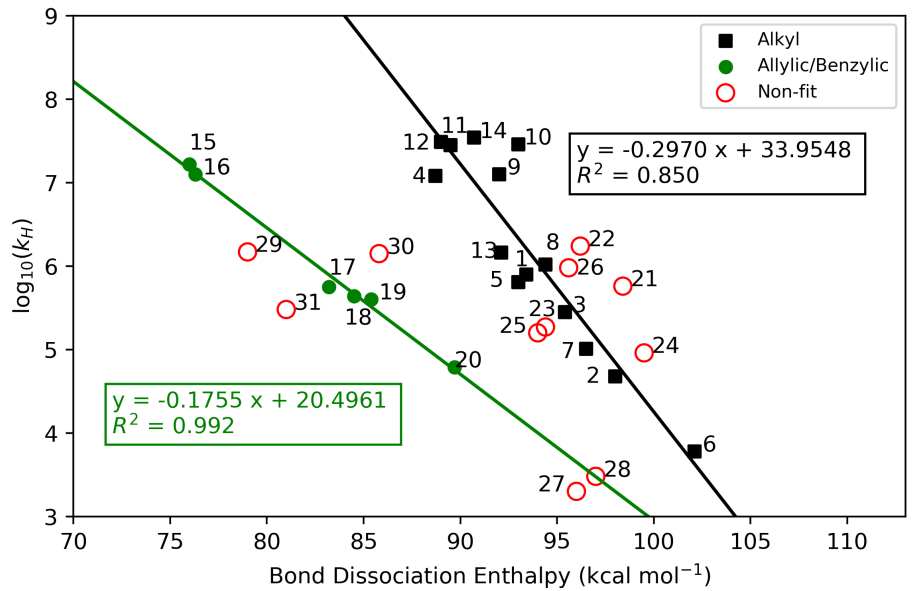
---

lipid models, by means of calculating BDEs.

A significant gap in the literature is the lack of applicability criterion for how broadly the BEP principle can be utilised. In this work, I explore this issue. In order to achieve this, I have studied HAT reactions involving the abstraction of C-H bonds by CumO<sup>•</sup>, for which many rate constants have been published.<sup>45,128,129,131,132,151–153</sup> Additional unpublished rate constants have been provided by our experimental colleagues in Rome. The above studies, as well as many other have used CumO<sup>•</sup> and the closely related *t*-butoxyl radical (*t*-BuO<sup>•</sup>) as models for reactive oxygen-centred radicals in studying oxidative damage of biomaterials,<sup>154–156</sup> as well as in studying the mechanism and efficiency of antioxidants.<sup>157–161</sup> Using these radicals has an important caveat: the fundamental chemistry of these radicals is less well understood than often assumed.<sup>35,36,162</sup>

These reactions are all exothermic, and thus have early transition state by the Hammond Postulate.<sup>163</sup> Plotting these rate constants against literature BDEs (Figure 4.2) there appears to be evidence for two BEP relations. This has led us to the hypothesis that there are two general for C-H bond: one in which the incipient radical is delocalised into a  $\pi$ -system (benzylic or allylic), and one in which the remaining alkyl radicals are largely localised.

#### 4.1. Introduction



1	1,4-diazobicyclo[2.2.2]octane	2	2,2-dimethylbutane
3	2,2-dimethylbutane	4	Benzaldehyde
5	Diethyl Ether	6	Dimethyl sulfoxide
7	Dioxane	8	Hexamethylphosphoramide
9	Morpholine	10	Piperazine
11	Piperidine	12	Pyrroldiine
13	Tetrahydrofuran	14	Triethylamine
15	1,4-cyclohexadiene	16	9,10-dihydroanthracene
17	Cumene	18	Diphenylmethane
19	Ethylbenzen	20	Toluene
21	Adamantane ( $2^\circ$ )	22	Adamantane ( $3^\circ$ )
23	Cycloheptane	24	Cyclohexane
25	Cyclooctane	26	Cyclopentane
27	Acetone	28	Acetonitrile
29	Benzyl alcohol	30	Dibenzyl ether
31	Triphenylmethane		

Figure 4.2: Bell-Evans-Polanyi plot of experimental rate constants (normalised for the number of equivalent hydrogen atoms) for HAT between CumO<sup>·</sup> and substrates against literature BDEs. BDEs for dimethyl sulfoxide and hexamethylphosphoramide are from Ref. 132, while all other BDEs are from Ref. 164.

## 4.2. Methods

---

There is a considerable amount of scatter in Figure 4.2, which may be due to differences in experimental procedures. BDEs are measurable using a large number of different experimental techniques, and a great deal of data exists in the literature. Much of this data has been compiled in the *de facto* reference for BDEs: the CRC Handbook of Bond Dissociation Enthalpies.<sup>164</sup> However, caution must be taken with experimentally determined BDEs, as not all experimental methods give reliable data. For example, BDEs from the Bordwell<sup>165</sup> thermochemical cycle are possibly unreliable.<sup>132,166</sup> This was demonstrated for the BDE of dimethyl sulfoxide, for which the experimentally determined BDE is about 8 kcal mol<sup>-1</sup> lower than the best computational estimate.<sup>132</sup> Therefore, quantum chemistry is a useful tool for studying BDEs, as it is facile to compute BDEs. For example, an arbitrary X–H bond strength is given by:

$$\Delta H(BDE) = H(X^\bullet) + H(H^\bullet) - H(X-H) \quad (4.1)$$

where  $\Delta H(BDE)$  is the BDE, and the right-hand terms are the enthalpies of the radical product, the hydrogen atom, and the substrate, respectively. The aim of this work was to compute the most accurate possible BDEs for

DFT-based methods have been shown to give reliable relative BDEs, however, highly correlated wave function based methods are required to predict chemically accurate (sub-kcal mol<sup>-1</sup>) BDEs.<sup>167–169</sup> For this purpose, we shall use composite quantum chemical procedures. Unfortunately, due to the computational cost of some of these procedures, calculations are often limited to small molecules. Additionally, there is currently no literature which compares the ability of common composite methods to predict accurate BDEs. Therefore, another aim of the work is to determine which composite procedure can be used to compute accurate BDEs for relatively large molecules.

## 4.2 Methods

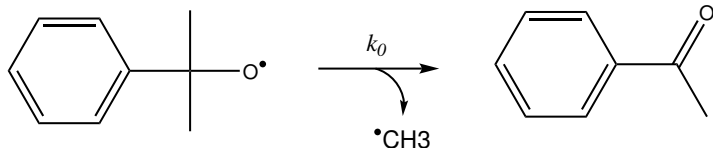
Experimental rate constants were have either provided from unpublished results from our colleagues, the Bietti group in Rome, or come from literature sources.<sup>45,128,129,131,132,151–153</sup> All rate constants come from laser flash photolysis (LFP) experiments of CumO<sup>•</sup> with the substrates of interest. Acetonitrile solvent and ambient conditions (298 K and 1 atm) were used in all cases. For those results which have are unpublished, CumO<sup>•</sup> is generated by laser pulses at either 266 nm or 355 nm in solutions of excess dicumyl peroxide. Many of the literature results are also from the Bietti group,

## 4.2. Methods

---

where the same procedure is used. Other results may have small variations in experimental details, however, all results are well time-resolved.

Observed rate constants ( $k_{obs}$ ) are obtained from transient absorption decay traces of CumO<sup>•</sup> monitored at 485 nm. The observed rate constant is plotted against concentration of substrate to provide the bimolecular HAT rate constant ( $k_H$ ) as the slope ( $k_{obs} = k_0 + k_H[\text{substrate}]$ ). The CumO<sup>•</sup> radical decays unimolecularly through the  $\beta$ -scission of a methyl group, giving acetophenone and a methyl radical, as shown in Scheme 4.1. The unimolecular decay rate constant<sup>170</sup> for CumO<sup>•</sup>( $k_0$ ) in acetonitrile is on the order of  $7.5 \times 10^5 \text{ s}^{-1}$  at 298 K.



Scheme 4.1: Unimolecular decay of the cumyloxy radical.

All quantum chemical calculations were performed using the Gaussian 09 software package.<sup>103</sup> Several composite quantum chemical method which are implemented in Gaussian 09 were used in this work: W1BD, CBS-QB3 and the restricted open-shell variant ROCBS-QB3, CBS-APNO, and G4 and the MP2 variant G4(MP2). An approach using ROCCSD(T) with locally-dense basis sets<sup>171,172</sup> (LDBS) was also utilised in order to approximate W1BD results. Each of these methods is briefly described below.

### 4.2.1 Quantum chemical composite procedures

#### W1BD

The highest accuracy method used is W1BD, which employs seven different calculations to obtain highly correlated electronic energies, as well as thermochemically corrected quantities. This method is very computationally expensive, and thus cannot be applied to the larger species of interest in this work. Geometries and thermochemical corrections come from DFT-based B3LYP calculations with nearly complete cc-pVTZ+d basis sets. A frequency scaling factor of 0.985 is used for harmonic frequency calculations. The electronic energy comes from several additive corrections involving the Brueckner Doubles<sup>83</sup> (BD) variation of coupled cluster and various large basis sets extrapolated to the complete basis set limit. Corrections for core-electron correlation and relativistic contributions are computed using an

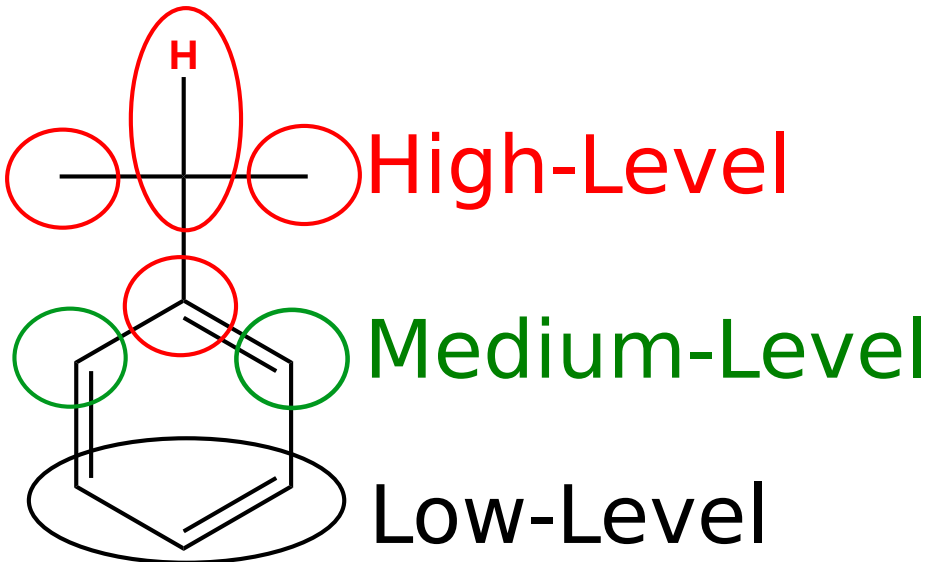
## 4.2. Methods

---

uncontracted variant of the cc-pVTZ+2df basis sets, known as MTsmall.<sup>173</sup>

### LDBS approach

Locally-dense basis sets have been used in the past to calculate BDEs for relatively large molecules.<sup>171,172</sup> The principle is to use large basis sets to treat the atoms in which chemistry takes place, and use progressively smaller basis sets for “remote” portions of the molecule, thus taking advantage of error cancellation. We chose a method which best approximates W1BD results for a small subset of molecules. The scheme utilised herein obtains geometries and scaled frequencies from DFT-based B3LYP/cc-pVTZ+d, as used in the W1BD procedure. Single-point energy calculations were then performed using ROCCSD(T) and an LDBS partitioning scheme we denote as pc-3/3/2/1, demonstrated in Scheme 4.2, which uses the polarisation consistent basis sets.<sup>58</sup>



Scheme 4.2: Locally-dense basis set partitioning used in the calculation of BDEs. The scheme is referred to as pc-3/3/2/1, where for the shown cumene molecule, the centre of C–H cleavage and the immediately adjacent groups are treated with high-level pc-3 basis sets. The next groups are treated with medium level pc-2 basis sets, and all other atoms are treated with low-level pc-1 basis sets.

### CBS methods

## 4.2. Methods

---

The Complete Basis Set (CBS) methods of Petersson and coworkers<sup>80–82,174</sup> are widely used because of the relatively low computational cost (compared to other composite procedures), and well established accuracy.<sup>175,176</sup> CBS-QB3<sup>80,81</sup> utilises DFT-based B3LYP optimisation and scaled frequencies (factor = 0.990) with modified triple-zeta Pople style basis sets. Electronic energies are obtained by extrapolation of medium basis set CCSD(T) and MP4SDQ. Small empirical corrections for are added to achieve more accurate results compared to the parametrisation sets.<sup>177</sup> ROCBS-QB3 is a similar procedure to CBS-QB3, except spin-restricted wave functions are used in place of unrestricted wave functions. This is done to eliminate spin contamination, and the use of an restricted open-shell definition has been shown to produce more accurate BDEs.<sup>167</sup> (RO)CBS-QB3 has been implemented for first, second, and third periods of elements.

Atomic pair natural orbital (APNO) expansions are a method used for averaging over multiple Slater determinants. The use of APNOs allows for small basis set extrapolation of higher order correlation energies to converge more rapidly to the complete basis set limit. This approach is used in the CBS-APNO method.<sup>82</sup> Geometries and scaled frequencies (factor = 0.989) are obtained at the QCISD/6-311G(d,p) level of theory. Similar to CBS-QB3, the extrapolation of moderate basis set MP4SDQ and QCISD(T) results gives the electronic energy. An empirical correction is also used in CBS-APNO. Even though CBS-APNO is more accurate, the expansion of APNOs makes CBS-APNO more computationally demanding than CBS-QB3. As a results, it has only been implemented for first and second row periods, and is thus less commonly used in literature.

### Gn methods

The Gaussian- $n$  (Gn) series of methods originate from the Pople group,<sup>178</sup> where G4 is the fourth generation. G4 utilises moderately large basis sets and extrapolation techniques with CCSD(T) calculations to obtained highly correlated electronic energies. G4(MP2) uses MP2 in place is CCSD(T) and is thus less computationally expensive, but also gives a less complete description of electron correlation. Both methods use the B3LYP/6-31(2df,p) level of theory for optimisation and frequency calculations with a frequency scaling factor of 0.9854. G4 results have been described as generally on par with CBS-QB3 results,<sup>175,176</sup> but calculations are more computationally expensive.

#### 4.2.2 Transition state calculations

Calculations were performed to identify the lowest energy TS complex of several reactions between CumO<sup>·</sup> and organic substrates. In all cases cisoid and transoid conformations were explored. All optimisation calculations were performed at the B3LYP-D3(BJ)/6-31+G\* level of theory, followed by single-point energy calculations at the LC- $\omega$ PBE-D3(BJ)/6-311+G\*\* level of theory. The latter DFT-based method was selected to minimise delocalisation error in the TS complex.<sup>99</sup> Transition states were visualised using the Chemcraft program<sup>179</sup> to confirm a single imaginary frequency connecting reactants to products. In some cases, a small secondary imaginary frequency was observed, indicating a TS complex which is not fully optimised. Necessary steps were taken to re-optimise the structures and eliminate the small imaginary frequencies, however, this was not always successful. Nonetheless, I am confident the structures reported herein sufficiently represent the true TS complex geometries and relative energies. Results from structures which are not fully optimised are indicated as such appropriately.

### 4.3 Comparison of composite method for the prediction of BDEs

In order to determine the best method for BEP principle analysis, and to investigate which is the most efficient yet accurate composite method, the BDEs of 49 species have been calculated. This set of species contains a wide variety of chemical functionalities with bond strengths ranging from 75–113 kcal mol<sup>-1</sup>, thus this set may be described as a comprehensive test of these methods for C-H BDEs. Given that W1BD is the most accurate method used, these results have been used for comparison to other composite method. However, BDEs for only 33 out of the 49 species studied were able to be calculated using W1BD due to computational cost restrictions: hard disk capacity was insufficient for large systems. Therefore, literature BDEs from Luo<sup>164</sup> for all species in the set are also used for comparison. The literature and calculated BDEs are listed in Table 4.1.

4.3. Comparison of composite method for the prediction of BDEs

Table 4.1: Bond dissociation enthalpies of the species used to investigate the accuracy of composite methods. All values are in kcal mol<sup>-1</sup>. Statistics are listed at the bottom of the table

Molecule	Lit. <sup>164</sup>	W1BD	LDBS	CBS-QB3	ROCBS-QB3	CBS-APNO	G4	G4(MP2)
1,3-pentadiene	83.0	82.9	82.2	80.9	81.7	81.8	81.6	82.1
1,4-diazabicyclo[2.2.2]-octane	93.4	98.9	98.9	98.8	98.5	96.7	95.6	
1,4-pentadiene	76.6	76.2	76.0	74.2	75.0	75.2	75.1	75.7
2,2-dimethylbutane	98.0	99.3	99.1	99.4	99.3	99.7	97.5	96.7
2,3-dimethylbutane	95.4	97.8	97.7	97.9	97.8	98.0	96.2	95.5
2-methylbutane	95.8	97.3	97.2	97.3	97.1	97.3	95.9	95.5
Acetaldehyde	94.3	95.9	95.3	95.3	95.7	95.5	94.9	94.8
Acetone	96.0	96.9	96.4	96.2	96.7	97.1	95.4	95.0
Acetonitrile	97.0	96.9	96.6	96.2	96.6	96.5	96.3	96.3
Adamantane (2°)	98.4		100.9	100.5	100.4	100.9	97.8	96.3
Adamantane (3°)	96.2		100.3	99.9	99.9	100.3		95.7
Benzaldehyde	88.7		90.9	91.5	91.4	91.0	89.3	88.2
Benzene	112.9	113.1	112.7	115.4	113.0			113.0
Benzyl Alcohol	79.0		84.4	84.3	83.2	83.9	83.4	83.6
Cumene	83.2		87.9	87.9	86.9		86.9	86.7
Cycloheptane	94.0		96.0	96.0	95.8	96.1	93.9	92.9
Cyclohexadiene	76.0	76.3	76.2	74.3	75.0	75.2	75.5	
Cyclohexane	99.5	99.2	99.1	99.4	99.3	99.6	97.5	96.8

4.3. Comparison of composite method for the prediction of BDEs

Cyclooctane	94.4	92.6	92.6	92.4	92.8	90.2	89.1
Cyclopentane	95.6	96.3	96.1	96.5	96.3	95.6	95.0
Cyclopropane	106.3	109.0	108.5	109.3	109.2	109.5	108.0
Dibenzyl ether	85.8		83.6	84.3	82.7		79.6
Diethyl ether	93.0	95.3	95.1	95.6	95.5	95.4	93.8
Dihydroanthracene	76.3		80.4	80.9	78.1		79.9
Dimethylamine	94.2	92.6	92.4	92.9	92.8	92.7	92.0
Dimethylsulfoxide	94.0	102.0	101.7	102.3	102.3		100.6
Dioxane	96.5	97.3	97.3	97.7	97.6	97.4	95.7
Diphenylmethane	84.5		84.1	85.3	82.8		84.5
Ethane	100.5	101.3	99.3	101.7	101.5	101.8	100.7
Ethylbenzene	85.4		88.3	88.6	87.6	89.3	87.6
Ethylene	110.9	110.8	110.3	110.6	110.9	111.1	109.9
Fluorene	82.0		82.4	83.6	81.9		81.2
Formaldehyde	88.0	88.6	88.0	89.1	88.9	88.2	88.2
Hexamethyl-phosphoramide			93.8	94.1	93.9		88.5
Indene	83.0		80.6	80.4	80.1	81.2	79.0
Methane	105.0	105.0	104.4	105.4	105.2	105.4	104.5
Methanol	96.1	96.4	96.0	96.9	96.8	96.6	96.0
Methylamine	93.9	93.1	92.8	93.4	93.3	93.3	92.7
Morpholine	92.0		93.4	93.4	93.3	93.3	91.8
N,N-dimethylacetamide (acetyl)	91.4	99.6	99.4	99.5	99.5	100.1	97.6
Piperazine	93.0	93.4	93.5	93.6	93.5	93.4	91.9

4.3. Comparison of composite method for the prediction of BDEs

		W1BD	LDBS	CBS-QB3	ROCBS-QB3	CBS-APNO	G4	G4(MP2)
<b>Statistics</b>	Lit.	49	33	50	50	40	43	50
<i>N</i>								
MAE (Lit.)		0.82	1.60	1.88	1.64	1.35	1.21	1.57
Max.		1.59	2.41	2.63	3.15	1.85	4.19	6.23
Min.		-8.22	-8.04	-8.26	-8.25	-8.74	-6.86	-6.58
MAE (W1BD)		0.22	0.32	0.18	0.20	0.70	0.88	
Max.		2.00	2.01	1.26	1.08	2.05	2.84	
Min.		-0.09	-2.37	-0.35	-1.39	0.37	0.02	

### 4.3. Comparison of composite method for the prediction of BDEs

Mean absolute error (MAE) is used to assess the quality of computational methods, where errors are calculated with respect to benchmark values for a given data set.<sup>180</sup> The MAE is calculated as

$$\text{MAE} = \frac{1}{N} \sum |E_{ref} - E_{calc}| \quad (4.2)$$

where, for a set of  $N$  reference values, the MAE is the average of the mean differences of the reference energy ( $E_{ref}$ ) and the calculated value ( $E_{calc}$ ). The MAE with respect to W1BD and literature shall be reported herein as “MAEW1BD (MAELit.)”. An additional semi-quantitative metric which I used to evaluate the accuracy of composite procedures to reproduce experimental results, is a bar chart which summarises the number of deviations from literature within given error ranges. This bar chart is reported in Figure 4.3. Also, an alternative method for visualising these data is through the use of one-to-one plots, in which BDEs from two methods are directly compared. An ideal plot should have a slope = 1 and y-intercept = 0.

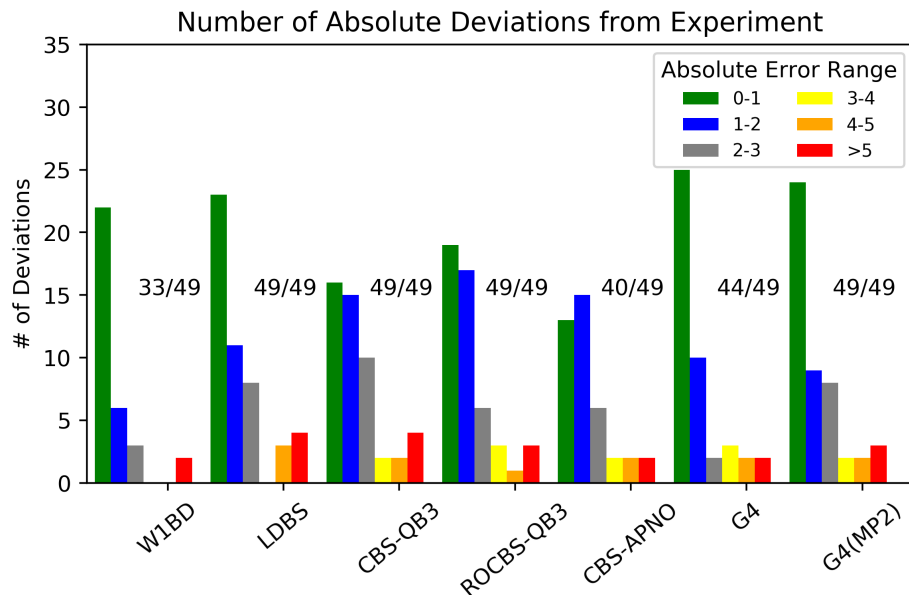


Figure 4.3: Summary of deviations of BDEs from literature or composite quantum chemical methods. Errors are units of kcal mol<sup>-1</sup> and are relative to Reference 164. Numbers out of 49 represent the total number of data points which were computed for the given method.

#### 4.3. Comparison of composite method for the prediction of BDEs

Comparing W1BD results to literature, the MAE is 0.82 kcal mol<sup>-1</sup>, where the majority of the data matching to within 1–2 kcal mol<sup>-1</sup> of literature. Thus, W1BD is largely consistent with the literature values. Additionally, the one-to-one plots comparing W1BD to literature in Figure 4.4, show reasonable agreement with slope of 0.98 and a y-intercept of 2.35. There are, however, two large outliers: dimethyl sulfoxide<sup>iv</sup> and *N,N*-dimethylacetamide, with experiment underestimating the BDEs by -8.0 and -8.2 kcal mol<sup>-1</sup>, respectively. These large outliers are consistent amongst all composite method, suggesting the literature BDEs for dimethyl sulfoxide and *N,N*-dimethylacetamide are incorrect.

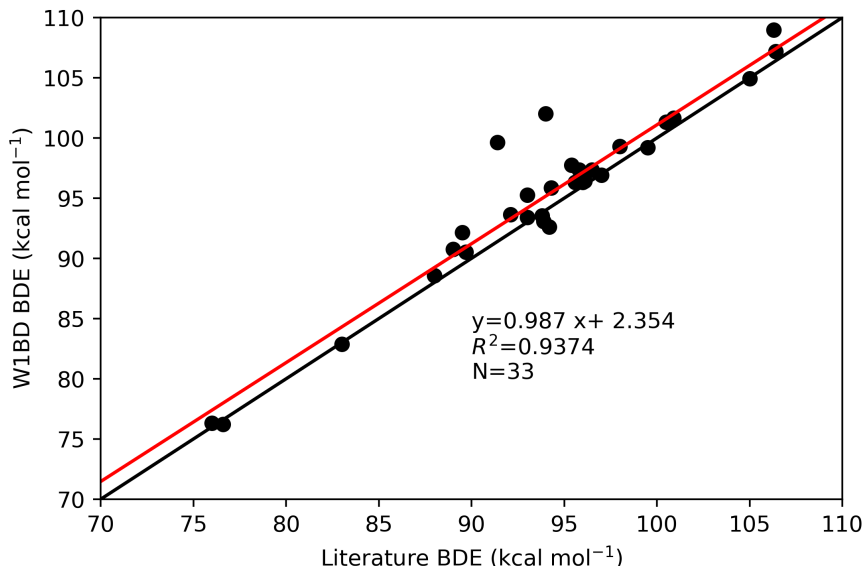


Figure 4.4: One-to-one plot of BDEs from literature<sup>164</sup> and as calculated by the W1BD composite method. The red line represents the least squares line of best fit, while black line represents a perfect one-to-one correlation.

The method which gives the best combined agreement with W1BD and literature is ROCBS-QB3 with an MAE = 0.18 (1.64) kcal mol<sup>-1</sup>. It is also apparent from the one-to-one plots in Figure 4.5, that ROCBS-QB3 matches well with literature and experiment. In comparison, CBS-QB3 has an MAE

<sup>iv</sup>The experimental BDE for dimethyl sulfoxide was previously identified as accurate by Salamone et al.<sup>132</sup>

### 4.3. Comparison of composite method for the prediction of BDEs

$= 0.32$  ( $1.88$ ) kcal mol $^{-1}$ , while CBS-APNO has an MAE =  $0.20$  ( $1.40$ ) kcal mol $^{-1}$ . The LDBS approach also performs well with an MAE =  $0.22$  ( $1.60$ ) kcal mol $^{-1}$ . The G4 method deviates from the W1BD reference by about  $0.5$  kcal mol $^{-1}$  more, however, it appears to give reasonable agreement with experimental results (MAE =  $0.70$  ( $1.21$ ) mol). The use of the MP2 variant of G4 gives somewhat questionable results, with an MAE of  $0.88$  ( $1.60$ ) kcal mol $^{-1}$ , as well as a large outlier of  $6.2$  kcal/mol that is not present in the other data from composite methods. One-to-one plots of all other methods are presented in Appendix A.

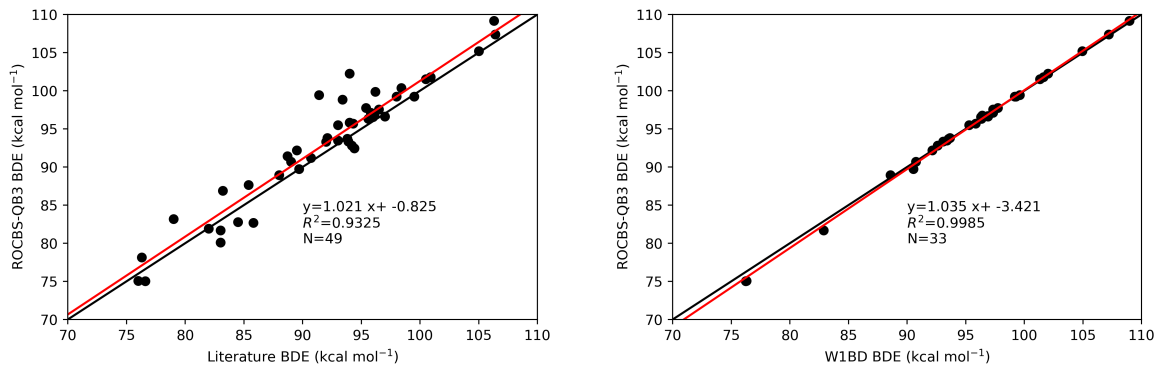


Figure 4.5: One-to-one plot comparing calculated BDEs calculated by the ROCBS-QB3 to reference literature<sup>164</sup> and W1BD BDE values, respectively. The red line represents the least squares line of best fit, while black line represents a perfect one-to-one correlation.

In summary, ROCBS-QB3 performs best for the calculation of C–H BDEs while G4(MP2) performs worst. Given these data, and considering the relative computational cost, the ROCBS-QB3 method is recommended for the calculation of accurate BDEs, particularly for large molecules for which more expensive computational methods are not possible. Importantly, we can now confidently continue investigating the BEP relationships using reliable calculated BDE data from the ROCBS-QB3 method. Furthermore, these results can be extended to even larger systems as the ROCBS-QB3 approach is one of the least computationally expensive composite methods. For example, for calculations on the cyclohexane molecule, which take about 20 minutes using ROCBS-QB3 on SGI Altix compute nodes with 6 processors and 8 GB RAM, while G4 takes about 27 times longer, the LDBS approach takes about 500 times longer, and W1BD takes about 1100 times longer.

#### *4.4. Analysis of the Bell-Evans-Polanyi principle*

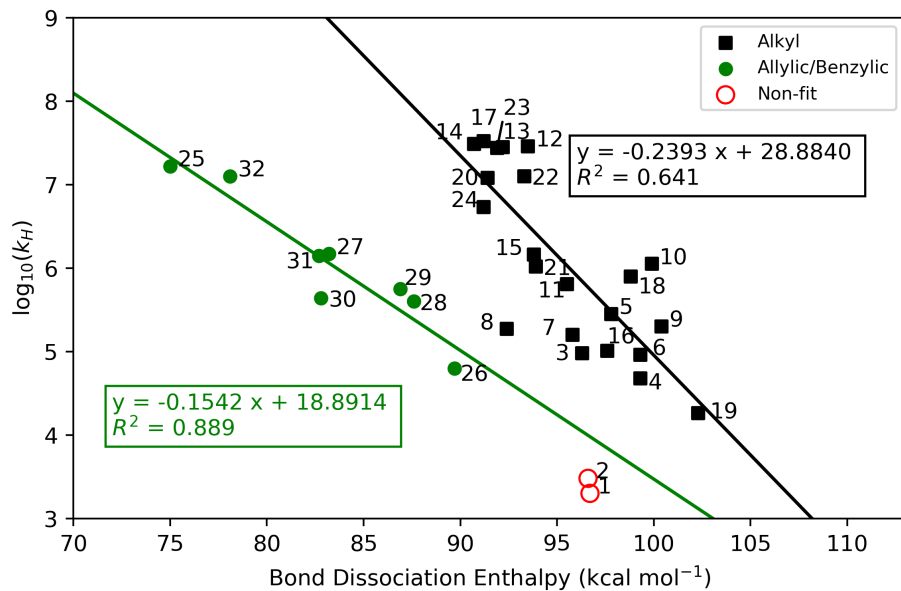
---

### **4.4 Analysis of the Bell-Evans-Polanyi principle**

We turn now to the application of accurate BDEs on the BEP principle. Experimental HAT rate constants have been collected for 32 reactions involving CumO<sup>•</sup>and organic substrates. The BEP plot of the logarithm of rate constants divided by the number of equivalent H atoms (i.e. normalised) against BDEs is shown in Figure 4.6.

There clearly exists two distinct regions in Figure 4.6, inline with our initial hypothesis that there should exist two linear relations: one for benzylic/allylic C-H bonds and another for alkyl C-H bonds. However, the correlation of one of these trends is poor, a result which is inconsistent with our hypothesis. For the series of C-H BDEs which result in a radical which is delocalised, the correlation coefficient is 0.89, suggesting a valid correlation. Therefore, there is predictive power from a BEP relation for C-H bond cleavage which results in a delocalised radical. Furthermore, this result is consistent with the correlation of rate constants with C-H BDEs for model unsaturated fatty acids, described by Pratt et al.<sup>150</sup>

#### 4.4. Analysis of the Bell-Evans-Polanyi principle



1	Acetone	2	Acetonitrile
3	Cyclopentane	4	2,2-dimethylbutane
5	2,3-dimethylbutane	6	Cyclohexane
7	Cycloheptane	8	Cyclooctane
9	Adamantane (2°)	10	Adamantane (3°)
11	Diethyl ether	12	Piperazine
13	Piperidine	14	Pyrrolidine
15	Tetrahydrofuran	16	Dioxane
17	Triethylamine	18	1,4-diazobicyclo[2.2.2]octane
19	Dimethyl sulfoxide	20	Benzaldehyde
21	Hexamethylphosphoramide	22	Morpholine
23	Diethylamine	24	Propylamine
25	1,4-cyclohexadiene	26	Toluene
27	Benzyl alcohol	28	Ethylbenzene
29	Cumene	30	Diphenylmethane
31	Dibenzyl ether	32	9,10-dihydroanthracene

Figure 4.6: Bell-Evans-Polanyi plot of experimental rate constants (normalised for the number of equivalent hydrogen atoms) for HAT between CumO<sup>·</sup> and substrates. Acetone and acetonitrile are note included in fitting as the experimental rate constants are approximate. Needs revision to move labels around.

#### 4.5. Transition state analysis

---

(fix) In contrast, the alkyl C-H BDEs shows very weak correlation with HAT rate constants, with a correlation coefficient of 0.63. However, with the exception of two larger outlier, cyclooctane and the secondary hydrogen position of adamantane, the majority of the data fall within half an order of magnitude of rate a rate constant which is consistent with the line of best fit. The two large outliers are approximately twice as far from the trendline. While this result may not seem positive, there is actually some predictive power in the BEP relation established for alkyl C-H bonds. This is because in the calculations of rate constants, an error of only 1.2 kcal mol<sup>-1</sup> can result in a order of magnitude difference in rate constant. Errors of this magnitude are not uncommon for DFT-based mechanistic studies. For example, barrier heights for a set<sup>181,182</sup> of 76 hydrogen transfer, heavy atom transfer, nucleophilic substitution, unimolecular, and association reactions calculated with at the B3LYP-D3(BJ)/Def2-QZVP level of theory give a mean absolute error of 5.20 kcal mol<sup>-1</sup>, with errors exceeding 11 kcal mol<sup>-1</sup>.<sup>183</sup>

In sum, these results suggest that the BEP principle is overly simple to directly correlate the large groups of allylic/benzylic and alkyl C-H bonds with HAT rate constant. Nonetheless, BEP relations offer predictive capabilities for rate constants to within an order of magnitude. Importantly, this result indicates that there are additional factors which contribute to the HAT rate constants studied herein.

## 4.5 Transition state analysis

In order to determine what effects appear to be most important, I have calculated TS structures for 20 of the reactions at the LC- $\omega$ PBE-D3(BJ)/6-311+G(2d,2p)//B3LYP-D3(BJ)/6-31+G\* level of theory. Comparing the calculated rate constants both with and without tunnelling corrections, there is a large degree of variability in the agreement with experiment. Figure 4.7 demonstrates that the calculated rate constants deviate rather significantly from the experimental rate constants, both with and without the inclusion of a tunnelling correction. This result is perhaps unsurprising given the neglect of solvent effects, and the fairly low level of theory used for optimisation. Note however, that the goal of these calculations was not to reproduce experimental rate constants, but to obtain TS complex structures to analyse the structural differences that may lead to the deviations from the BEP principle.

The first factor which may lead to deviations from the BEP is the pos-

#### 4.5. Transition state analysis

---

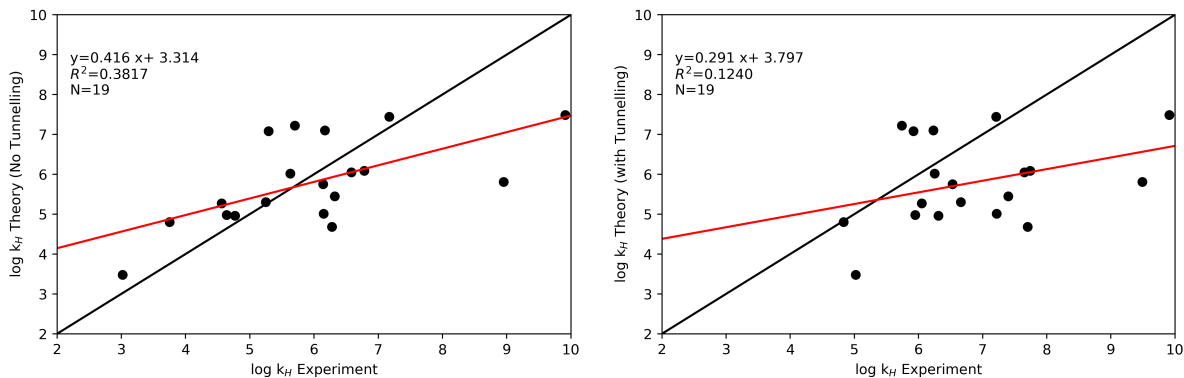


Figure 4.7: One-to-one plots of theoretically determined logarithm of rate constant for HAT reactions between CumO<sup>•</sup> and organic substrates against experimental values. The plot on the left does not include a tunnelling correction while the plot on the right includes the Eckart potential tunnelling correction.

sibility for different HAT reaction mechanisms, i.e. direct HAT or PCET. Consider first the reaction of toluene with CumO<sup>•</sup>. As this reaction is similar to the self-exchange reaction of the benzyl-toluene couple as described by DiLabio and Johnson,<sup>25</sup> one might expect the reaction to proceed via PCET. The lowest energy TS complex has a partially  $\pi$ -stacked conformation with the rings oriented about 40° relative to one another. Surprisingly, examination of the SOMO and HOMO reveals no  $\pi$ - $\pi$  partial bonding interaction, as can be seen in Figure 4.8. The electron density of the SOMO is largely localised on the toluene portion of the complex. This is likely due to the additional non-conjugated carbon centre of CumO<sup>•</sup>, which prevent an additional electron channel for PCET to occur. Therefore, this reaction takes place through direct HAT. This behaviour is specific to the CumO<sup>•</sup> radical, thus all the reactions likely also take place through a direct HAT mechanism, and this should not factor into the deviations in the observed BEP principle relationships.

There are several other possible deviations which may arise from differences in intermolecular interactions due to structural differences in the substrates. For example, cyclooctane may deviate from the trend observed due to the many possible conformations of the ring which are comparable in energy.<sup>184</sup> Alternatively, the position of the TS complex along the reaction coordinate may differ between the various reactions. This would break

#### 4.6. Summary

---

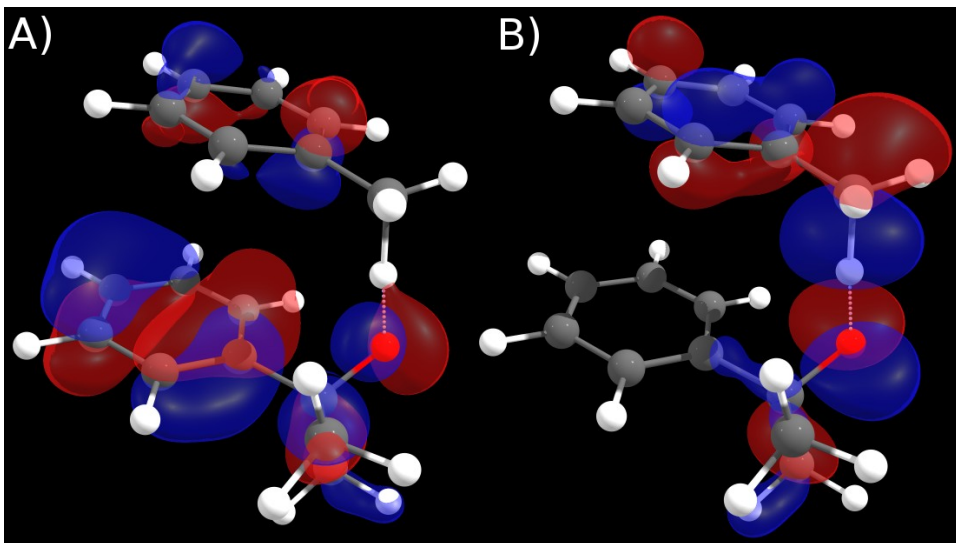


Figure 4.8: Insert better images of CumO<sup>•</sup>-toluene TS complex with A) SOMO and B) HOMO.

the assumption of the BEP principle, and may result in deviation from the expected trend.

(I am having a hard time finding further explanations from the data I have. Any input here is greatly appreciated.)

## 4.6 Summary

Firstly, a number of composite quantum mechanical methods were tested for the accurate prediction of C-H BDEs. The ROCBS-QB3 method was determined to be the most efficient accurate method for this purpose. Additionally, the widespread applicability of the BEP principle was investigated through utilisation of these accurate C-H BDEs and experimental HAT rate constants for reaction of CumO<sup>•</sup> with organic substrates.

As was hypothesised, two relationships exist for the BEP principle when investigating a wide range of HAT reactions from C-H bonds. C-H bonds which result in a radical which can be delocalised into neighbour  $\pi$  systems (benzylic/allylic) correlate well with experimental rate constants. The remaining alkyl C-H bonds, correlate weakly with experimental rate constants and offer only order of magnitude predictions of rate constants. Altogether, these results suggest that the BEP principle must be carefully applied if

#### *4.6. Summary*

---

accurate rate constants are the desired target, however, they also suggest that as the BEP principle holds as a reasonably general principle.

# Chapter 5

## Do non-redox active metal cations have the potentials to behave as chemo-protective agents? The Effects on Metal Cations on HAT Reaction Barrier Heights

### 5.1 Benchmarking Density Functional Theory for the Binding of Alkali and Alkaline Earth Metals

#### 5.1.1 Background

In order to study the central hypothesis proposed in this work, we must carefully select a computational method. In particular, we wish to use density-functional theory (DFT), which is known to be prone to various problems such as self-interaction error,<sup>185</sup> delocalization error,<sup>99</sup> and the inability to treat non-covalent interactions.<sup>95,186</sup> The latter of these can be corrected by the selection of a method capable correcting the non-covalent corrections such as a pair-wise dispersion model ([\cite{D3}](#)), or atom centered potentials developed by our group ([\cite{DCPS}](#)). Other errors can be ignored through the careful selection of a DFT method.

We are interested in selecting a method which can accurately treat the interactions between alkali and alkaline earth metal cations, and organic substrates and radicals. To this end, there exists little literature, with one notable paper<sup>187</sup> which examines the binding of calcium cations to organic substrates. In this paper, Suárez et al.<sup>187</sup> provide accurate energetic,

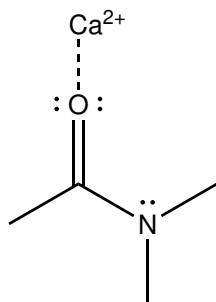
## 5.1. Benchmarking Density Functional Theory for the Binding of Alkali and Alkaline Earth Metals

---

electronic, and structural results for the binding of calcium to organic neutral and charged species, as well as assess the performance of four different DFT methods. They also analyze the nature of ligand-metal bonding interactions using a symmetry-adapted perturbation theory approach (SAPT) ([EXPAND ON THIS](#))

Due to our interest in alkali and alkaline earth metal cations in FHT, we determined it necessary to prepare benchmark quality data for binding to organic substrates and radicals.

([Calcium prefers to bind to O, with binding to S or N is rare<sup>188</sup>](#)) In N,N-dimethylacetamide for example, calcium binds preferentially to the lone pairs of the carbonyl oxygen over the nitrogen lone pair. This is shown in Scheme 5.1.



Scheme 5.1: Binding of the calcium cation ( $\text{Ca}^{2+}$ ) to the oxygen lone pairs of N,N-dimethylacetamide.

### 5.1.2 Methods

Conformers were generated using Hyperchem with the AM1 semi-empirical molecular orbital (MO) method ([\-citehyperchem](#)) followed by optimization calculations of 5-10 lowest energy structures using at the ([\(\(currently unpublished\)\)](#) BLYP-D3/pc1 level of theory, including our own groups basis set incomplete potential (BSIPs).([\(\(CITATIONS\)\)](#))

On the basis of the work by Otero-de-la-Roza et al.<sup>99</sup>, which showed that in systems which are halogen bonded, erroneous charge transfer can be significant, and given the charge on the metal cations, the LC- $\omega$ PBE density functional with D3 dispersion correction and moderate 6-31+G(2d,2p) ([\(\(CITATIONS for DFT and D3\)\)](#)) basis sets were applied to determine the most strongly bound complexes of substrates and metal cations. Global minima monomers and complexes were optimized with the LC- $\omega$ PBE-D3 method

## 5.1. Benchmarking Density Functional Theory for the Binding of Alkali and Alkaline Earth Metals

---

near the basis set limit (6-311+G(3df,3pd)). Highly correlated wavefunction results were obtained at the CCSD(T) level of theory with extrapolation to the complete basis set limit. ([CITATION](#)) Calculations were performed using the Gaussian 09 package,<sup>103</sup> and wavefunction calculations were performed using the TURBOMOLE<sup>61</sup> package.

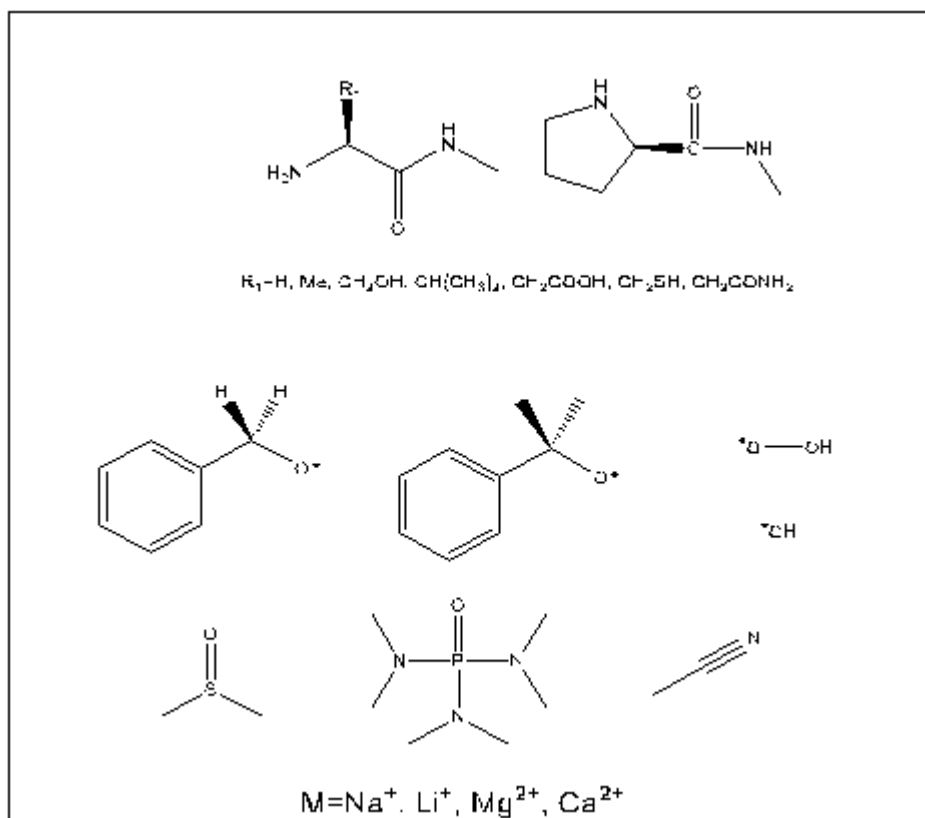
### 5.1.3 Benchmark systems

The purpose of this work is to provide high-level binding energies for organic substrates which are of interest directly for this project, but also which may be useful for future work. The substrates proposed were to be relevant to simple biological models such as dipeptide like molecules and the hydroxyl and hydroperoxyl radical. We also wanted to incorporate substrates which are important to the physical organic experiments that are performed to probe these systems, thus solvents such as acetonitrile and dimethyl sulfoxide and the benzyloxy and cumyloxy radicals were also included. This set is shown in Scheme 5.2([FIND CDX](#)).

Benchmark quality binding energies are generally calculated using the “gold standard” approach, CCSD(T)/CBS, where correlation consistent basis sets ([\(CITATION\)](#)) (cc-pV<sub>X</sub>Z, X=T,Q,5) developed by Dunning and co-workers are used for complete basis set extrapolation. These basis sets have limited availability for the metals of interest. Specifically, basis sets for K are not available, and only non-augmented basis sets for Li, Na, Mg, and Ca. It is necessary to include core correlation of the n-1 shell in alkali and alkaline earth metals, thus it is advantageous to use core valence basis sets such as cc-pCV<sub>X</sub>Z. These basis sets are even more limited, thus we opted for the augmented version of the polarization consistent basis sets of Jensen and co-workers (aug-pc-*N*, *N*=2,3,4). ([CITATIONS FOR GOLD STANDARD AND BASIS SETS, NEED THEORY SECTION ON DIFFERENT BASIS SETS](#))

While performing CCSD(T)/CBS calculations, we noticed that the metal cations (and neutral metal atoms), did not converge smoothly to the complete basis set limit. Given this, and the limited computational resources, we decided to re-evaluate the size scope of the benchmark set being used. In order to facilitate future DFT work and probe the issue of basis set convergence of alkali and alkaline earth metals, a benchmark set of small substrates was proposed. This new set is shown in Scheme 5.3. The new, small benchmark set was selected to include important functional groups and radicals for biological systems and the most common solvent used in physical organic experiments, acetonitrile.

### 5.1. Benchmarking Density Functional Theory for the Binding of Alkali and Alkaline Earth Metals



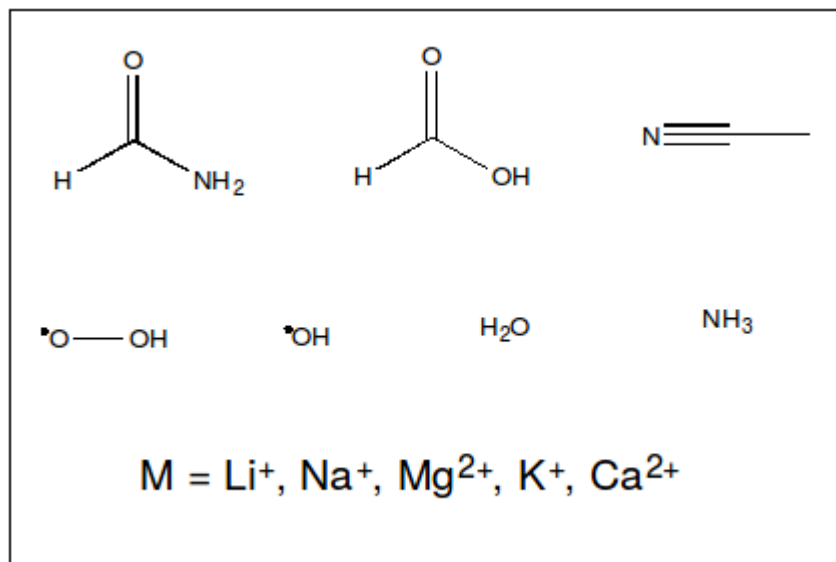
Scheme 5.2: Initial proposed benchmark set of molecules and cations. Note this set consists of all combinations of substrates and metal cation, thus there are 60 complexes in the set.

#### 5.1.4 Metal cation basis set convergence

#### 5.1.5 High level results and evaluation of various density-functional theory methods

5.1. Benchmarking Density Functional Theory for the Binding of Alkali and Alkaline Earth Metals

---



Scheme 5.3: Revised benchmark set of small substrates and cations. Note this set consists of all combinations of substrates and metal cation, thus there are 35 complexes in the set.

# **Chapter 6**

# **Conclusion**

Here comes the conclusion.

*Chapter 6. Conclusion*

---

Your conclusion can go on for several pages.

# References

- [1] Halliwell, B.; Gutteridge, J. M. *Free Radicals in Biology and Medicine*; Oxford University Press, USA, 2015.
- [2] Barnham, K. J.; Masters, C. L.; Bush, A. I. Neurodegenerative diseases and oxidative stress. *Nat. Rev. Drug Discovery* **2004**, *3*, 205–214.
- [3] Valko, M.; Leibfritz, D.; Moncol, J.; Cronin, M. T. D.; Mazur, M.; Telser, J. Free radicals and antioxidants in normal physiological functions and human disease. *International Journal of Biochemistry & Cell Biology* **2007**, *39*, 44–84.
- [4] Hwang, O. Role of oxidative stress in Parkinson’s disease. *Experimental Neurobiology* **2013**, *22*, 11–17.
- [5] Halliwell, B. Oxidative stress and cancer: have we moved forward? *Biochem. J.* **401**, 1–11.
- [6] Turrens, J. F. Mitochondrial formation of reactive oxygen species. *J. Physiol. (Lond.)* **2003**, *552*, 335–344.
- [7] Kozmér, Z.; Arany, E.; Alapi, T.; Takács, E.; Wojnárovits, L.; Dombi, A. Determination of the rate constant of hydroperoxyl radical reaction with phenol. *Radiat. Phys. Chem.* **2014**, *102*, 135–138.
- [8] Berlett, B. S.; Stadtman, E. R. Protein Oxidation in Aging, Disease, and Oxidative Stress. *1997*, *272*, 20313–20316.
- [9] Davies, M. J. Protein oxidation and peroxidation. *Biochem. J.* **2016**, *473*, 805–825.
- [10] Davies, M. J. The oxidative environment and protein damage. *Biochim. Biophys. Acta* **2005**, *1703*, 93–109.
- [11] Rauk, A.; Armstrong, D. A. Influence of  $\beta$ -Sheet Structure on the Susceptibility of Proteins to Backbone Oxidative Damage: Preference for

---

## References

---

- $\alpha$ C-Centered Radical Formation at Glycine Residues of Antiparallel  $\beta$ -Sheets. *J. Am. Chem. Soc.* **2000**, *122*, 4185–4192.
- [12] Stadtman, E. R. Role of oxidant species in aging. *Curr. Med. Chem.* **2004**, *11*, 1105–1112.
- [13] Mulder, P.; Korth, H.-G.; Pratt, D. A.; DiLabio, G. A.; Valgimigli, L.; Pedulli, G. F.; Ingold, K. U. Critical Re-evaluation of the O-H Bond Dissociation Enthalpy in Phenol. *J. Phys. Chem. A* **2005**, *109*, 2647–2655.
- [14] Stadtman, E. R.; Levine, R. L. Free radical-mediated oxidation of free amino acids and amino acid residues in proteins. *Amino Acids* **2003**, *25*, 207–218.
- [15] Garrison, W. M.; Jayko, M.; Bennett, W. Radiation-induced oxidation of protein in aqueous solution. *Radiat Res* **1962**, *16*, 483–502.
- [16] Garrison, W. M. Reaction mechanisms in the radiolysis of peptides, polypeptides, and proteins. *Chem. Rev.* **1987**, *87*, 381–398.
- [17] Halliwell, B. Oxidative stress and neurodegeneration: where are we now? *J. Neurochem.* **2006**, *97*, 1634–1658.
- [18] Kochi, J., Ed. *Free Radicals, Vols. 1 and 2*; Wiley, New York, 1973.
- [19] Parsons, A. F. *An Introduction to Free Radical Chemistry*; Wiley-Blackwell, 2000.
- [20] Litwinienko, G.; Ingold, K. U. Solvent Effects on the Rates and Mechanisms of Reaction of Phenols with Free Radicals. *Acc. Chem. Res.* **2007**, *40*, 222–230.
- [21] Cukier, R. I.; Nocera, D. G. Proton-coupled electron transfer. *Annu. Rev. Phys. Chem.* **1998**, *49*, 337–369.
- [22] Mayer, J. M.; Hrovat, D. A.; Thomas, J. L.; Borden, W. T. Proton-coupled electron transfer versus hydrogen atom transfer in benzyl/toluene, methoxyl/methanol, and phenoxy/phenol self-exchange reactions. *J. Am. Chem. Soc.* **2002**, *124*, 11142–11147.
- [23] Stubbe, J.; Nocera, D. G.; Yee, C. S.; Chang, M. C. Radical initiation in the class I ribonucleotide reductase: long-range proton-coupled electron transfer? *Chem. Rev.* **2003**, *103*, 2167–2202.

---

## References

---

- [24] Mayer, J. M. Proton-coupled electron transfer: a reaction chemist's view. *Annu. Rev. Phys. Chem.* **2004**, *55*, 363–390.
- [25] DiLabio, G. A.; Johnson, E. R. Lone Pair- $\pi$  and  $\pi$ - $\pi$  Interactions Play an Important Role in Proton-Coupled Electron Transfer Reactions. *J. Am. Chem. Soc.* **129**, 6199–6203.
- [26] Huynh, M. H. V.; Meyer, T. J. Proton-coupled electron transfer. *Chem. Rev.* **2007**, *107*, 5004–5064.
- [27] Hammes-Schiffer, S.; Soudackov, A. V. Proton-coupled electron transfer in solution, proteins, and electrochemistry. *J. Phys. Chem. B* **2008**, *112*, 14108–14123.
- [28] Mayer, J. M. Understanding hydrogen atom transfer: from bond strengths to Marcus theory. *Acc. Chem. Res.* **2010**, *44*, 36–46.
- [29] Weinberg, D. R.; Gagliardi, C. J.; Hull, J. F.; Murphy, C. F.; Kent, C. A.; Westlake, B. C.; Paul, A.; Ess, D. H.; McCafferty, D. G.; Meyer, T. J. Proton-coupled electron transfer. *Chem. Rev.* **2012**, *112*, 4016–4093.
- [30] Hammes-Schiffer, S. Proton-coupled electron transfer: Moving together and charging forward. *J. Am. Chem. Soc.* **2015**, *137*, 8860–8871.
- [31] Muñoz-Rugeles, L.; Galano, A.; Alvarez-Idaboy, J. R. Non-Covalent  $\pi$ - $\pi$  Stacking Interactions Turn Off Non-Adiabatic Effects in Proton-Coupled Electron Transfer Reactions. *Phys. Chem. Chem. Phys.* **2017**,
- [32] Hatcher, E.; Soudackov, A. V.; Hammes-Schiffer, S. Proton-coupled electron transfer in soybean lipoxygenase: dynamical behavior and temperature dependence of kinetic isotope effects. *J. Am. Chem. Soc.* **2007**, *129*, 187–196.
- [33] Sirjoosinh, A.; Hammes-Schiffer, S. Proton-coupled electron transfer versus hydrogen atom transfer: generation of charge-localized diabatic states. *J. Phys. Chem. A* **2011**, *115*, 2367–2377.
- [34] Salamone, M.; Bietti, M. Tuning Reactivity and Selectivity in Hydrogen Atom Transfer from Aliphatic C–H Bonds to Alkoxy Radicals: Role of Structural and Medium Effects. *Acc. Chem. Res.* **2015**, *48*, 2895–2903.

---

## References

---

- [35] Finn, M.; Friedline, R.; Suleman, N. K.; Wohl, C. J.; Tanko, J. M. Chemistry of the t-Butoxyl Radical: Evidence that Most Hydrogen Abstractions from Carbon are Entropy-Controlled. *J. Am. Chem. Soc.* **2004**, *126*, 7578–7584.
- [36] Salamone, M.; Anastasi, G.; Bietti, M.; DiLabio, G. A. Diffusion Controlled Hydrogen Atom Abstraction from Tertiary Amines by the Benzyloxyl Radical. The Importance of C-H/N Hydrogen Bonding. *Org. Lett.* **2011**, *13*, 260–263.
- [37] Kreilick, R. W.; Weissman, S. I. Hydrogen Atom Transfer between Free Radicals and Their Diamagnetic Precursors. *J. Am. Chem. Soc.* **1966**, *88*, 2645–2652.
- [38] Johnson, E. R.; Dilabio, G. A. Radicals as hydrogen bond donors and acceptors. *Interdisciplinary Sciences: Computational Life Sciences* **2009**, *1*, 133–140.
- [39] DiLabio, G. A.; Ingold, K. U. A Theoretical Study of the Iminoxyl/Oxime Self-Exchange Reaction. A Five-Center, Cyclic Proton-Coupled Electron Transfer. *127*, 6693–6699.
- [40] Tedder, J. M. Which factors determine the reactivity and regioselectivity of free radical substitution and addition reactions? *Angew. Chem. Int. Ed.* **1982**, *21*, 401–410.
- [41] Wijtmans, M.; Pratt, D. A.; Valgimigli, L.; DiLabio, G. A.; Pedulli, G. F.; Porter, N. A. 6-Amino-3-Pyridinols: Towards Diffusion-Controlled Chain-Breaking Antioxidants. *Angew. Chem. Int. Ed.* **2003**, *42*, 4370–4373.
- [42] Pratt, D. A.; DiLabio, G. A.; Mulder, P.; Ingold, K. U. Bond Strengths of Toluenes, Anilines, and Phenols: To Hammett or Not. *37*, 334–340.
- [43] Bell, R. P. The Theory of Reactions Involving Proton Transfers. *Proceedings of the Royal Society A: Mathematical, Physical and Engineering Sciences* **1936**, *154*, 414–429.
- [44] Evans, M. G.; Polanyi, M. Inertia and driving force of chemical reactions. *Trans. Faraday Soc.* **1938**, *34*, 11.
- [45] Salamone, M.; Milan, M.; DiLabio, G. A.; Bietti, M. Reactions of the Cumyloxyl and Benzyloxyl Radicals with Tertiary Amides. Hydrogen

---

## References

---

- Abstraction Selectivity and the Role of Specific Substrate-Radical Hydrogen Bonding. *J. Org. Chem.* **2013**, *78*, 5909–5917.
- [46] Salamone, M.; Carboni, G.; Mangiacapra, L.; Bietti, M. Binding to Redox-Inactive Alkali and Alkaline Earth Metal Ions Strongly Deactivates the C–H Bonds of Tertiary Amides toward Hydrogen Atom Transfer to Reactive Oxygen Centered Radicals. *J. Org. Chem.* **2015**, *80*, 9214–9223.
- [47] Salamone, M.; Mangiacapra, L.; Carboni, G.; Bietti, M. Hydrogen atom transfer from tertiary alkanamides to the cumyloxyl radical. The role of substrate structure on alkali and alkaline earth metal ion induced C–H bond deactivation. *Tetrahedron* **2016**,
- [48] Griffiths, D. J. *Introduction to quantum mechanics*; Cambridge University Press, 2016.
- [49] Heisenberg, W. Mehrkörperproblem und Resonanz in der Quantenmechanik. *Zeitschrift für Physik* **1926**, *38*, 411–426.
- [50] Dirac, P. A. M. On the Theory of Quantum Mechanics. *Proceedings of the Royal Society A: Mathematical, Physical and Engineering Sciences* **1926**, *112*, 661–677.
- [51] Slater, J. C. The Theory of Complex Spectra. *Phys. Rev.* **1929**, *34*, 1293–1322.
- [52] Roothaan, C. C. J. New Developments in Molecular Orbital Theory. *Rev. Mod. Phys.* **1951**, *23*, 69–89.
- [53] Gill, P. M. *Advances in Quantum Chemistry*; Elsevier BV, 1994; pp 141–205.
- [54] Szabo, A.; Ostlund, N. S. Modern Quantum Chemistry: Intro to Advanced Electronic Structure Theory. **1996**,
- [55] Jensen, F. Atomic orbital basis sets. *WIREs Comput Mol Sci* **2012**, *3*, 273–295.
- [56] Hehre, W. J.; Stewart, R. F.; Pople, J. A. Self-Consistent Molecular-Orbital Methods. I. Use of Gaussian Expansions of Slater-Type Atomic Orbitals. *The Journal of Chemical Physics* **1969**, *51*, 2657–2664.

---

## References

---

- [57] Dunning, T. H. Gaussian basis sets for use in correlated molecular calculations. I. The atoms boron through neon and hydrogen. *J. Chem. Phys.* **1989**, *90*, 1007–1023.
- [58] Jensen, F. Polarization consistent basis sets: Principles. *115*, 9113.
- [59] Schäfer, A.; Horn, H.; Ahlrichs, R. Fully optimized contracted Gaussian basis sets for atoms Li to Kr. *J. Chem. Phys.* **1992**, *97*, 2571–2577.
- [60] Weigend, F.; Ahlrichs, R. Balanced basis sets of split valence, triple zeta valence and quadruple zeta valence quality for H to Rn: Design and assessment of accuracy. *Phys. Chem. Chem. Phys.* **2005**, *7*, 3297.
- [61] TURBOMOLE V6.3 2011, a development of University of Karlsruhe and Forschungszentrum Karlsruhe GmbH, 1989-2007, TURBOMOLE GmbH, since 2007; available from <http://www.turbomole.com>.
- [62] Cramer, C. J. *Essentials of Computational Chemistry*; Wiley John + Sons, 2004.
- [63] Leininger, M. L.; Allen, W. D.; Schaefer, H. F.; Sherrill, C. D. Is Möller–Plesset perturbation theory a convergent ab initio method? *J. Chem. Phys.* **2000**, *112*, 9213–9222.
- [64] Crawford, T. D.; Schaefer, H. F. *Reviews in Computational Chemistry*; Wiley-Blackwell, 2000; pp 33–136.
- [65] Levine, I. N. *Quantum Chemistry*; Prentice Hall, 2013.
- [66] Pople, J. A.; Head-Gordon, M.; Raghavachari, K. Quadratic configuration interaction. A general technique for determining electron correlation energies. *J. Chem. Phys.* **1987**, *87*, 5968–5975.
- [67] Truhlar, D. G. Basis-set extrapolation. *Chem. Phys. Lett.* **1998**, *294*, 45–48.
- [68] Feller, D. Application of systematic sequences of wave functions to the water dimer. *J. Chem. Phys.* **1992**, *96*, 6104–6114.
- [69] Feller, D. The use of systematic sequences of wave functions for estimating the complete basis set, full configuration interaction limit in water. *J. Chem. Phys.* **1993**, *98*, 7059–7071.

---

## References

---

- [70] Helgaker, T.; Klopper, W.; Koch, H.; Noga, J. Basis-set convergence of correlated calculations on water. *J. Chem. Phys.* **1997**, *106*, 9639–9646.
- [71] Halkier, A.; Helgaker, T.; Jørgensen, P.; Klopper, W.; Koch, H.; Olsen, J.; Wilson, A. K. Basis-set convergence in correlated calculations on Ne, N<sub>2</sub>, and H<sub>2</sub>O. *Chem. Phys. Lett.* **1998**, *286*, 243–252.
- [72] Kupka, T.; Lim, C. Polarization-Consistent versus Correlation-Consistent Basis Sets in Predicting Molecular and Spectroscopic Properties. *J. Phys. Chem. A* **2007**, *111*, 1927–1932.
- [73] Shiozaki, T.; Kamiya, M.; Hirata, S.; Valeev, E. F. Explicitly correlated coupled-cluster singles and doubles method based on complete diagrammatic equations. *J. Chem. Phys.* **2008**, *129*, 071101.
- [74] Köhn, A.; Richings, G. W.; Tew, D. P. Implementation of the full explicitly correlated coupled-cluster singles and doubles model CCSD-F12 with optimally reduced auxiliary basis dependence. *J. Chem. Phys.* **2008**, *129*, 201103.
- [75] Ten-no, S.; Noga, J. Explicitly correlated electronic structure theory from R12/F12 anszte. *WIREs Comput Mol Sci* **2012**, *2*, 114–125.
- [76] Feller, D. Benchmarks of improved complete basis set extrapolation schemes designed for standard CCSD(T) atomization energies. *J. Chem. Phys.* **2013**, *138*, 074103.
- [77] Karton, A. A computational chemist's guide to accurate thermochemistry for organic molecules. *WIREs Comput Mol Sci* **2016**, *6*, 292–310.
- [78] Curtiss, L. A.; Redfern, P. C.; Raghavachari, K. Gaussian-4 theory. *J. Chem. Phys.* **2007**, *126*, 084108.
- [79] Curtiss, L. A.; Redfern, P. C.; Raghavachari, K. Gaussian-4 theory using reduced order perturbation theory. *J. Chem. Phys.* **2007**, *127*, 124105.
- [80] Montgomery, J. A.; Frisch, M. J.; Ochterski, J. W.; Petersson, G. A. A complete basis set model chemistry. VI. Use of density functional geometries and frequencies. *J. Chem. Phys.* **1999**, *110*, 2822–2827.
- [81] Montgomery, J. A.; Frisch, M. J.; Ochterski, J. W.; Petersson, G. A. A complete basis set model chemistry. VII. Use of the minimum population localization method. *J. Chem. Phys.* **2000**, *112*, 6532–6542.

---

## References

---

- [82] Ochterski, J. W.; Petersson, G. A.; Montgomery, J. A. A complete basis set model chemistry. V. Extensions to six or more heavy atoms. *J. Chem. Phys.* **1996**, *104*, 2598–2619.
- [83] Barnes, E. C.; Petersson, G. A.; Montgomery, J. A.; Frisch, M. J.; Martin, J. M. L. Unrestricted Coupled Cluster and Brueckner Doubles Variations of W1 Theory. *J. Chem. Theory Comput.* **2009**, *5*, 2687–2693.
- [84] Hohenberg, P.; Kohn, W. Inhomogeneous Electron Gas. *Phys. Rev.* **1964**, *136*, B864–B871.
- [85] Koch, W.; Holthausen, M. C. *A Chemist's Guide to Density Functional Theory: An Introduction*; Wiley-VCH, 2000.
- [86] Kohn, W.; Sham, L. J. Self-Consistent Equations Including Exchange and Correlation Effects. *Phys. Rev.* **1965**, *140*, A1133–A1138.
- [87] Perdew, J. P.; Ruzsinszky, A.; Tao, J.; Staroverov, V. N.; Scuseria, G. E.; Csonka, G. I. Prescription for the design and selection of density functional approximations: More constraint satisfaction with fewer fits. *J. Chem. Phys.* **2005**, *123*, 062201.
- [88] Goerigk, L.; Grimme, S. Double-hybrid density functionals. *WIREs Comput Mol Sci* **2014**, *4*, 576–600.
- [89] Becke, A. D. Density-functional thermochemistry. III. The role of exact exchange. *J. Chem. Phys.* **1993**, *98*, 5648–5652.
- [90] Lee, C.; Yang, W.; Parr, R. G. Development of the Colle-Salvetti correlation-energy formula into a functional of the electron density. *Phys. Rev. B* **1988**, *37*, 785–789.
- [91] Zhao, Y.; Schultz, N. E.; Truhlar, D. G. Design of Density Functionals by Combining the Method of Constraint Satisfaction with Parametrization for Thermochemistry, Thermochemical Kinetics, and Noncovalent Interactions. *J. Chem. Theory Comput.* **2006**, *2*, 364–382.
- [92] Zhao, Y.; Truhlar, D. G. The M06 suite of density functionals for main group thermochemistry, thermochemical kinetics, noncovalent interactions, excited states, and transition elements: two new functionals and systematic testing of four M06-class functionals and 12 other functionals. *Theor. Chem. Acc.* **2006**, *120*, 215–241.

---

## References

---

- [93] Parr, R. G.; Yang, W. *Density-Functional Theory of Atoms and Molecules*; Oxford University Press, 1995.
- [94] Cohen, A. J.; Mori-Sánchez, P.; Yang, W. Challenges for Density Functional Theory. *Chem. Rev.* **2012**, *112*, 289–320.
- [95] DiLabio, G. A.; Otero-de-la-Roza, A. *Reviews in Computational Chemistry*; Wiley-Blackwell, 2016; pp 1–97.
- [96] Grimme, S.; Antony, J.; Ehrlich, S.; Krieg, H. A consistent and accurate ab initio parametrization of density functional dispersion correction (DFT-D) for the 94 elements H-Pu. *The Journal of Chemical Physics* **2010**, *132*, 154104.
- [97] Johnson, E. R.; Becke, A. D. A post-Hartree-Fock model of intermolecular interactions: Inclusion of higher-order corrections. *J. Chem. Phys.* **2006**, *124*, 174104.
- [98] Mori-Sánchez, P.; Cohen, A. J.; Yang, W. Localization and Delocalization Errors in Density Functional Theory and Implications for Band-Gap Prediction. *Phys. Rev. Lett.* **2008**, *100*.
- [99] Otero-de-la-Roza, A.; Johnson, E. R.; DiLabio, G. A. Halogen Bonding from Dispersion-Corrected Density-Functional Theory: The Role of Delocalization Error. *J. Chem. Theory Comput.* **2014**, *10*, 5436–5447.
- [100] Csonka, G. I.; Johnson, B. G. Inclusion of exact exchange for self-interaction corrected H 3 density functional potential energy surface. *Theor. Chem. Acc.* **1998**, *99*, 158–165.
- [101] Heidrich, D.; Kliesch, W.; Quapp, W. *Properties of Chemically Interesting Potential Energy Surfaces*; Springer Berlin Heidelberg, 1991.
- [102] Hratchian, H. P.; Schlegel, H. B. *Theory and Applications of Computational Chemistry*; Elsevier, 2005; pp 195–249.
- [103] Frisch, M. J. et al. Gaussian 09, Revision D. 01. 2009.
- [104] Wilson, E. B.; Decius, J. C.; Cross, P. C. *Molecular Vibrations: The Theory of Infrared and Raman Vibrational Spectra (Dover Books on Chemistry)*; Dover Publications, 1980.
- [105] McQuarrie, D. A.; Simon, J. D. *Molecular Thermodynamics*; University Science Books, 1999.

---

## References

---

- [106] McQuarrie, D. A. *Statistical Mechanics*; UNIV SCIENCE BOOKS, 2000.
- [107] Note that  $Q$  is actually a function of the number of moles, volume of a system, and temperature. This description, denoted as  $Q(N, V, T)$  has been omitted for simplicity.
- [108] Mennucci, B., Cammi, R., Eds. *Continuum Solvation Models in Chemical Physics: From Theory to Applications*; John Wiley & Sons Inc., 2007.
- [109] Marenich, A. V.; Cramer, C. J.; Truhlar, D. G. Universal Solvation Model Based on Solute Electron Density and on a Continuum Model of the Solvent Defined by the Bulk Dielectric Constant and Atomic Surface Tensions. *J. Phys. Chem. B* **2009**, *113*, 6378–6396.
- [110] Ho, J.; Klamt, A.; Coote, M. L. Comment on the Correct Use of Continuum Solvent Models. *J. Phys. Chem. A* **2010**, *114*, 13442–13444.
- [111] McQuarrie, D. A.; Simon, J. D. *Physical Chemistry: A Molecular Approach*; University Science Books, 1997.
- [112] Steinfeld, J. I.; Francisco, J. S.; Hase, W. L. *Chemical Kinetics and Dynamics*, 2nd ed.; Prentice Hall, 1998.
- [113] Truhlar, D. G.; Garrett, B. C. Variational Transition State Theory. *Annu. Rev. Phys. Chem.* **1984**, *35*, 159–189.
- [114] McMahon, R. J. Chemical Reactions Involving Quantum Tunneling. *Science* **2003**, *299*, 833–834.
- [115] Bell, R. P. *The Tunnel Effect in Chemistry*; Springer Nature, 1980.
- [116] Johnston, H. S.; Heicklen, J. Tunnelling Corrections For Unsymmetrical Eckart Potential Energy Barriers. *J. Phys. Chem.* **1962**, *66*, 532–533.
- [117] Mader, E. A.; Larsen, A. S.; Mayer, J. M. Hydrogen Atom Transfer from Iron(II)-Tris[2,2'-bi(tetrahydropyrimidine)] to TEMPO: A Negative Enthalpy of Activation Predicted by the Marcus Equation. *J. Am. Chem. Soc.* **2004**, *126*, 8066–8067.
- [118] Mahoney, L. R.; DaRooge, M. A. Kinetic and thermochemical study of the reaction of 2,4,6-tri-tert-butylphenoxy radical with substituted phenols. *J. Am. Chem. Soc.* **1970**, *92*, 890–899.

---

## References

---

- [119] DaRooge, M. A.; Mahoney, L. R. Reaction of 2,4,6-tri-tert-butylphenoxy radical with unhindered phenols. *J. Org. Chem.* **1967**, *32*, 1–6.
- [120] Howard, J. A.; Furimsky, E. Arrhenius Parameters for Reaction of tert -Butylperoxy Radicals with some Hindered Phenols and Aromatic Amines. *Can. J. Chem.* **1973**, *51*, 3738–3745.
- [121] Foti, M.; Ingold, K. U.; Lusztyk, J. The Surprisingly High Reactivity of Phenoxy Radicals. *J. Am. Chem. Soc.* **1994**, *116*, 9440–9447.
- [122] Chenier, J. H. B.; Furimsky, E.; Howard, J. A. Arrhenius Parameters for Reaction of the tert -Butylperoxy and 2-Ethyl-2-propylperoxy Radicals with some Nonhindered Phenols, Aromatic Amines, and Thiophenols. *Can. J. Chem.* **1974**, *52*, 3682–3688.
- [123] Chenier, J. H. B.; Howard, J. A. A Kinetic Electron Spin Resonance Study of the Transfer of a Hydrogen Atom from  $\alpha$ -Tetralin Hydroperoxide to a Tertiary Alkylperoxy Radical. *Can. J. Chem.* **1975**, *53*, 623–627.
- [124] Lucarini, M.; Pedrielli, P.; Pedulli, G. F.; Cabiddu, S.; Fattuoni, C. Bond Dissociation Energies of O-H Bonds in Substituted Phenols from Equilibration Studies. *J. Org. Chem.* **1996**, *61*, 9259–9263.
- [125] Mahoney, L. R.; DaRooge, M. A. Equilibrium reaction of 2,4,6-tri-tert-butylphenol and organic peroxy radicals. *J. Am. Chem. Soc.* **1970**, *92*, 4063–4067.
- [126] Mahoney, L. R.; DaRooge, M. A. Kinetic behavior and thermochemical properties of phenoxy radicals. *J. Am. Chem. Soc.* **1975**, *97*, 4722–4731.
- [127] Korcek, S.; Chenier, J. H. B.; Howard, J. A.; Ingold, K. U. Absolute Rate Constants for Hydrocarbon Autoxidation. XXI. Activation Energies for Propagation and the Correlation of Propagation Rate Constants with Carbon–Hydrogen Bond Strengths. *Can. J. Chem.* **1972**, *50*, 2285–2297.
- [128] Salamone, M.; DiLabio, G. A.; Bietti, M. Hydrogen Atom Abstraction Selectivity in the Reactions of Alkylamines with the Benzyloxyl and Cumyloxyl Radicals. The Importance of Structure and of Substrate Radical Hydrogen Bonding. *J. Am. Chem. Soc.* **2011**, *133*, 16625–16634.

---

## References

---

- [129] Pischel, U.; Nau, W. M. Switch-Over in Photochemical Reaction Mechanism from Hydrogen Abstraction to Exciplex-Induced Quenching: Interaction of Triplet-Excited versus Singlet-Excited Acetone versus Cumyloxy Radical with Amines. *J. Am. Chem. Soc.* **2001**, *123*, 9727–9737.
- [130] Griller, D.; Howard, J. A.; Marriott, P. R.; Scaiano, J. C. Absolute rate constants for the reactions of tert-butoxyl, tert-butylperoxyl, and benzophenone triplet with amines: the importance of a stereoelectronic effect. *J. Am. Chem. Soc.* **1981**, *103*, 619–623.
- [131] Bietti, M.; Martella, R.; Salamone, M. Understanding Kinetic Solvent Effects on Hydrogen Abstraction Reactions from Carbon by the Cumyloxy Radical. *Org. Lett.* **2011**, *13*, 6110–6113.
- [132] Salamone, M.; DiLabio, G. A.; Bietti, M. Reactions of the Cumyloxy and Benzyloxy Radicals with Strong Hydrogen Bond Acceptors. Large Enhancements in Hydrogen Abstraction Reactivity Determined by Substrate/Radical Hydrogen Bonding. *J. Org. Chem.* **77**, 10479–10487.
- [133] Malatesta, V.; Scaiano, J. C. Absolute rate constants for the reactions of tert-butoxyl with ethers: importance of the stereoelectronic effect. *J. Org. Chem.* **1982**, *47*, 1455–1459.
- [134] Salamone, M.; Milan, M.; DiLabio, G. A.; Bietti, M. Absolute Rate Constants for Hydrogen Atom Transfer from Tertiary Amides to the Cumyloxy Radical: Evaluating the Role of Stereoelectronic Effects. *J. Org. Chem.* **2014**, *79*, 7179–7184.
- [135] Becke, A. D. Density-functional exchange-energy approximation with correct asymptotic behavior. *Phys. Rev. A* **1988**, *38*, 3098–3100.
- [136] Andzelm, J.; Klobukowski, M.; Radzio-andzelm, E.; Sakai, Y.; Tatewaki, H. In *Gaussian Basis Sets For Molecular Calculation*; Huzinaga, S., Ed.; Elsevier, 1984; Valence Scale Factors From John Deisz Of North Dakota State University.
- [137] The Escher program<sup>189</sup> was used to generate a Z-matrix with specific dihedral angles. This geometry was then systematically scanned using simple shell scripts.
- [138] Vydrov, O. A.; Scuseria, G. E. Assessment of a long-range corrected hybrid functional. *J. Chem. Phys.* **2006**, *125*, 234109.

---

## References

---

- [139] Vydrov, O. A.; Heyd, J.; Krukau, A. V.; Scuseria, G. E. Importance of short-range versus long-range Hartree-Fock exchange for the performance of hybrid density functionals. *J. Chem. Phys.* **2006**, *125*, 074106.
- [140] Johnson, E. R.; Otero-de-la-Roza, A.; Dale, S. G.; DiLabio, G. A. Efficient basis sets for non-covalent interactions in XDM-corrected density-functional theory. *J. Chem. Phys.* **2013**, *139*, 214109.
- [141] Řezáč, J.; Riley, K. E.; Hobza, P. S66: A Well-balanced Database of Benchmark Interaction Energies Relevant to Biomolecular Structures. *J. Chem. Theory Comput.* **2011**, *7*, 2427–2438.
- [142] Benson, S. W. *Thermochemical kinetics*, 2nd ed.; Wiley: New York, 1976.
- [143] Kim, K.; Jordan, K. Theoretical calculation of the height of the barrier for OH rotation in phenol. *Chem. Phys. Lett.* **1994**, *218*, 261–269.
- [144] Isborn, C.; Hrovat, D. A.; Borden, W. T.; Mayer, J. M.; Carpenter, B. K. Factors controlling the barriers to degenerate hydrogen atom transfers. *J. Am. Chem. Soc.* **2005**, *127*, 5794–5795.
- [145] Jeffrey, G. A. *An Introduction to Hydrogen Bonding*; Oxford University Press, 1997.
- [146] Johnson, E. R.; Keinan, S.; Mori-Sánchez, P.; Contreras-García, J.; Cohen, A. J.; Yang, W. Revealing Noncovalent Interactions. *J. Am. Chem. Soc.* **2010**, *132*, 6498–6506.
- [147] Contreras-García, J.; Johnson, E. R.; Keinan, S.; Chaudret, R.; Piquemal, J.-P.; Beratan, D. N.; Yang, W. NCIPLOT: A Program for Plotting Noncovalent Interaction Regions. *J. Chem. Theory Comput.* **2011**, *7*, 625–632.
- [148] Dill, K. A.; Bromberg, S. *Molecular Driving Forces: Statistical Thermodynamics in Chemistry & Biology*; Garland Science, 2003.
- [149] Brønsted, J. N.; Pedersen, K. Stöchiometrie und Verwandtschaftslehre. *J. Zeitschrift für Phys. Chemie* **1924**, *108*, 185–235.
- [150] Pratt, D. A.; Mills, J. H.; Porter, N. A. Theoretical calculations of carbon-oxygen bond dissociation enthalpies of peroxy radicals formed in the autoxidation of lipids. *J. Am. Chem. Soc.* **2003**, *125*, 5801–5810.

## References

---

- [151] Bietti, M.; Salamone, M. Kinetic Solvent Effects on Hydrogen Abstraction Reactions from Carbon by the Cumyloxy Radical. The Role of Hydrogen Bonding. *Org. Lett.* **2010**, *12*, 3654–3657.
- [152] Salamone, M.; Martella, R.; Bietti, M. Hydrogen Abstraction from Cyclic Amines by the Cumyloxy and Benzyloxy Radicals. The Role of Stereoelectronic Effects and of Substrate/Radical Hydrogen Bonding. *J. Org. Chem.* **2012**, *77*, 8556–8561.
- [153] Salamone, M.; Mangiacapra, L.; Bietti, M. Kinetic Solvent Effects on the Reactions of the Cumyloxy Radical with Tertiary Amides. Control over the Hydrogen Atom Transfer Reactivity and Selectivity through Solvent Polarity and Hydrogen Bonding. *J. Org. Chem.* **2015**, *80*, 1149–1154.
- [154] Adam, W.; Grimm, G. N.; Saha-Mller, C. R.; Dall'Acqua, F.; Miolo, G.; Vedaldi, D. DNA Damage by tert-Butoxyl Radicals Generated in the Photolysis of a Water-Soluble, DNA-Binding Peroxyester Acting as a Radical Source. *Chem. Res. Toxicol.* **1998**, *11*, 1089–1097.
- [155] Adam, W.; Marquardt, S.; Kemmer, D.; Saha-Mller, C. R.; Schreier, P. 2'-Deoxyguanosine (DG) Oxidation and Strand-Break Formation in DNA by the Radicals Released in the Photolysis of N-tert-Butoxy-2-pyridone. Are tert-Butoxyl or Methyl Radicals Responsible for the Photooxidative Damage in Aqueous Media? *Org. Lett.* **2002**, *4*, 225–228.
- [156] Jones, C. M.; Burkitt, M. J. EPR Spin-Trapping Evidence for the Direct, One-Electron Reduction of tert-Butylhydroperoxide to the tert-Butoxyl Radical by Copper(II): Paradigm for a Previously Overlooked Reaction in the Initiation of Lipid Peroxidation. *J. Am. Chem. Soc.* **2003**, *125*, 6946–6954.
- [157] MacFaul, P. A.; Ingold, K. U.; Lusztyk, J. Kinetic Solvent Effects on Hydrogen Atom Abstraction from Phenol, Aniline, and Diphenylamine. The Importance of Hydrogen Bonding on Their Radical-Trapping (Antioxidant) Activities 1. *The Journal of Organic Chemistry* **1996**, *61*, 1316–1321.
- [158] Valgimigli, L.; Ingold, K. U.; Lusztyk, J. Antioxidant Activities of Vitamin E Analogues in Water and a Kamlet-Taft  $\beta$ -Value for Water1. *J. Am. Chem. Soc.* **1996**, *118*, 3545–3549.

---

## References

---

- [159] Valgimigli, L.; Banks, J. T.; Lusztyk, J.; Ingold, K. U. Solvent Effects on the Antioxidant Activity of Vitamin E. *J. Org. Chem.* **1999**, *64*, 3381–3383.
- [160] Jovanovic, S. V.; Steenken, S.; Boone, C. W.; Simic, M. G. H-Atom Transfer Is A Preferred Antioxidant Mechanism of Curcumin. *J. Am. Chem. Soc.* **1999**, *121*, 9677–9681.
- [161] Sortino, S.; Petralia, S.; Foti, M. C. Absolute rate constants and transient intermediates in the free-radical-induced peroxidation of  $\gamma$ -terpinene, an unusual hydrocarbon antioxidant. *New J. Chem.* **2003**, *27*, 1563–1567.
- [162] Tanko, J. M.; Friedline, R.; Suleman, N. K.; Castagnoli, N. tert-Butoxyl as a Model for Radicals in Biological Systems: Caveat Empor. *J. Am. Chem. Soc.* **2001**, *123*, 5808–5809.
- [163] Russell, G. A. In *Free Radicals*; Kochi, J. K., Ed.; Wiley: New York, 1973; Chapter Reactivity, Selectivity, and Polar Effects in Hydrogen Atom Transfer Reactions, pp 1–13.
- [164] Luo, Y.-R. *Handbook of Bond Dissociation Energies in Organic Compounds*; CRC Press, 2002.
- [165] Bordwell, F.; Cheng, J. P.; Harrelson, J. A. Homolytic bond dissociation energies in solution from equilibrium acidity and electrochemical data. *J. Am. Chem. Soc.* **1988**, *110*, 1229–1231.
- [166] Miller, D. C.; Tarantino, K. T.; Knowles, R. R. Proton-Coupled Electron Transfer in Organic Synthesis: Fundamentals, Applications, and Opportunities. *Top. Curr. Chem.* **2016**, *374*, 145–203.
- [167] DiLabio, G. A.; Pratt, D. A.; LoFaro, A. D.; Wright, J. S. Theoretical Study of X-H Bond Energetics (X = C, N, O, S): Application to Substituent Effects, Gas Phase Acidities, and Redox Potentials. *J. Phys. Chem. A* **1999**, *103*, 1653–1661.
- [168] Chan, B.; Radom, L. BDE261: A Comprehensive Set of High-Level Theoretical Bond Dissociation Enthalpies. *J. Phys. Chem. A* **2012**, *116*, 4975–4986.
- [169] Wiberg, K. B.; Petersson, G. A. A Computational Study of RXHn X–H Bond Dissociation Enthalpies. *J. Phys. Chem. A* **2014**, *118*, 2353–2359.

---

## References

---

- [170] Avila, D. V.; Ingold, K. U.; Lusztyk, J.; Green, W. H.; Procopio, D. R. Dramatic Solvent Effects on the Absolute Rate Constants for Abstraction of the Hydroxylic Hydrogen Atom from tert-Butyl Hydroperoxide and Phenol by the Cumyloxy Radical. The Role of Hydrogen Bonding. *J. Am. Chem. Soc.* **1995**, *117*, 2929–2930.
- [171] DiLabio, G. A. Using Locally Dense Basis Sets for the Determination of Molecular Properties. *J. Phys. Chem. A* **1999**, *103*, 11414–11424.
- [172] Wright, J. S.; Johnson, E. R.; DiLabio, G. A. Predicting the Activity of Phenolic Antioxidants: Theoretical Method, Analysis of Substituent Effects, and Application to Major Families of Antioxidants. *J. Am. Chem. Soc.* **2001**, *123*, 1173–1183.
- [173] Martin, J. M. L.; de Oliveira, G. Towards standard methods for benchmark quality ab initio thermochemistry—W1 and W2 theory. *J. Chem. Phys.* **1999**, *111*, 1843–1856.
- [174] Wood, G. P. F.; Radom, L.; Petersson, G. A.; Barnes, E. C.; Frisch, M. J.; Montgomery, J. A. A restricted-open-shell complete-basis-set model chemistry. *J. Chem. Phys.* **2006**, *125*, 094106.
- [175] Somers, K. P.; Simmie, J. M. Benchmarking Compound Methods (CBS-QB3, CBS-APNO, G3, G4, W1BD) against the Active Thermochemical Tables: Formation Enthalpies of Radicals. *J. Phys. Chem. A* **2015**, *119*, 8922–8933.
- [176] Simmie, J. M.; Somers, K. P. Benchmarking Compound Methods (CBS-QB3, CBS-APNO, G3, G4, W1BD) against the Active Thermochemical Tables: A Litmus Test for Cost-Effective Molecular Formation Enthalpies. *J. Phys. Chem. A* **2015**, *119*, 7235–7246.
- [177] Petersson, G. A. *Understanding Chemical Reactivity*; Kluwer Academic Publishers, 2001; pp 99–130.
- [178] Pople, J. A.; Head-Gordon, M.; Fox, D. J.; Raghavachari, K.; Curtiss, L. A. Gaussian-1 theory: A general procedure for prediction of molecular energies. *J. Chem. Phys.* **1989**, *90*, 5622–5629.
- [179] Andrienko, G. A. Chemcraft. 2015; <http://www.chemcraftprog.com>.
- [180] Savin, A.; Johnson, E. R. *Topics in Current Chemistry*; Springer International Publishing, 2014; pp 81–95.

---

## References

---

- [181] Zhao, Y.; González-García, N.; Truhlar, D. G. Benchmark Database of Barrier Heights for Heavy Atom Transfer, Nucleophilic Substitution, Association, and Unimolecular Reactions and Its Use to Test Theoretical Methods. *J. Phys. Chem. A* **2005**, *109*, 2012–2018.
- [182] Zhao, Y.; Tishchenko, O.; Gour, J. R.; Li, W.; Lutz, J. J.; Piecuch, P.; Truhlar, D. G. Thermochemical Kinetics for Multireference Systems: Addition Reactions of Ozone. *J. Phys. Chem. A* **2009**, *113*, 5786–5799.
- [183] Goerigk, L.; Grimme, S. A thorough benchmark of density functional methods for general main group thermochemistry, kinetics, and non-covalent interactions. *Phys. Chem. Chem. Phys.* **2011**, *13*, 6670.
- [184] Dorofeeva, O. V.; Mastryukov, V. S.; Allinger, N. L.; Almenningen, A. The molecular structure and conformation of cyclooctane as determined by electron diffraction and molecular mechanics calculations. *J. Phys. Chem.* **1985**, *89*, 252–257.
- [185] Dutoi, A. D.; Head-Gordon, M. Self-interaction error of local density functionals for alkali–halide dissociation. *Chem. Phys. Lett.* **2006**, *422*, 230–233.
- [186] Johnson, E. R.; Mackie, I. D.; DiLabio, G. A. Dispersion interactions in density-functional theory. *J. Phys. Org. Chem.* **2009**, *22*, 1127–1135.
- [187] Suárez, D.; Rayón, V. M.; Díaz, N.; Valdés, H. Ab initio benchmark calculations on Ca (II) complexes and assessment of density functional theory methodologies. *115*, 11331–11343.
- [188] Harding, M. M. The geometry of metal–ligand interactions relevant to proteins. *Acta Crystallogr., Sect. D: Biol. Crystallogr.* **1999**, *55*, 1432–1443.
- [189] Otero-de-la-Roza, A. Escher. Accessed Apr. 3, 2017: <https://github.com/aoterodelaroza/escher>.

# **Appendix**

## Appendix A

### BDE data

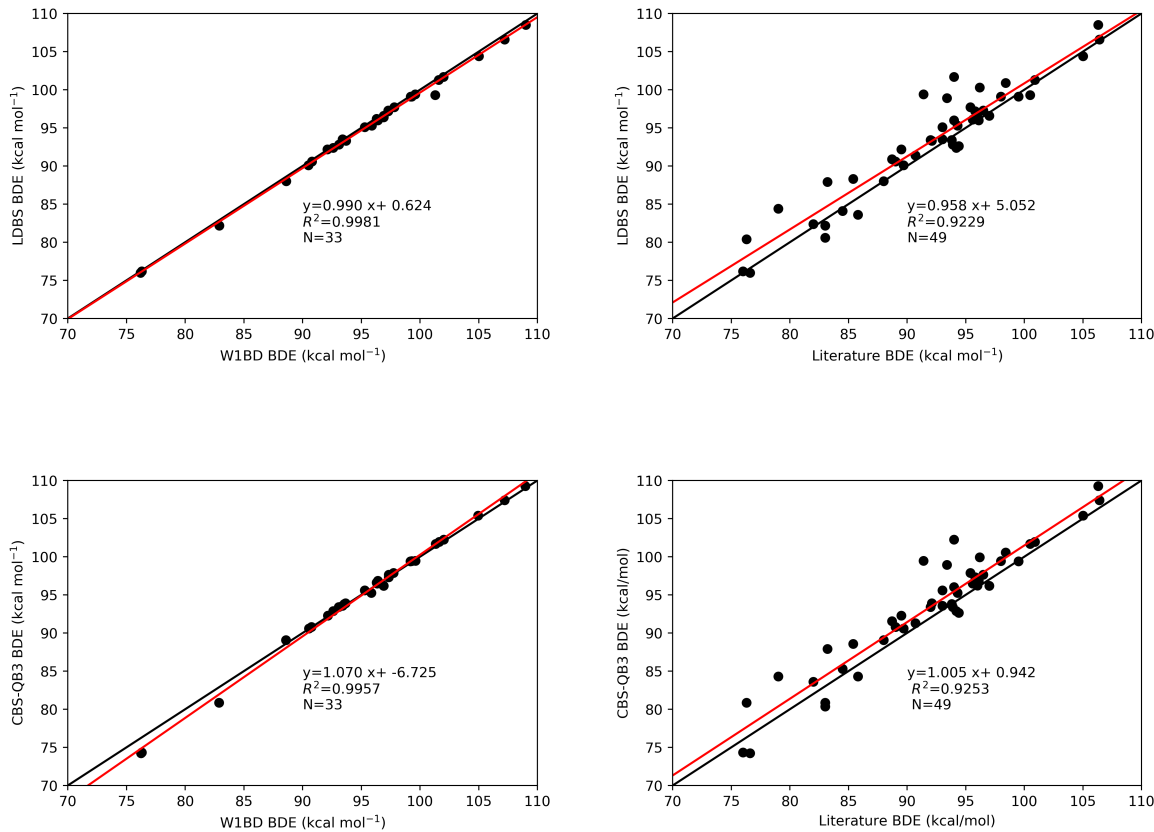


Table A.1: Summary of experimental rate constants ( $M^{-1}s^{-1}$ ) and literature<sup>164</sup> bond dissociation enthalpies (BDEs, kcal mol<sup>-1</sup>).

Molecule	$k_H$	Normalized $k_H$	BDE
1,4-cyclohexadiene	$6.60 \times 10^7$	$1.65 \times 10^7$	76

1,4-diazabicyclo-[2.2.2]octane	$9.60 \times 10^6$	$8.00 \times 10^5$	93.4
2,2-dimethylbutane	$9.50 \times 10^4$	$4.75 \times 10^4$	98
2,3-dimethylbutane	$5.60 \times 10^5$	$2.80 \times 10^5$	95.4
9,10-dihydroanthracene	$5.04 \times 10^7$	$1.26 \times 10^7$	76.3
Acetone	$< 1 \times 10^4$	$2 \times 10^3$	96
Acetonitrile	$< 1 \times 10^4$	$3 \times 10^3$	97
Adamantane (2°)	$6.90 \times 10^6$	$5.75 \times 10^5$	98.4
Adamantane (3°)	$6.90 \times 10^6$	$1.73 \times 10^6$	96.2
Benzaldehyde	$1.20 \times 10^7$	$1.20 \times 10^7$	88.7
Benzyl alcohol	$2.97 \times 10^6$	$1.49 \times 10^6$	79
Cumene	$5.60 \times 10^5$	$5.60 \times 10^5$	83.2
Cycloheptane	$2.20 \times 10^6$	$1.57 \times 10^5$	94
Cyclohexane	$1.10 \times 10^6$	$9.17 \times 10^4$	99.5
Cyclooctane	$2.98 \times 10^6$	$1.86 \times 10^5$	94.4
Cyclopentane	$9.54 \times 10^6$	$9.54 \times 10^5$	95.6
Dibenzyl ether	$5.60 \times 10^6$	$1.40 \times 10^6$	85.8
Diethyl ether	$2.60 \times 10^6$	$6.50 \times 10^5$	93
Dimethyl sulfoxide	$1.80 \times 10^4$	$6.00 \times 10^3$	94
Dioxane	$8.20 \times 10^5$	$1.03 \times 10^5$	96.5
Diphenylmethane	$8.71 \times 10^5$	$4.36 \times 10^5$	84.5
Ethylbenzene	$7.90 \times 10^5$	$3.95 \times 10^5$	85.4
Hexamethylphosphoramide	$1.87 \times 10^7$	$1.04 \times 10^6$	
Morpholine	$5.00 \times 10^7$	$1.25 \times 10^7$	92
Piperazine	$2.30 \times 10^8$	$2.90 \times 10^7$	93
Piperidine	$1.10 \times 10^8$	$2.80 \times 10^7$	89.5
Pyrrolidine	$1.20 \times 10^8$	$3.10 \times 10^7$	89
Tetrahydrofuran	$5.80 \times 10^6$	$1.45 \times 10^6$	92.1
Toluene	$1.85 \times 10^5$	$6.17 \times 10^4$	89.7
Triethylamine	$2.10 \times 10^8$	$3.5 \times 10^7$	90.7
Triphenylmethane	$3.04 \times 10^5$	$3.04 \times 10^5$	81

